nature neuroscience

Article

https://doi.org/10.1038/s41593-023-01514-1

Inferring neural activity before plasticity as a foundation for learning beyond backpropagation

Received: 18 May 2022

Accepted: 2 November 2023

Published online: 03 January 2024

Check for updates

Yuhang Song[1,2,3] ✉, Beren Millidge[2], Tommaso Salvatori[1,4,5], Thomas Lukasiewicz[1,4] ✉, Zhenghua Xu[1,6] ✉ & Rafal Bogacz[2] ✉

For both humans and machines, the essence of learning is to pinpoint which components in its information processing pipeline are responsible for an error in its output, a challenge that is known as 'credit assignment'. It has long been assumed that credit assignment is best solved by backpropagation, which is also the foundation of modern machine learning. Here, we set out a fundamentally different principle on credit assignment called 'prospective configuration'. In prospective configuration, the network first infers the pattern of neural activity that should result from learning, and then the synaptic weights are modified to consolidate the change in neural activity. We demonstrate that this distinct mechanism, in contrast to backpropagation, (1) underlies learning in a well-established family of models of cortical circuits, (2) enables learning that is more efficient and effective in many contexts faced by biological organisms and (3) reproduces surprising patterns of neural activity and behavior observed in diverse human and rat learning experiments.

The credit assignment problem[1] lies at the very heart of learning. Backpropagation[2], as a simple yet effective credit assignment theory, has powered notable advances in artificial intelligence since its inception[3–5] and has also gained a predominant place in understanding learning in the brain[1,6–8]. Due to this success, much recent work has focused on understanding how biological neural networks could learn in a way similar to backpropagation[9–12]; although many proposed models do not implement backpropagation exactly, they nevertheless try to approximate backpropagation, and much emphasis is placed on how close this approximation is[9,11,13,14]. However, learning in the brain is superior to backpropagation in many critical aspects. For example, compared to the brain, backpropagation requires many more exposures to a stimulus to learn[15] and suffers from catastrophic interference of newly and previously stored information[16]. This raises the question of whether using backpropagation to understand learning in the brain should be the main focus of the field.

Here, we propose that the brain instead solves credit assignment with a fundamentally different principle, which we call 'prospective configuration'. In prospective configuration, before synaptic weights are modified, neural activity changes across the network so that output neurons better predict the target output; only then are the synaptic weights (hereafter termed 'weights') modified to consolidate this change in neural activity. By contrast, in backpropagation, the order is reversed; weight modification takes the lead, and the change in neural activity is the result that follows.

We identify prospective configuration as a principle that is implicitly followed by a well-established family of neural models with solid biological groundings, namely, energy-based networks.

[1]Department of Computer Science, University of Oxford, Oxford, UK. [2]Medical Research Council Brain Network Dynamics Unit, University of Oxford, Oxford, UK. [3]Fractile, Ltd., London, UK. [4]Institute of Logic and Computation, Vienna University of Technology, Vienna, Austria. [5]VERSES AI Research Lab, Los Angeles, CA, USA. [6]State Key Laboratory of Reliability and Intelligence of Electrical Equipment, School of Health Sciences and Biomedical Engineering, Hebei University of Technology, Tianjin, China. ✉e-mail: yuhang.song@bndu.ox.ac.uk; thomas.lukasiewicz@cs.ox.ac.uk; zhenghua.xu@hebut.edu.cn; rafal.bogacz@ndcn.ox.ac.uk

These networks include Hopfield networks[17] and predictive coding networks[18], which have been successfully used to describe information processing in the cortex[19]. To support the theory of prospective configuration, we show that it can both yield efficient learning, which humans and animals are capable of, and reproduce data from experiments on human and animal learning. Thus, on the one hand, we demonstrate that prospective configuration performs more efficient and effective learning than backpropagation in various situations faced by biological systems, such as learning with deep structures, online learning, learning with a limited amount of training examples, learning in changing environments, continual learning with multiple tasks and reinforcement learning. On the other hand, we demonstrate that patterns of neural activity and behavior in diverse human and animal learning experiments, including sensorimotor learning, fear conditioning and reinforcement learning, can be naturally explained by prospective configuration but not by backpropagation.

Guided by the belief that backpropagation is the foundation of biological learning, previous work showed that energy-based networks can closely approximate backpropagation. However, to achieve it, the networks were set up in an unnatural way, such that the neural activity was prevented from substantially changing before weight modification by constraining the supervision signal to be infinitely small (for example, as in equilibrium propagation[11] and in previous studies using predictive coding networks[12,20]) or last an infinitely short time[14,21]. By contrast, we reveal that energy-based networks without these unrealistic constraints follow the distinct principle of prospective configuration rather than backpropagation and are superior in both learning efficiency and accounting for data on biological learning.

Here, we introduce prospective configuration with an intuitive example, show how it originates from energy-based networks and describe its advantages and quantify them in a rich set of biologically relevant learning tasks. We show that prospective configuration naturally explains patterns of neural activity and behavior in diverse learning experiments.

Results

Prospective configuration: an intuitive example

To optimally plan behavior, it is critical for the brain to predict future stimuli, for example, to predict sensations in some modalities on the basis of other modalities[22]. If the observed outcome differs from the prediction, the weights in the whole network need to be updated so that predictions in the 'output' neurons are corrected. Backpropagation computes how the weights should be modified to minimize the error on the output, and this weight update results in a change in neural activity when the network next makes the prediction. By contrast, we propose that neural activity is first adjusted to a new configuration so that the output neurons better predict the observed outcome (target pattern); the weights are then modified to reinforce this configuration of neural activity. We call this configuration of neural activity 'prospective' because it is the neural activity that the network should produce to correctly predict the observed outcome. In agreement with the proposed mechanism of prospective configuration, it has indeed been widely observed in biological neurons that presenting the outcome of a prediction triggers changes in neural activity; for example, in tasks requiring animals to predict a juice delivery, the reward triggers rapid changes in activity not only in the gustatory cortex but also in multiple cortical regions[23,24].

To highlight the difference between backpropagation and prospective configuration, consider a simple example (Fig. 1a). Imagine a bear seeing a river. In the bear's mind, the sight generates predictions of hearing water and smelling salmon. On that day, the bear indeed smelled the salmon but did not hear the water, perhaps due to an ear injury, and thus the bear needs to change its expectation related to the sound. Backpropagation (Fig. 1b) would proceed by backpropagating the negative error to reduce the weights on the path between the visual and auditory neurons. However, this also entails a reduction of the weights between visual and olfactory neurons that would compromise the expectation of smelling the salmon the next time the river is visited, even though the smell of salmon was present and correctly predicted. These undesired and unrealistic side effects of learning with backpropagation are closely related with the phenomenon of catastrophic interference, where learning a new association destroys previously learned memories[16]. This example shows that, with backpropagation, even learning one new aspect of an association may interfere with the memory of other aspects of the same association.

By contrast, prospective configuration assumes that learning starts with the neurons being configured to a new state, which corresponds to a pattern enabling the network to correctly predict the observed outcome. The weights are then modified to consolidate this state. This behavior can 'foresee' side effects of potential weight modifications and compensate for them dynamically (Fig. 1c). To correct the negative error on the incorrect output, the hidden neurons settle to their prospective state of lower activity, and, as a result, a positive error is revealed and allocated to the correct output. Consequently, prospective configuration increases the weights connecting to the correct output, whereas backpropagation does not (Fig. 1b,c). Hence, prospective configuration is able to correct the side effects of learning an association effectively and efficiently and with little interference.

Origin of prospective configuration: energy-based networks

To show how prospective configuration naturally arises in energy-based networks, we introduce a physical machine analog, which provides an intuitive understanding of energy-based networks and how they produce the mechanism of prospective configuration.

Energy-based networks have been widely and successfully used in describing biological neural systems[17,25]. In these models, a neural circuit is described by a dynamical system driven by reducing an abstract 'energy', for example, reflecting errors made by neurons (Methods). Neural activity and weights change to reduce this energy; hence, they can be considered 'movable parts' of the dynamical system. We show that energy-based networks are mathematically equivalent to a physical machine (we call it 'energy machine'), where the energy function has an intuitive interpretation, and its dynamics are straightforward; the energy machine simply adjusts its movable parts to reduce energy.

The energy machine includes nodes sliding on vertical posts connected with each other via rods and springs (Fig. 2a,b). Translating from energy-based networks to the energy machine, neural activity maps to the vertical position of a solid node, a connection maps to a rod (blue arrow) pointing from one node to another (where the weight determines how the end position of the rod relates to the initial position), and the energy function maps to the elastic potential energy of springs with nodes attached on both ends (the natural length of the springs is 0). Different energy functions and network structures result in different energy-based networks, corresponding to energy machines with different configurations and combinations of nodes, rods and springs. In Fig. 2, we present the energy machine of predictive coding networks[12,18] because they are most accessible and are established to be closely related to backpropagation[12,14].

The dynamics of energy-based networks, which are driven by minimizing the energy function, map to relaxation of the energy machine, which is driven by reducing the total elastic potential energy on the springs. A prediction with energy-based networks involves clamping the input neurons to the provided stimulus and updating the activity of the other neurons, which corresponds to fixing one side of the energy machine and letting the energy machine relax by moving nodes (Fig. 2a). Learning with energy-based networks involves clamping the input and output neurons to the corresponding stimulus, first letting the activities of the remaining neurons converge and then updating weights, which corresponds to fixing both sides of the energy machine and letting the energy machine relax first by moving nodes and then tuning rods (Fig. 2b).

https://doi.org/10.1038/s41593-023-01514-1

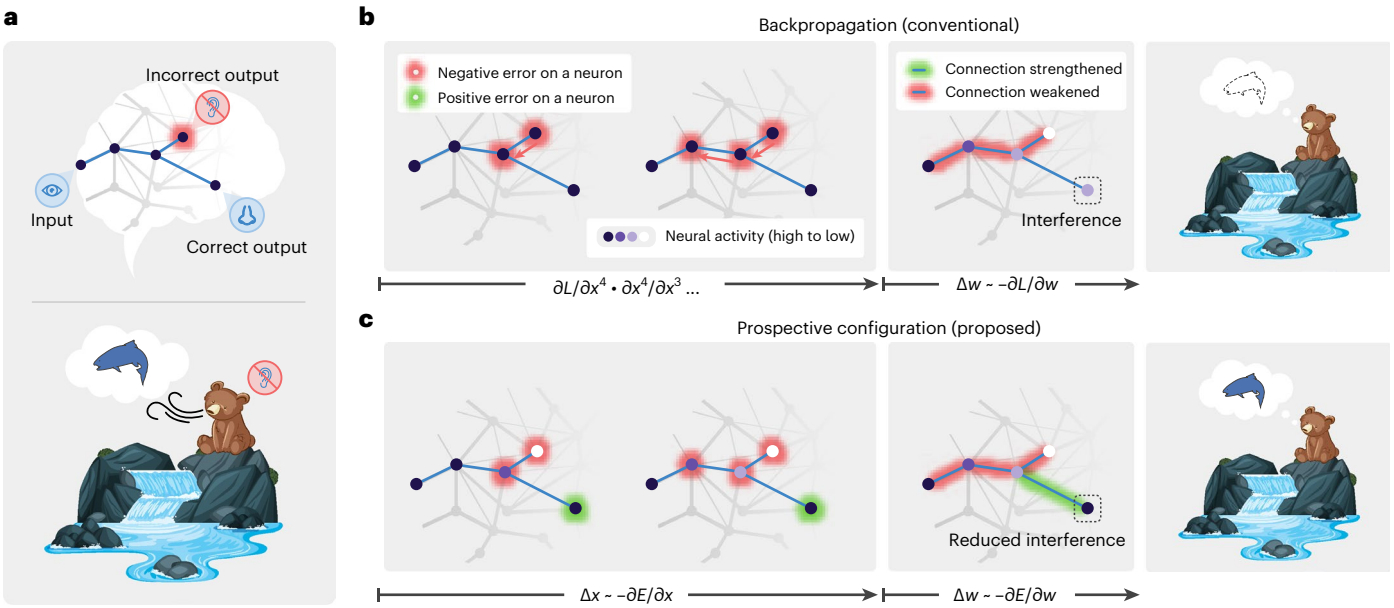

Fig. 1 | Prospective configuration avoids interference during learning. a, Abstract (top) and concrete (bottom) examples of a task inducing interference during learning. One stimulus input (seeing the water) triggers two prediction outputs (hearing the water and smelling the salmon). One output is correct (smelling the salmon), whereas the other output is an error (not hearing the water). **b**,**c**, Backpropagation produces interference during learning; not hearing the water reduces the expectation of smelling the salmon (**b**), although the salmon was indeed smelled. Prospective configuration, on the other hand, avoids such interference (**c**). In backpropagation, negative error propagates from the error output to hidden neurons (**b**; left). This causes a weakening of some connections, which, on the next trial, improves the incorrect output but also reduces the prediction of the correct output, thus introducing interference (**b**; middle and right). In prospective configuration, neural activity settles into a new configuration (different intensities of purple) before weight modification (**c**; left). This configuration corresponds to the activity that should be produced after learning, that is, is 'prospective'. Hence, it foresees the positive error on the correct output and modifies the connections to improve the incorrect output while maintaining the correct output (**c**; middle and right).

The energy machine reveals the essence of energy-based networks; relaxation before weight modification lets the network settle to a new configuration of neural activity corresponding to the neural activity that would have occurred after the error was corrected by the modification of weights, that is, prospective activity (thus, we call this mechanism prospective configuration). For example, the second-layer 'neuron' in Fig. 2b increases its activity, and this increase in activity would also be caused by the subsequent weight modification (of the connection between the first and second neurons). In simple terms, relaxation in energy-based networks infers the prospective neural activity after learning, toward which the weights are then modified. This distinguishes it from backpropagation, where weight modification takes the lead, and the change in neural activity is the result that follows.

The bottom of Fig. 2c shows the connectivity of a predictive coding network[12,18], which has dynamics mathematically equivalent to those of the energy machine shown above it. Predictive coding networks include neurons (blue) corresponding to nodes on the posts and separate neurons encoding prediction errors (red) corresponding to springs. For details, see Methods and Supplementary Fig. 1, where we list equations describing predictive coding networks and show how they map on the neural implementation and the proposed energy machine.

Using the energy machine, Fig. 2d simulates the learning problem from Fig. 1. Here, we can see that prospective configuration indeed foresees the result of learning and its side effects through relaxation. Hence, it corrects the side effects within one iteration, which would otherwise take multiple iterations for backpropagation.

Advantages of prospective configuration: reduced interference and faster learning

Here, we quantify interference in the above scenario and demonstrate how reduced interference translates into an advantage in performance. In all simulations in the main text, prospective configuration is implemented in predictive coding networks (other energy-based models are considered in the Supplementary Notes, Section 2.1). We also compare the performance of predictive coding networks against artificial neural networks (ANNs) trained with backpropagation because they are closely related, which makes the comparisons fair. In particular, although predictive coding networks include recurrent connections, they generate the same prediction for a given input (when inputs are constrained but outputs are not; Fig. 2a) as standard feedforward ANNs if their weights are set to corresponding values[12,14]. Therefore, loss is the same function of weights in both models, so direct minimization of loss with gradient descent in predictive coding networks (which is not their natural way of training) would produce the same weight changes as backpropagation in ANNs. Hence, comparing predictive coding networks and backpropagation enables isolation of the effects of the learning algorithm (prospective configuration versus direct minimization of loss as in backpropagation).

In Fig. 3a, we compare the activity of output neurons in the example in Fig. 1 between backpropagation and prospective configuration. Initially both output neurons are active (top right), and the output should change toward a target in which one of the neurons is inactive (red vector). Learning with prospective configuration results in changes on the output (purple solid vector) that are aligned better with the target than those for backpropagation (purple dotted vector).

Following the first weight update, we simulate multiple iterations until the network is able to correctly predict the target. Here, 'iteration' refers to each time the agent is presented with stimuli and conducts one weight update because of the stimulus. Although the output from backpropagation can reach the target after multiple iterations, the output for the 'correct neuron' diverges from the target during learning and then comes back; this is a particularly undesired effect in biological learning, where networks can be 'tested' at any point during the learning process, because it may lead to incorrect decisions

https://doi.org/10.1038/s41593-023-01514-1

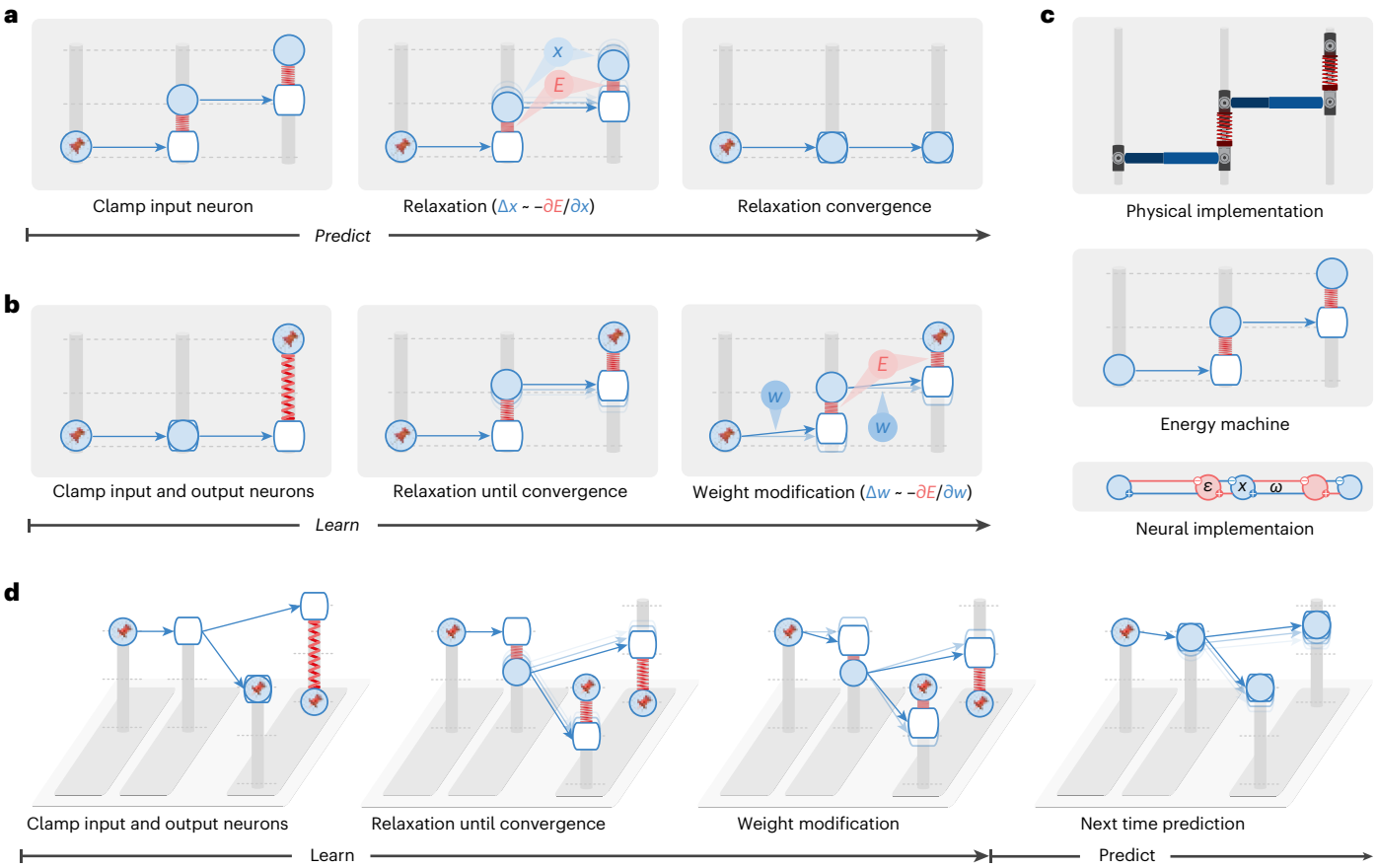

Fig. 2 | The energy machine reveals a new understanding of energy-based networks, the mechanism of prospective configuration and its theoretical advantages. A subset of energy-based networks can be visualized as mechanical machines that perform equivalent computations. Here, we present the energy machine corresponding to predictive coding networks[12,18]. In the energy machine, the activity of a neuron corresponds to the height of a node (represented by a solid circle) sliding on a post. The input to the neuron is represented by a hollow node on the same post. A synaptic connection corresponds to a rod pointing from a solid node to a hollow node. The weight determines how the input to a postsynaptic neuron depends on the activity of a presynaptic neuron; hence, it influences the angle of the rod. In energy-based networks, relaxation (that is, neural dynamics) and weight modification (that is, weight dynamics) are both driven by minimizing the energy, which corresponds to relaxation of the energy machine by moving the nodes and tuning the rods, respectively. **a**,**b**, Predictions (**a**) and learning (**b**) in energy-based networks visualized by the energy machine. The pin indicates that neural activity is fixed to the input or target pattern. Here, it is revealed that relaxation infers prospective neural activity, toward which the weights are then modified, a mechanism that we call prospective configuration. **c**, Physical implementation (top) and connectivity of a predictive coding network[12,18] (bottom), which has dynamics mathematically equivalent to those of the energy machine in the middle (see Methods for details). **d**, The learning problem in Fig. 1 visualized by the energy machine, which learns to improve the incorrect output while not interfering with the correct output, thanks to the mechanism of prospective configuration.

affecting chances for survival. By contrast, prospective configuration substantially reduces this effect.

Although backpropagation modifies weights to directly reduce cost in the space of weights (that is, performs gradient descent), surprisingly, and rather subversively, it does not push the resulting output activity directly toward the target. To illustrate this, Fig. 3a visualizes the cost with contour lines. Changing the activity of output neurons according to the gradient of the cost would correspond to a change orthogonal to the contour lines, that is, that indicated by the red arrow. However, backpropagation changes the output in a different direction shown by a dashed arrow. Optimizing the weights independently, without considering the effect of updating other weights, leads to output activity not updating toward the target directly due to different weight updates to different layers interfering with each other. By contrast, prospective configuration considers the results of updating other weights by finding a desired configuration of neural activity first. Such a mechanism is missing in backpropagation but is natural in energy-based networks. Supplementary Fig. 2 shows a direct comparison of how these two models evolve in weight and output spaces during learning.

Interference can be quantified by the angle between the direction of the target (from current output to target) and learning (from current output to output after learning, both measured without the target provided), and we define 'target alignment' as the cosine of this angle (Fig. 3b); hence, high interference corresponds to low target alignment (Fig. 3c).

It is useful to highlight that target alignment is affected little by the learning rate (Fig. 3d), demonstrating that the learning rate has little effect on the direction and trajectory that output neurons take. The difference in target alignment demonstrated in Fig. 3a is also present for deeper and larger (randomly generated) networks (Fig. 3e). When a network has no hidden layers, the target alignment is equal to 1 (Supplementary Notes, Section 2.4.1). The target alignment drops for backpropagation as the network gets deeper because changes in weights in one layer interfere with changes in other layers (Fig. 1), and the backpropagated errors do not lead to appropriate modification of weights in hidden layers (Supplementary Fig. 2). Because backpropagation modifies the weights in the direction reducing loss, it has positive target alignment for small learning rates but not necessarily

https://doi.org/10.1038/s41593-023-01514-1

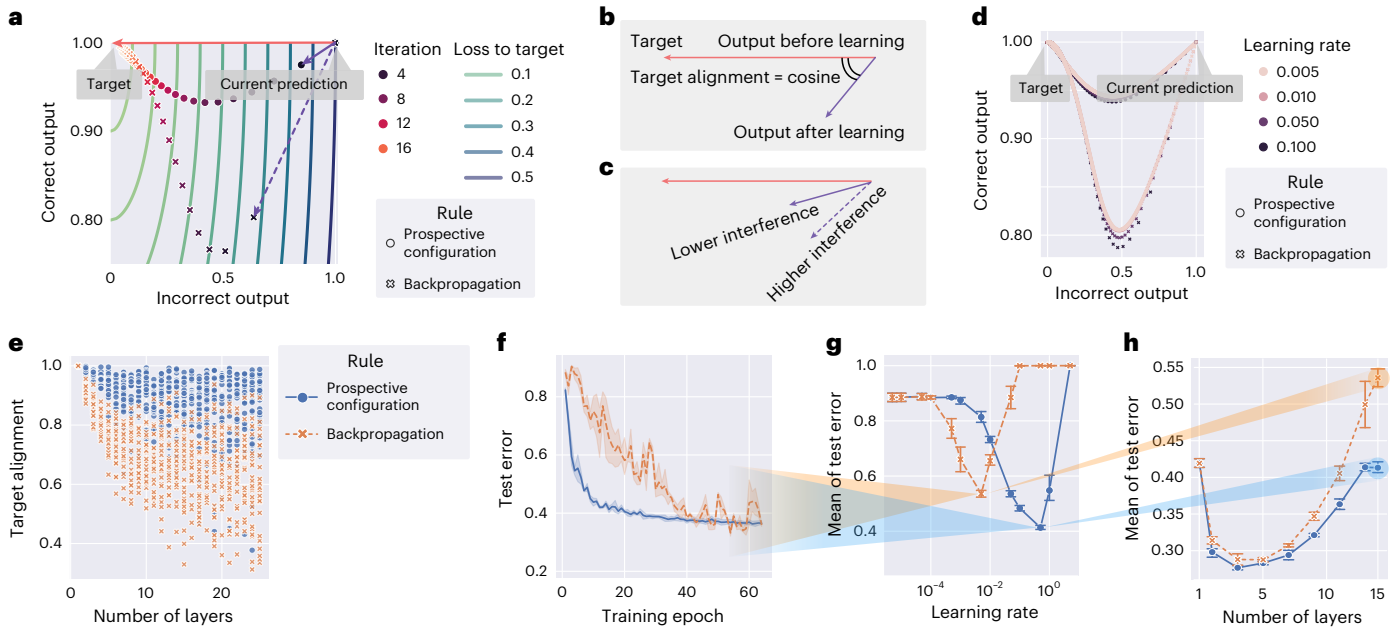

Fig. 3 | Learning with prospective configuration changes the activity of output neurons in a direction more aligned toward the target. a, Simulation of the network from Fig. 1 showing changes in the correct and incorrect output neurons during training ('Iteration') trained with both learning rules. Here, learning with prospective configuration (purple solid vector) aligns better with the target (red vector) than learning with backpropagation (purple dashed vector). **b**, Interference can be quantified by 'target alignment', the cosine similarity of the direction of the target (red vector) and the direction of learning (purple vector). **c**, Higher target alignment indicates less interference and vice versa. **d**, The same experiment as in **a** repeated with a learning rate ranging from 0.005 to 0.5 represented by the size of the markers, where it is shown that the choice of learning rate changes the trajectories for both methods slightly, but the conclusion holds irrespective of the learning rate. **e**, Target alignment of randomly generated networks trained with both learning rules as a function of depth of the network. Each symbol shows target alignment resulting from training on a single randomly generated pattern. **f**, Test error during training on the FashionMNIST[60] dataset containing images of clothing belonging to different categories for both learning rules with a deep neural network of 15 layers. Here, 'test error' refers to the ratio of incorrectly classified samples among all samples in the test set. **g**, Mean of the test error over training epochs (reflecting how fast test error drops) as a function of learning rate. Results in **f** and **h** are for the learning rates giving the minima of the corresponding curves in **g**. **h**, Mean of test error of other network depths. Each point is from a learning rate independently optimized for each learning rule in the corresponding setup of network depth. In **e**–**h**, prospective configuration demonstrates a notable advantage as the structure gets deeper. Each experiment in **f**–**h** was repeated with $n = 3$ random seeds. Error bars and bands represent the 68% confidence interval.

close to 1. By contrast, prospective configuration maintains a much higher value along the way. This higher target alignment of prospective configuration can be theoretically explained by the following: (1) there exists a close link between prospective configuration and an algorithm called target propagation[26] (shown in Supplementary Fig. 3 and Supplementary Notes, Section 2.2), and (2) under certain conditions, target propagation[26] has a target alignment of 1 (ref. 27; demonstrated in Supplementary Fig. 4 and Supplementary Notes, Section 2.4.2). Thus, the link with target propagation provides theoretical insight (with numerical verification) into why prospective configuration has a higher target alignment.

Higher target alignment directly translates to the efficiency of learning. Test error during training in a visual classification task with a deep neural network of 15 layers decreases faster for prospective configuration than for backpropagation (Fig. 3f).

Throughout the data presented here, if learning rate is not presented in a plot, the plot corresponds to the best learning rate optimized independently for each rule under the setup via a grid search. The optimization target is either learning performance or similarity to experimental data (details can be found in the methods for each experiment). Thus, for example, Fig. 3f shows the test errors as training progress, with the learning rates optimized independently for each learning rule. The optimization target is the 'mean of test error' during training, reflecting how fast the test error decreases during training. Fig. 3g plots this mean of test error for different learning rates for both learning rules, and the learning rates giving the minima of the curves were used in Fig. 3f. Fig. 3h repeats the experiment on networks of other depths and shows the mean of the test error during training as a function of network depth. The mean error is higher for lower depths, as these networks are unable to learn the task, and for greater depths, as it takes longer to train deeper networks. Importantly, the gap between backpropagation and prospective configuration widens for deeper networks, paralleling the difference in target alignment. Efficient training with deeper networks is important for biological neural systems known to be deep, for example, the primate visual cortex[28].

In Section 2.3 of the Supplementary Notes, we develop a formal theory of prospective configuration and provide further illustrations and analyses of its advantages. Supplementary Fig. 5 formally defines prospective configuration and demonstrates that it is indeed commonly observed in different energy-based networks. Supplementary Figs. 6 and 7 empirically verify and generalize the advantages expected from the theory and show that prospective configuration yields more accurate error allocation and less erratic weight modification, respectively.

Advantages of prospective configuration: effective learning in biologically relevant scenarios

Inspired by these advantages, we show empirically that prospective configuration indeed handles various learning problems that biological systems would face better than backpropagation. Because the field of machine learning has developed effective benchmarks for testing learning performance, we use variants of classic machine

https://doi.org/10.1038/s41593-023-01514-1

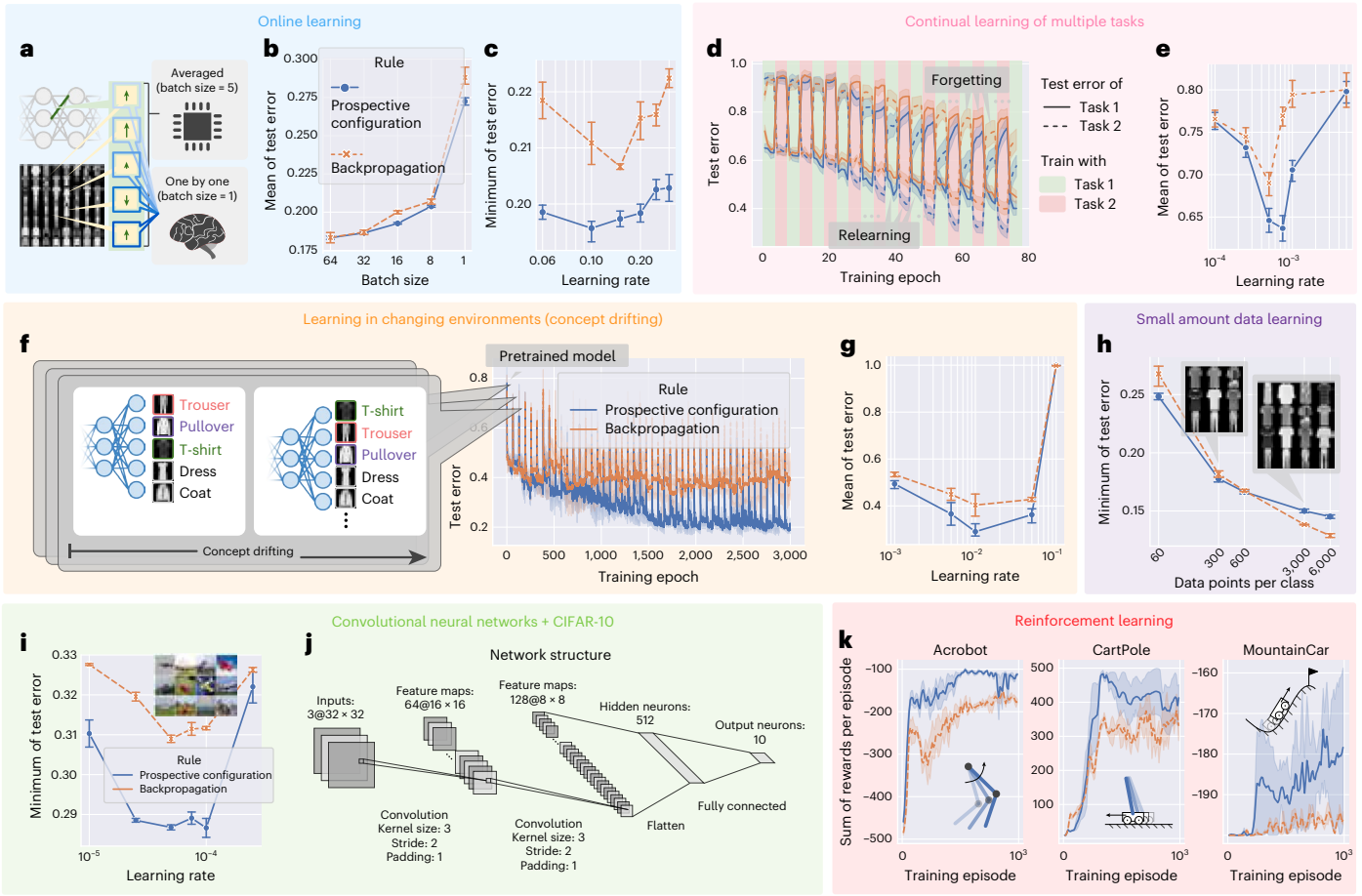

Fig. 4 | Prospective configuration achieves a superior performance over backpropagation in various learning situations faced by biological systems. **a**–**k**, Learning situations include online learning[29] (**a**–**c**), continual learning of multiple tasks[30] (**d**–**e**), learning in changing environments[31] (**f**–**g**), learning with a limited amount of training examples (**h**) and reinforcement learning[4] (**k**). Graphs corresponding to each situation are grouped together with the same background color. Simulations of each situation differ from the 'default setup' described in the Methods in a single aspect unique to this task. For example, the default setup involves training with minibatches, so the batch size was only set to 1 in **a**–**c** for investigating online learning, whereas it was set to a larger default value in rest of the groups. In supervised learning setups, fully connected networks (**a**–**h**) were evaluated on the FashionMNIST[60] dataset, and convolutional neural networks[35] (**i** and **j**) were evaluated on the CIFAR-10 (ref. 36) dataset. In the reinforcement learning setup (**k**), fully connected networks were evaluated on three classic control problems. If the learning rate was not presented, each point (a setup of an experiment) in the plot corresponds to the best learning rate optimized independently for each rule under that setup. **a**, Difference in training setup between computers that can average weight modifications for individual examples to get a 'statistically good' value and biological systems that must apply one modification before computing another. **b**, Mean of the test errors during training as a function of batch size. **c**, Minimum of test error during training as a function of learning rate. **d**, Test error during continual learning of two tasks. **e**, Mean of test error of both tasks during training as a function of learning rate. **f**, Test error during training when learning with concept drifting. **g**, Mean of test error during training with concept drifting as a function of learning rate. **h**, Minimum of test error during training with different amounts of training examples (data points per class). **i**, Minimum of test error during training of a convolutional neural network trained with prospective configuration and backpropagation on the CIFAR-10 (ref. 36) dataset. **j**, Structure detail of the convolutional neural network used in **i**. **k**, Sum of rewards per episode during training on three classic reinforcement learning tasks (insets). An episode is a period from initialization of environment to reaching a terminate state. Each experiment in **a**–**h** was repeated with $n = 10$ random seeds. Each experiment in **i**–**k** was repeated with $n = 3$ random seeds because these experiments are more expensive. Error bars and bands represent the 68% confidence interval.

learning problems that share key features with learning in natural environments. Such problems include online learning, where weights must be updated after each experience (rather than a batch of training examples)[29], continual learning with multiple tasks[30], learning in changing environments[31], learning with a limited amount of training examples and reinforcement learning[4]. In all aforementioned learning problems, prospective configuration demonstrates a notable superiority over backpropagation.

First, based on the example in Fig. 1, we expect prospective configuration to require fewer episodes for learning than backpropagation. Before presenting the comparison, we describe how backpropagation is used to train ANNs. Typically, the weights are only modified after a batch of training examples based on the average of updates derived from individual examples (Fig. 4a). In fact, backpropagation relies heavily on averaging over multiple experiences to reach human-level performance[32], as it needs to stabilize training[33]. By contrast, biological systems must update the weights after each experience, and we compare learning performance in such a setting. Sampling efficiency can be quantified by mean of test error during training, which is shown in Fig. 4b as a function of batch size (number of experiences that the updates are averaged over). Efficiency strongly depends on batch size for backpropagation because it requires batch training to average out erratic weight updates, whereas this dependence is weaker for prospective configuration, where weight changes are intrinsically less erratic and batch averaging is required less (Supplementary Fig. 7). Importantly, prospective configuration learns faster with smaller batch sizes, as in

https://doi.org/10.1038/s41593-023-01514-1

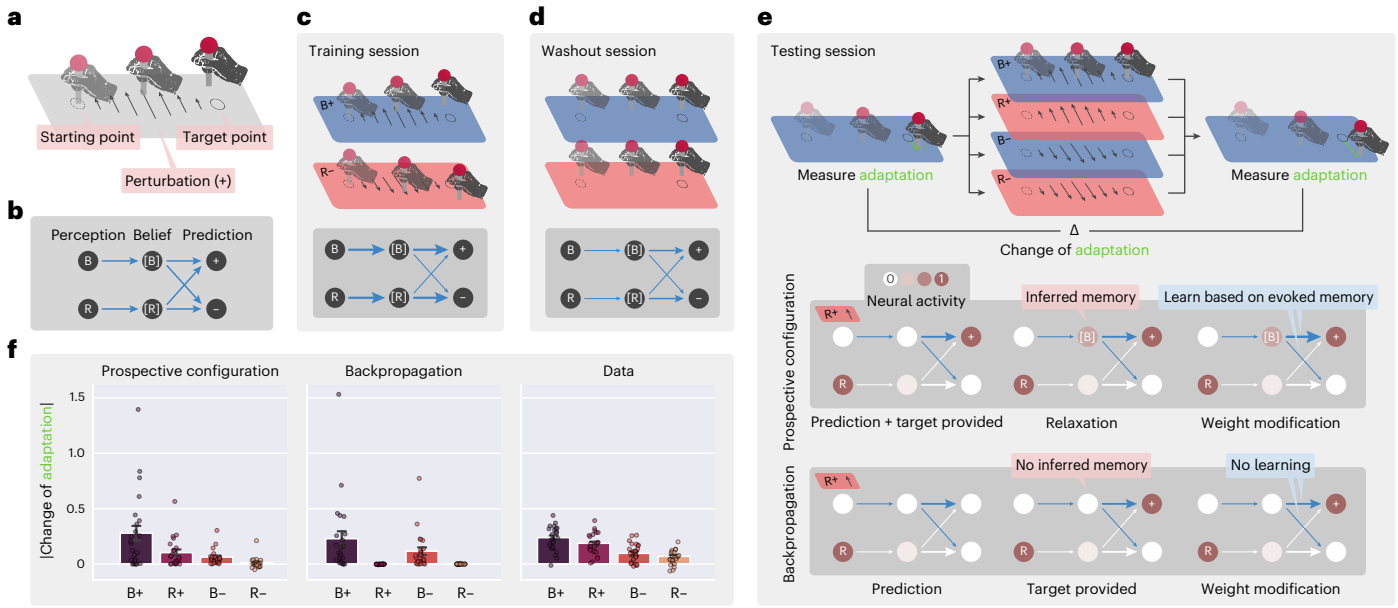

Fig. 5 | Prospective configuration explains contextual inference in human sensorimotor learning. a, Structure of an experimental trial where participants were asked to move a stick from the starting point to the target point while experiencing perturbations. **b**, The minimal network for the task, including six connections encoding the associations from the backgrounds (B and R) to the belief of contexts ([B] and [R]) and from the belief of contexts to the prediction of perturbations (+ and −). **c**–**e**, Sequence of sessions the participants experienced, including training (**c**), washout (**d**) and testing (**e**). Darker gray boxes show the expected network after the session, where thickness represents the strength of connections. In the testing session, the darker box explains how the two learning rules learn differently on the R+ trial, leading to the differences in **f**. **f**, Predictions of the two learning rules compared to behavioral data measured from human participants, where prospective configuration reproduces the key patterns of data, but backpropagation does not. Each experiment was repeated with $n = 24$ random seeds, as there were 24 participants in the behavioral experiment.

biological settings. Additionally, final performance can be quantified by the minimum of the test error, which is shown in Fig. 4c, when trained with a batch size equal to 1. Here, prospective configuration also demonstrates a notable advantage over backpropagation.

Second, biological organisms need to sequentially learn multiple tasks, while ANNs show catastrophic forgetting. When trained on a new task, performance on previously learned tasks is largely destroyed[16,34]. The data in Fig. 4d show performance when trained on two tasks alternately (task 1 is classifying five randomly selected classes in the FashionMNIST dataset, and task 2 is classifying the remaining five classes). Prospective configuration outperforms backpropagation both in terms of avoiding forgetting previous tasks and relearning current tasks. The results are summarized in Fig. 4e.

Third, biological systems often need to rapidly adapt to changing environments. A common way to simulate this is 'concept drifting'[31], where a part of the mapping between the output neurons to the semantic meaning is shuffled regularly, each time a certain number of training iterations has passed (Fig. 4f). Test error during training with concept drifting is presented in Fig. 4f. Before epoch 0, both learning rules are initialized with the same pretrained model (trained with backpropagation); thus, epoch 0 is the first time the model experiences concept drift. The results are summarized in Fig. 4g and show that, for this task, there is a particularly large difference in mean error (for optimal learning rates). This large advantage of prospective configuration is related to it being able to optimally detect which weights to modify (Supplementary Fig. 6) and to preserve existing knowledge while adapting to changes (Fig. 1). This ability to maintain important information while updating other information is critical for survival in natural environments that are bound to change, and prospective configuration has a very substantial advantage in this respect.

Furthermore, biological learning is also characterized by limited data availability. Prospective configuration outperforms backpropagation when the model is trained with fewer examples (Fig. 4h).

To demonstrate that the advantage of prospective configuration also scales up to larger networks and problems, we evaluated convolutional neural networks[35] on CIFAR-10 (ref. 36) trained with both learning rules (Fig. 4i), where prospective configuration showed notable advantages over backpropagation. The detailed structure of the convolutional networks is provided in Fig. 4j.

Another key challenge for biological systems is to decide which actions to take. Reinforcement learning theories (for example, *Q* learning) propose that it is solved by learning the expected reward resulting from different actions in different situations[37]. Such prediction of rewards can be made by neural networks[4], which can be trained with prospective configuration or backpropagation. The sum of rewards per episode during training on three classic reinforcement learning tasks is reported in Fig. 4k, where prospective configuration demonstrates a notable advantage over backpropagation. This large advantage may arise because reinforcement learning is particularly sensitive to erratic changes in network weights (as the target output depends on reward predicted by the network itself for a new state; Methods).

Based on the superior learning performance of prospective configuration, we may expect that this learning mechanism has been favored by evolution; thus, in the next sections, we investigate if it can account for neural activity and behavior during learning better than backpropagation.

Evidence for prospective configuration: inferring the latent state during learning

Prospective configuration is related to theories proposing that before learning, the brain first infers a latent state of the environment from feedback[38–40]. Here, we propose that this inference can be achieved in neural circuits through prospective configuration, where, following feedback, neurons in 'hidden layers' converge to a prospective pattern of activity that encodes this latent state. We demonstrate that data from various previous studies, which involved the inference of a

https://doi.org/10.1038/s41593-023-01514-1

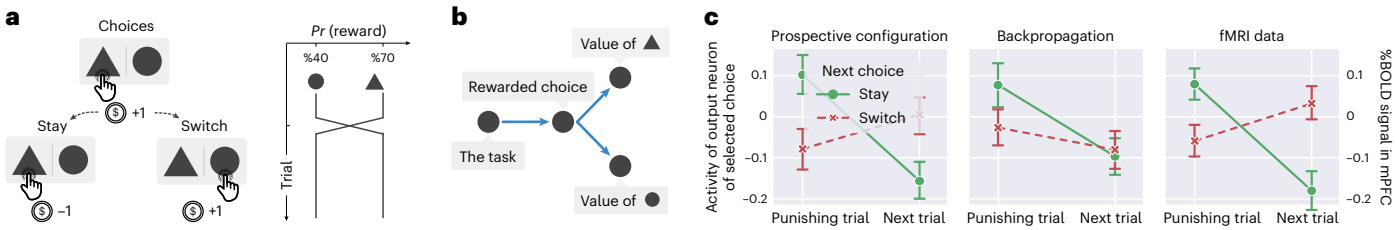

Fig. 6 | Prospective configuration can discover the underlying task structure during reinforcement learning. a, Reinforcement learning task. Human participants were required to choose between two options, leading to either reward (gaining coins) or punishment (losing coins) with different probabilities. The probability of reward was occasionally reversed between the two options. **b**, The minimal network encoding the essential elements of the task. **c**, Activity of the output neuron corresponding to the selected option from networks trained with prospective configuration and backpropagation compared with fMRI data measured in human participants (that is, peak blood oxygenation level-dependent (%BOLD) signal in the mPFC). Prospective configuration reproduces the key finding that the expected value (encoded in %BOLD signal in the mPFC) increases if the next choice after a punishing trial is to switch to the other option. The number of trials is not mentioned in the original paper, so we simulated for $n = 128$ trials for both learning rules. Error bars represent the 68% confidence interval.

latent state, can be explained by prospective configuration. These data were previously explained by complex and abstract mechanisms, such as Bayesian models[38,39], whereas here, we mechanistically show with prospective configuration how such inference can be performed by minimal networks encoding only the essential elements of the tasks.

The dynamical inference of a latent state from feedback has been recently proposed to take place during sensorimotor learning[39]. In this experiment, participants received different motor perturbations in different contexts and learned to compensate for these perturbations. Behavioral data suggest that, after receiving feedback, participants first used the feedback to infer context and then adapted the force for the inferred context. We demonstrate that prospective configuration is able to reproduce these behavioral data, whereas backpropagation cannot.

Specifically, in the task (Fig. 5a), participants were asked to move a stick from a starting point to a target point while experiencing perturbations. The participants experienced a sequence of blocks of trials (Fig. 5c–e), including training, washout and testing. During the training session, different directions of perturbations, positive (+) or negative (−), were applied in different contexts, blue (B) or red (R) backgrounds, respectively. We denote these trials as B+ and R−. These trials may be associated with latent states, which we denote [B] and [R]; for example, the latent state [B] may be associated with both background B and perturbation +. The next stage of the task was designed to investigate if the latent state [B] can be activated by perturbation + even if no background B is shown. Thus, participants experienced different trials including R+ (that is, perturbation + but no background B). Specifically, after a washout session (during which no perturbation was provided), in the testing session, participants experienced one of the four possible test trials: B+, R+, B− and R−. To evaluate learning on the test trials, motor adaptation (that is, the difference between the final and target stick positions) was measured before and after the test trial in two trials with the blue background (Fig. 5e). Change in the adaptation between these two trials is a reflection of learning about blue context that occurred at the test trial. If participants only associated feedback with the background color (B), then the change in adaptation would only occur with test trials B+ and B−. However, experimental data (Fig. 5f) show that there was also substantial adaptation change with R+ trials (which was even bigger than with B− trials).

To model learning in this task, we considered a neural network (Fig. 5b) where input nodes encode the background color, and outputs encode movement compensations in the two directions. Importantly, this network also includes hidden neurons encoding belief of being in the contexts associated with the two backgrounds ([B] and [R]). Trained with the exact procedure of the experiment[39] from randomly initialized weights, prospective configuration with this minimal network can reproduce the behavioral data, whereas backpropagation cannot (Fig. 5f).

Prospective configuration can produce change in adaptation with the R+ test trial because after + feedback, it is able to also activate context [B] that was associated with this feedback during training and then learn compensation for this latent state. To shed light on how this inference takes place in the model, schematics in Fig. 5c,d show evolution of the weights of the network over sessions (thickness represents the strength of connections). The schematic in Fig. 5e shows the difference between the two learning rules after exposure to R+; although B is not perceived, prospective configuration infers a moderate excitation of the belief of blue context [B] because the positive connection from [B] to + was built during the training session. The activity of [B] enables the learning of weights from [B] to + and −, while backpropagation does not modify any weights originating from [B].

For simplicity of explanation, we presented simulations with minimal networks; however, Supplementary Fig. 8 shows that networks with a general fully connected structure and more hidden neurons can replicate the above data when using prospective configuration but not when using backpropagation.

Studies of animal conditioning have also observed that feedback in learning tasks involving multiple stimuli may trigger learning about non-presented stimuli[41,42]. One example is provided in Supplementary Fig. 9, where we show that it can be explained by prospective configuration but not by backpropagation.

Evidence for prospective configuration: discovering task structure during learning

Prospective configuration is also able to discover the underlying task structure in reinforcement learning. Specifically, we consider a task where reward probabilities of different options were not independent[38]. In this study, humans were choosing between two options where the reward probabilities were constrained such that one option had a higher reward probability than the other (Fig. 6a). Occasionally the reward probabilities were swapped, so if one probability was increased, the other was decreased by the same amount. Remarkably, the recorded functional magnetic resonance imaging (fMRI) data suggested that participants learned that the values of the two options were negatively correlated and on each trial updated the value estimates of both options in opposite ways. This conclusion was drawn from analysis of the signal from the medial prefrontal cortex (mPFC), which encoded the expected value of reward. The data presented in Fig. 6c compare this signal after making a choice on two consecutive trials: a trial in which the reward was not received ('punish trial') and the next trial. If the participant selected the same option on both trials ('stay'), the signal decreased, indicating that the reward expected by the participant was reduced. Remarkably, if the participant selected the other option on the next trial ('switch'), the signal increased, suggesting that negative feedback for

one option increased the value estimate for the other. Such learning is not predicted by standard reinforcement learning models[38].

This task can be conceptualized as having a latent state encoding which option is superior, and this latent state determines the reward probabilities for both options. Consequently, we consider a neural network reflecting this structure (Fig. 6b) that includes an input neuron encoding being in the task (equal to 1 in simulations), a hidden neuron encoding the latent state and two output neurons encoding the reward probabilities for the two options. Trained with the exact procedure of the experiment[38] from randomly initialized weights, prospective configuration with this minimal network can reproduce the data, whereas backpropagation cannot (Fig. 6c). In Supplementary Fig. 10, we show that prospective configuration reproduces these data because it can infer the rewarded choice by updating the activity of the hidden neuron based on feedback.

Taken together, the presented simulations illustrate that prospective configuration is a common principle that can explain a range of surprising learning effects in diverse tasks.

Discussion

Our paper identifies the principle of prospective configuration, according to which learning relies on neurons first optimizing their pattern of activity to match the correct output and then reinforcing these prospective activities through synaptic plasticity. Although it was known that in energy-based networks the activity of neurons shifts before weight update, it has been previously thought that this shift is a necessary cost of error propagation in biological networks, and several methods have been proposed to suppress it[11,12,14,20,21] to approximate backpropagation more closely. By contrast, we demonstrate that this reconfiguration of neural activity is the key to achieving learning performance superior to that of backpropagation and to explaining experimental data from diverse learning tasks. Prospective configuration further offers a range of experimental predictions distinct from those of backpropagation (Supplementary Figs. 11 and 12). Together, we have demonstrated that prospective configuration enables more efficient learning than backpropagation by reducing interference, demonstrates superior performance in situations faced by biological organisms, requires only local computation and plasticity and matches experimental data across a wide range of tasks.

Our theory addresses a long-standing question of how the brain solves the plasticity-stability dilemma, for example, how it is possible that, despite adjustment of representation in the primary visual cortex during learning[43], we can still understand the meaning of visual stimuli we learned over our lifetime. According to prospective configuration, when some weights are modified, compensatory changes are made to other weights to ensure the stability of correctly predicted outputs. Thus, prospective configuration reduces interference between different weight modifications while learning a single association. Previous computational models have proposed mechanisms that reduce interference between new and previously acquired information while learning multiple associations[34,44]. It is highly likely that such mechanisms and prospective configuration operate in the brain in parallel to minimize both types of interference.

Prospective configuration is related to inference and learning procedures in statistical modeling. If the 'energy' in energy-based schemes is variational free energy, prospective configuration can be seen as an implementation of variational Bayes that subsumes inference and learning[45]. For example, dynamic expectation maximization[46,47] can be regarded as a generalization of predictive coding networks in which the D-step optimizes representations of latent states (analogously to relaxation until convergence during inference) while the E-step optimizes model parameters (analogously to weight modification during learning).

Other recent work[48,49] also noticed that the natural form of energy-based networks ('strong control' in their words) performs different learning than backpropagation. Their analysis concentrates on an architecture of deep feedback control, and they demonstrated that a particular form of their model is equivalent to predictive coding networks[49]. The unique contribution of our paper is to show the benefits of such strong control and explain why they arise. The principle of prospective configuration is also present in other recent models. For example, Gilra and Gerstner[50] developed a spiking model in which feedback about the error on the output directly affects the activity of hidden neurons before plasticity takes place. Haider et al.[51] developed a faster inference algorithm for energy-based models that computes a value to which the activity is likely to converge, termed latent equilibrium[51]. Iteratively setting each neuron's output based on its latent equilibrium leads to much faster inference[51] and enables efficient computation of the prospective configuration.

Predictive coding networks require symmetric forward and backward weights between layers of neurons, so a question arises concerning how such symmetry may develop in the brain. If predictive coding networks are initialized with symmetric weights (as in our simulations), the symmetry will persist because the changes in weight between neurons A and B are the same as those for feedback weight (between neurons B and A). Even if the weights are not initialized symmetrically, the symmetry may develop if synaptic decay is included in the model[52] because then the initial asymmetric values decay away, and weight values become more influenced by recent changes that are symmetric. Nevertheless, weight symmetry is not generally required for effective credit assignment[53,54].

Here, we assumed for simplicity that the convergence of neural activity to an equilibrium happens rapidly after the stimuli are provided so that the synaptic weight modification after convergence may take place while the stimuli are still present. Nevertheless, predictive coding networks can still work even if weight modification takes place while the neural activity is converging. Specifically, Song et al. demonstrated that if neural activities are only updated for the first few steps, the update of the weights is equivalent to that in backpropagation[14]. As a reminder, we demonstrate here that if the neural activities are updated to equilibrium, the update of the weights follows the principle of prospective configuration and possesses the desirable demonstrated properties. Thus, a learning rule where neural activities and weights are updated in parallel will experience a weight update that is equivalent to backpropagation at the start and then move to prospective configuration as the system converges to equilibrium[55]. Furthermore, predictive coding networks have been extended to describe recurrent structures[56–58], and it has been shown that such networks can learn to predict dynamically changing stimuli even if weights are modified before the activity converged for a given 'frame' of the stimulus[57].

The advantages of prospective configuration suggest that it may be profitably applied in machine learning to improve the efficiency and performance of deep neural networks. An obstacle for this is that the relaxation phase is computationally expensive. However, recent work demonstrated that by modifying weights after each step of relaxation, the model becomes comparably fast to backpropagation and easier for parallelization[55].

Most intriguingly, it has been demonstrated that the speed of energy-based networks can be greatly increased by implementing the relaxation on analog hardware[59], potentially resulting in energy-based networks being faster than backpropagation. Therefore, we anticipate that our discoveries may change the blueprint of next-generation machine learning hardware, switching from the current digital tensor base to analog hardware and being closer to the brain and potentially far more efficient.

Online content

Any methods, additional references, Nature Portfolio reporting summaries, source data, extended data, supplementary information, acknowledgements, peer review information; details of author contributions and competing interests; and statements of data and code availability are available at https://doi.org/10.1038/s41593-023-01514-1.

References

1. Lillicrap, T. P., Santoro, A., Marris, L., Akerman, C. J. & Hinton, G. Backpropagation and the brain. *Nat. Rev. Neurosci.* **21**, 335–346 (2020).
2. Rumelhart, D. E., Hinton, G. E. & Williams, R. J. *Learning Internal Representations by Error Propagation* (Univ. California, San Diego, Institute for Cognitive Science, 1985).
3. Krizhevsky, A., Sutskever, I. & Hinton, G. E. ImageNet classification with deep convolutional neural networks. In *Advances in Neural Information Processing Systems (NeurIPS)* (eds Bartlett, P. et al.) 1097–1105 (Curran Associates, 2012).
4. Mnih, V. et al. Human-level control through deep reinforcement learning. *Nature* **518**, 529–533 (2015).
5. Silver, D. et al. Mastering the game of go with deep neural networks and tree search. *Nature* **529**, 484–489 (2016).
6. Richards, B. A. et al. A deep learning framework for neuroscience. *Nat. Neurosci.* **22**, 1761–1770 (2019).
7. Singer, Y. et al. Sensory cortex is optimized for prediction of future input. *eLife* **7**, e31557 (2018).
8. Yamins, D. L. K. et al. Performance-optimized hierarchical models predict neural responses in higher visual cortex. *Proc. Natl Acad. Sci. USA* **111**, 8619–8624 (2014).
9. Sacramento, J., Costa, R. P., Bengio, Y. and Senn, W. Dendritic cortical microcircuits approximate the backpropagation algorithm. In *Advances in Neural Information Processing Systems (NeurIPS)* (eds Bengio, S. et al.) 8721–8732 (Curran Associates, 2018).
10. Guerguiev, J., Lillicrap, T. P. & Richards, B. A. Towards deep learning with segregated dendrites. *eLife* **6**, e22901 (2017).
11. Scellier, B. & Bengio, Y. Equilibrium propagation: bridging the gap between energy-based models and backpropagation. *Front. Comput. Neurosci.* **11**, 24 (2017).
12. Whittington, J. C. R. & Bogacz, R. An approximation of the error backpropagation algorithm in a predictive coding network with local hebbian synaptic plasticity. *Neural Comput.* **29**, 1229–1262 (2017).
13. Whittington, J. C. R. & Bogacz, R. Theories of error back-propagation in the brain. *Trends Cogn. Sci.* **23**, 235–250 (2019).
14. Song, Y., Lukasiewicz, T., Xu, Z. & Bogacz, R. Can the brain do backpropagation? Exact implementation of backpropagation in predictive coding networks. In *Advances in Neural Information Processing Systems (NeurIPS)* (eds Larochell, H. et al.) 22566–22579 (Curran Associates, 2020).
15. Tsividis, P. A., Pouncy, T., Xu, J. L., Tenenbaum, J. B. & Gershman, S. J. Human learning in Atari. In *2017 AAAI Spring Symposium Series* 643–646 (Association for the Advancement of Artificial Intelligence, 2017).
16. McCloskey, M. & Cohen, N. J. Catastrophic interference in connectionist networks: the sequential learning problem. *Psychol. Learn. Motiv.* **24**, 109–165 (1989).
17. Hopfield, J. J. Neural networks and physical systems with emergent collective computational abilities. *Proc. Natl Acad. Sci. USA* **79**, 2554–2558 (1982).
18. Rao, R. P. & Ballard, D. H. Predictive coding in the visual cortex: a functional interpretation of some extra-classical receptive-field effects. *Nat. Neurosci.* **2**, 79–87 (1999).
19. Friston, K. The free-energy principle: a unified brain theory? *Nat. Rev. Neurosci.* **11**, 127–138 (2010).
20. Millidge, B., Tschantz, A. & Buckley, C. L. Predictive coding approximates backprop along arbitrary computation graphs. *Neural Comput.* **34**, 1329–1368 (2022).
21. Bengio, Y. & Fischer, A. Early inference in energy-based models approximates back-propagation. Preprint at https://doi.org/10.48550/arXiv.1510.02777 (2015).
22. O'Reilly, R. C. & Munakata, Y. *Computational Explorations in Cognitive Neuroscience: Understanding the Mind by Simulating the Brain* (MIT Press Cambridge, 2000).
23. Quilodran, R., Rothe, M. & Procyk, E. Behavioral shifts and action valuation in the anterior cingulate cortex. *Neuron* **57**, 314–325 (2008).
24. Wallis, J. D. & Kennerley, S. W. Heterogeneous reward signals in prefrontal cortex. *Curr. Opin. Neurobiol.* **20**, 191–198 (2010).
25. Friston, K. A theory of cortical responses. *Philos. Trans. R. Soc. Lond. B Biol. Sci.* **360**, 815–836 (2005).
26. Bengio, Y. How auto-encoders could provide credit assignment in deep networks via target propagation. Preprint at https://doi.org/10.48550/arXiv.1407.7906 (2014).
27. Meulemans, A., Carzaniga, F., Suykens, J., Sacramento, J. & Grewe, B. F. A theoretical framework for target propagation. In *Advances in Neural Information Processing Systems (NeurIPS)* (eds Larochelle, H. et al.) 20024–20036 (Curran Associates, 2020).
28. Felleman, D. J. & Van Essen, D. C. Distributed hierarchical processing in the primate cerebral cortex. *Cereb. Cortex* **1**, 1–47 (1991).
29. Fontenla-Romero, Ó., Guijarro-Berdiñas, B., Martinez-Rego, D., Pérez-Sánchez, B. & Peteiro-Barral, D. Online machine learning. In *Efficiency and Scalability Methods for Computational Intellect* (eds Igelnik, B. & Zurada, J. M.) 27–54 (IGI Global, 2013).
30. Hassabis, D., Kumaran, D., Summerfield, C. & Botvinick, M. Neuroscience-inspired artificial intelligence. *Neuron* **95**, 245–258 (2017).
31. Gama, J., Žliobaitė, I., Bifet, A., Pechenizkiy, M. & Bouchachia, A. A survey on concept drift adaptation. *ACM Comput. Surv.* **46**, 1–37 (2014).
32. Puri, R., Kirby, R., Yakovenko, N. & Catanzaro, B. Large scale language modeling: converging on 40 GB of text in four hours. In *2018 30th International Symposium on Computer Architecture and High Performance Computing (SBAC-PAD)* 290–297 (IEEE, 2018).
33. Ioffe, S. & Szegedy, C. Batch normalization: accelerating deep network training by reducing internal covariate shift. In *Proceedings of the International Conference on Machine Learning (ICML)* (eds Bach, F. & Blei, D.) 448–456 (PMLR, 2015).
34. Zenke, F., Poole, B. & Ganguli, S. Continual learning through synaptic intelligence. In *Proc. 34th International Conference on Machine Learning* (eds Precup, D. & Teh, Y. W.) 3987–3995 (PMLR, 2017).
35. O'Shea, K. & Nash, R. An introduction to convolutional neural networks. Preprint at https://doi.org/10.48550/arXiv.1511.08458 (2015).
36. Krizhevsky, A. & Hinton, G. *Learning Multiple Layers of Features from Tiny Images*. Master's thesis, Univ. Toronto (2009).
37. Sutton, R. S. & Barto, A. G. *Introduction to Reinforcement Learning*, Vol. 2 (MIT Press Cambridge, 1998).
38. Hampton, A. N., Bossaerts, P. & O'Doherty, J. P. The role of the ventromedial prefrontal cortex in abstract state-based inference during decision making in humans. *J. Neurosci.* **26**, 8360–8367 (2006).
39. Heald, J. B., Lengyel, M. & Wolpert, D. M. Contextual inference underlies the learning of sensorimotor repertoires. *Nature* **600**, 489–493 (2021).
40. Larsen, T., Leslie, D. S., Collins, E. J. & Bogacz, R. Posterior weighted reinforcement learning with state uncertainty. *Neural Comput.* **22**, 1149–1179 (2010).
41. Kaufman, M. A. & Bolles, R. C. A nonassociative aspect of overshadowing. *Bull. Psychonomic Soc.* **18**, 318–320 (1981).
42. Matzel, L. D., Schachtman, T. R. & Miller, R. R. Recovery of an overshadowed association achieved by extinction of the overshadowing stimulus. *Learn. Motiv.* **16**, 398–412 (1985).
43. Poort, J. et al. Learning enhances sensory and multiple non-sensory representations in primary visual cortex. *Neuron* **86**, 1478–1490 (2015).

44. McClelland, J. L., McNaughton, B. L. & O'Reilly, R. C. Why there are complementary learning systems in the hippocampus and neocortex: insights from the successes and failures of connectionist models of learning and memory. *Psychol. Rev.* **102**, 419–457 (1995).
45. Dauwels, J. On variational message passing on factor graphs. In *2007 IEEE International Symposium on Information Theory*, 2546–2550 (IEEE, 2007).
46. Anil Meera, A. & Wisse, M. Dynamic expectation maximization algorithm for estimation of linear systems with colored noise. *Entropy* **23**, 1306 (2021).
47. Friston, K. Hierarchical models in the brain. *PLoS Comput. Biol.* **4**, e1000211 (2008).
48. Meulemans, A., Farinha, M. T., Cervera, M. R., Sacramento, J. & Grewe, B. F. Minimizing control for credit assignment with strong feedback. In *Proc. of Machine Learning Research* (eds Chaudhuri, K. et al.) 15458–15483 (PMLR, 2022).
49. Meulemans, A., Zucchet, N., Kobayashi, S., von Oswald, J. & Sacramento, J. The least-control principle for learning at equilibrium. *Adv. Neural Inf. Process. Syst.* **35**, 33603–33617 (2022).
50. Gilra, A. & Gerstner, W. Predicting non-linear dynamics by stable local learning in a recurrent spiking neural network. *eLife* **6**, e28295 (2017).
51. Haider, P. et al. Latent equilibrium: a unified learning theory for arbitrarily fast computation with arbitrarily slow neurons. In *Advances in Neural Information Processing Systems (NeurIPS)* (eds Ranzato, M. et al.) 17839–17851 (2021).
52. Akrout, M., Wilson, C., Humphreys, P., Lillicrap, T. & Tweed, D. B. Deep learning without weight transport. In *Advances in Neural Information Processing Systems (NeurIPS)* (eds Wallach, H. et al.) (Curran Associates, 2019).
53. Lillicrap, T. P., Cownden, D., Tweed, D. B. & Akerman, C. J. Random synaptic feedback weights support error backpropagation for deep learning. *Nat. Commun.* **7**, 13276 (2016).
54. Millidge, B., Tschantz, A. & Buckley, C. L. Relaxing the constraints on predictive coding models. Preprint at https://doi.org/10.48550/arXiv.2010.01047 (2020).
55. Salvatori, T. et al. Incremental predictive coding: a parallel and fully automatic learning algorithm. Preprint at https://doi.org/10.48550/arXiv.2212.00720 (2022).
56. Friston, K. J., Trujillo-Barreto, N. & Daunizeau, J. Dem: a variational treatment of dynamic systems. *NeuroImage* **41**, 849–885 (2008).
57. Millidge, B., Tang, M., Osanlouy, M. & Bogacz, R. Predictive coding networks for temporal prediction. Preprint at *bioRxiv* https://doi.org/10.1101/2023.05.15.540906 (2023).
58. Salvatori, T. et al. Learning on arbitrary graph topologies via predictive coding. In *Advances in Neural Information Processing Systems (NeurIPS)* (eds Koyejo, S. et al.) 38232–38244 (Curran Associates, 2022).
59. Foroushani, A. N., Assaf, H., Noshahr, F. H., Savaria, Y. & Sawan, M. Analog circuits to accelerate the relaxation process in the equilibrium propagation algorithm. In *2020 IEEE International Symposium on Circuits and Systems (ISCAS)* 1–5 (IEEE, 2020).
60. Xiao, H., Rasul, K. & Vollgraf, R. Fashion MNIST: a novel image dataset for benchmarking machine learning algorithms. Preprint at https://doi.org/10.48550/arXiv.1708.07747 (2017).

Methods

This section provides the necessary details for replication of the results described in the main text.

Models

Throughout this work, we compare the established theory of backpropagation to the proposed new principle of prospective configuration. As explained in the main text, backpropagation is used to train ANNs, where the activity of a neuron is fixed to a value based on its input, whereas prospective configuration occurs in energy-based networks, where the activity of a neuron is not fixed.

Because in ANNs the activity of neurons $\boldsymbol{x}$ is determined by their input, the output of the network can be obtained by propagating the inputs 'forward' through the computational graph. The output can then be compared to a target pattern to get a measure of difference known as a loss. Because the value of a node (activity of a neuron) in the computational graph is explicitly computed as a function of its input, the computational graph is usually differentiable. Thus, training ANNs with backpropagation modifies the weights $\boldsymbol{w}$ to take a step toward the negative gradient of loss $\mathcal{L}$,

$$\Delta \boldsymbol{w} = -\alpha \frac{\partial \mathcal{L}}{\partial \boldsymbol{w}}, \tag{1}$$

during which the activities of neurons $\boldsymbol{x}$ are fixed, and α is the learning rate. The weights $\boldsymbol{w}$ requiring modification might be many steps away from the output on the computational graph, where the loss $\mathcal{L}$ is computed; thus, $\frac{\partial \mathcal{L}}{\partial \boldsymbol{w}}$ is often obtained by applying the chain rule of computing a derivative through intermediate variables (activity of output and hidden neurons). For example, consider a network with four layers, and let $\boldsymbol{x}^l$ denote the activity of neurons in layer l and $\boldsymbol{w}^l$ denote the weights of connections between layers l and $l+1$. The change in weights originating from the first layer is then computed: $\frac{\partial \mathcal{L}}{\partial \boldsymbol{w}^1} = \frac{\partial \mathcal{L}}{\partial \boldsymbol{x}^4} \cdot \frac{\partial \boldsymbol{x}^4}{\partial \boldsymbol{x}^3} \cdots \frac{\partial \boldsymbol{x}^2}{\partial \boldsymbol{w}^1}$. This enables the loss to be backpropagated through the graph to provide a direction of update for all weights.

In contrast to ANNs, in energy-based networks, the activity of neurons $\boldsymbol{x}$ is not fixed to the input from a previous layer. Instead, an energy function E is defined as a function of the neural activity $\boldsymbol{x}$ and weights $\boldsymbol{w}$. For networks organized in layers (considered in this paper), the energy can be decomposed into a sum of local energy terms E^l,

$$E = \sum_l E^l\left(\boldsymbol{x}^l, \boldsymbol{w}^{l-1}, \boldsymbol{x}^{l-1}\right). \tag{2}$$

Here, E^l is called local energy because it is a function of $\boldsymbol{x}^l, \boldsymbol{x}^{l-1}$ and $\boldsymbol{w}^{l-1}$, which are neighbors and connected to each other. This ensures that the optimization of energy E can be implemented by local circuits because the derivative of E with respect to any neural activity (or weights) results in an equation containing only the local activity (or weights) and the activity of adjacent neurons. Predictions with energy-based networks are computed by clamping the input neurons to an input pattern and then modifying the activity of all other neurons to decrease the energy:

$$\Delta \boldsymbol{x} = -\gamma \frac{\partial E}{\partial \boldsymbol{x}}, \tag{3}$$

where γ is the integration step of the neural dynamics. Because the terms in E can be divided into local energy terms, this results in an equation that can be implemented with local circuits. This process of modifying neural activity to decrease the energy is called relaxation, and we refer to the equation describing relaxation as neural dynamics because it describes the dynamics of the neural activity in energy-based networks. After convergence of relaxation, the activities of the output neurons are taken as the prediction made by the energy-based network. Different energy-based networks are trained in slightly different ways. For predictive coding networks[12,18], training involves clamping the input and output neurons to input and target patterns, respectively. Then, relaxation is run until convergence ($\boldsymbol{x} = \overset{*}{\boldsymbol{x}}$), after which the weights are updated using the activity at convergence to further decrease the energy:

$$\Delta \boldsymbol{w} = -\alpha \frac{\partial E}{\partial \boldsymbol{w}}\Big|_{\boldsymbol{x}=\overset{*}{\boldsymbol{x}}}. \tag{4}$$

This will also result in an equation that can be implemented with local plasticity because it is just a gradient descent on the local energy. We refer to such an equation as weight dynamics, because it describes the dynamics of the weights in energy-based networks.

Backpropagation and prospective configuration are not restricted to specific models. Depending on the structure of the network and the choice of the energy function, one can define different models that implement the principle of backpropagation or prospective configuration. In the main text and most of the Supplementary Notes, we investigate the most standard layered network. In this case, both ANNs and energy-based networks include L layers of weights $\boldsymbol{w}^1, \boldsymbol{w}^2, \ldots, \boldsymbol{w}^L$ and $L+1$ layers of neurons $\boldsymbol{x}^1, \boldsymbol{x}^2, \ldots, \boldsymbol{x}^{L+1}$, where $\boldsymbol{x}^1$ and $\boldsymbol{x}^{L+1}$ are the input and output neurons, respectively. We consider the relationship between activities in adjacent layers for ANNs given by

$$\boldsymbol{x}^l = \boldsymbol{w}^{l-1} f\left(\boldsymbol{x}^{l-1}\right), \tag{5}$$

and the energy function for EBNs described by

$$E^l = \frac{1}{2}\left(\boldsymbol{x}^l - \boldsymbol{w}^{l-1} f\left(\boldsymbol{x}^{l-1}\right)\right)^2. \tag{6}$$

This defines the ANNs to be the standard multilayer perceptrons (MLPs) and the energy-based networks to be the predictive coding network. In Eq. (6) and below, the square operator $(\boldsymbol{v})^2$ denotes the inner product of vector $\boldsymbol{v}$ with itself. The comparison between backpropagation and prospective configuration in the main text is thus between the above MLPs and predictive coding networks; this choice is justified as (1) they are the most standard models[61] and (2) it is established that the two are closely related[12,14] (that is, they make the same prediction with the same weights and input pattern), thus enabling a fair comparison. Nevertheless, we show that the theory (Supplementary Fig. 5) and empirical comparison (Supplementary Figs. 6 and 7) between backpropagation and prospective configuration generalize to other choices of network structures and energy functions, that is, other energy-based networks and ANNs, such as GeneRec[62] and Almeida–Pineda[63–65].

Putting Eqs. (5) and (6) into the general framework, we can obtain the equations that describe MLPs and predictive coding networks, respectively. Assume that the input and target patterns are $\boldsymbol{s}^{\text{in}}$ and $\boldsymbol{s}^{\text{target}}$, respectively. Prediction with MLPs is

$$\boldsymbol{x}^1 = \boldsymbol{s}^{\text{in}} \text{ and } \boldsymbol{x}^l = \boldsymbol{w}^{l-1} f\left(\boldsymbol{x}^{l-1}\right) \text{ for } l > 1, \tag{7}$$

where $\boldsymbol{x}^{L+1}$ is the prediction. Training MLPs with backpropagation is described by

$$\Delta \boldsymbol{w}^l = -\alpha \frac{\partial \mathcal{L}}{\partial \boldsymbol{w}^l} = -\alpha \frac{\partial \mathcal{L}}{\partial \boldsymbol{x}^{L+1}} \cdot \frac{\partial \boldsymbol{x}^{L+1}}{\partial \boldsymbol{x}^L} \cdots \frac{\partial \boldsymbol{x}^{l+1}}{\partial \boldsymbol{w}^l} \text{ where } \mathcal{L} = \frac{1}{2}\left(\boldsymbol{s}^{\text{target}} - \boldsymbol{x}^{L+1}\right)^2, \tag{8}$$

which backpropagates the error $\frac{\partial \mathcal{L}}{\partial \boldsymbol{x}^l}$ layer by layer from output neurons.

The neural dynamics of predictive coding networks can be obtained using Eq. (2):

$$\Delta \boldsymbol{x}^l = -\gamma \frac{\partial E}{\partial \boldsymbol{x}^l} = -\gamma \frac{\partial (E^l + E^{l+1})}{\partial \boldsymbol{x}^l}. \tag{9}$$

Similarly, the weight dynamics of predictive coding networks can be found,

$$\Delta \boldsymbol{w}^l = -\alpha \frac{\partial E}{\partial \boldsymbol{w}^l} = -\alpha \frac{\partial E^{l+1}}{\partial \boldsymbol{w}^l}. \tag{10}$$

To reveal the neural implementation of predictive coding networks, we define the prediction errors to be

$$\boldsymbol{\varepsilon}^l = \boldsymbol{x}^l - \boldsymbol{w}^{l-1} f\left(\boldsymbol{x}^{l-1}\right). \tag{11}$$

The neural and weight dynamics of predictive coding networks can be expressed (by evaluating derivatives in Eqs. (9) and (10)) as

$$\Delta \boldsymbol{x}^l = -\gamma \boldsymbol{\varepsilon}^l + f'\left(\boldsymbol{x}^l\right) \circ \left(\boldsymbol{w}^l\right)^T \boldsymbol{\varepsilon}^{l+1} \text{ and} \tag{12}$$

$$\Delta \boldsymbol{w}^l = \alpha \boldsymbol{\varepsilon}^{l+1} \left(f\left(\boldsymbol{x}^l\right)\right)^T, \tag{13}$$

where the symbol $\circ$ denotes element-wise multiplication. Assuming that $\boldsymbol{\varepsilon}^l$ and $\boldsymbol{x}^l$ are encoded in the activity of error and value neurons, respectively, Eqs. (11) and (12) can be realized with the neural implementation in Fig. 2c. In particular, error $\boldsymbol{\varepsilon}$ and value $\boldsymbol{x}$ neurons are represented by red and blue nodes, respectively; excitatory + and inhibitory − connections are represented by connections with solid and hollow nodes, respectively. Thus, Eqs. (11) and (12) are implemented with red and blue connections, respectively. It should also be noted that the weight dynamics are also realized locally. The weight change described by Eq. (13) corresponds to simple Hebbian plasticity[66] in the neural implementation of Fig. 2c; that is, the change in a weight is proportional to the product of activity of presynaptic and postsynaptic neurons. Thus, a predictive coding network, as an energy-based network, can be implemented with local circuits only due to the local nature of energy terms (as argued earlier in this section). Note that when the network is expressive enough such that learning can reduce the energy E to 0, the loss $\mathcal{L}$ must also become 0 as $\mathcal{L}$ is one of the terms in energy E, that is $\mathcal{L} = E^{L+1}$, and, in this case, the predictive coding network is guaranteed to minimize the loss, just like backpropagation[67].

The full algorithm of the predictive coding network is summarized in Algorithm 1. In all simulations in this paper (unless stated otherwise), the integration step of the neural dynamics (that is, relaxation) is set to $\gamma = 0.1$, and the relaxation is performed for 128 steps ($\mathcal{T}$ in Algorithm 1). During relaxation, if the overall energy is not decreased from the last step, the integration step is reduced by 50%; if the integration step is reduced two times (that is, reaching 0.025), relaxation is terminated early. By monitoring the number of relaxation steps performed, we notice that in most of the tasks we performed, relaxation is terminated early at around 60 iterations.

Algorithm 1. Learn with a predictive coding network[12,18]

Input: input pattern $\boldsymbol{s}^{\text{in}}$; target pattern $\boldsymbol{s}^{\text{target}}$; synaptic weights $\left\{\boldsymbol{w}^1, \boldsymbol{w}^2, \cdots, \boldsymbol{w}^L\right\}$
Output: updated synaptic weights $\left\{\boldsymbol{w}^1, \boldsymbol{w}^2, \cdots, \boldsymbol{w}^L\right\}$

$\boldsymbol{x}^1 = \boldsymbol{s}^{\text{in}}$; // Clamp input neurons to input pattern
$\boldsymbol{x}^{L+1} = \boldsymbol{s}^{\text{target}}$; // Clamp output neurons to target pattern
for $l = 2;\ l < L+1;\ l = l+1$ **do** // Initialize $\boldsymbol{x}$
  $\boldsymbol{x}^l = \boldsymbol{0}$;
end
for $t = 0;\ t < \mathcal{T};\ t = t+1$ **do** // Relaxation
  for $l = 1;\ l < L+1;\ l = l+1$ **do**
    $\boldsymbol{\varepsilon}^{l+1} = \boldsymbol{x}^{l+1} - \boldsymbol{w}^l f\left(\boldsymbol{x}^l\right)$; // according to Eq. (11)
  end
  for $l = 2;\ l < L+1;\ l = l+1$ **do**
    $\Delta \boldsymbol{x}^l = \gamma\left(-\boldsymbol{\varepsilon}^l + f'\left(\boldsymbol{x}^l\right) \circ \left(\left(\boldsymbol{w}^l\right)^T \boldsymbol{\varepsilon}^{l+1}\right)\right)$; // according to Eq. (12)
    $\boldsymbol{x}^l = \boldsymbol{x}^l + \Delta \boldsymbol{x}^l$;
  end
end
for $l = 1;\ l < L+1;\ l = l+1$ **do** // Update weights
  $\Delta \boldsymbol{w}^l = \alpha \boldsymbol{\varepsilon}^{l+1} \left(f\left(\boldsymbol{x}^l\right)\right)^T$;
  $\boldsymbol{w}^l = \boldsymbol{w}^l + \Delta \boldsymbol{w}^l$;
end

In the Supplementary Information, we also investigate other choices of network structures and energy functions, resulting in other ANNs and energy-based networks. Overall, the energy-based networks investigated include predictive coding networks[12,18], target predictive coding networks and GeneRec[62], and the ANNs investigated include backpropagation and Almeida–Pineda[63–65]. Details of all the models can be found in corresponding previous work and are also given in the Supplementary Notes, Section 2.1.

Interference and measuring interference (that is, target alignment)

In Fig. 3a, because it simulates the example in Fig. 1, the network has one input neuron, one hidden neuron and two output neurons; weights were all initialized to 1, the input pattern was [1], and the target pattern was [0, 1]. Learning rates of both learning rules were 0.2, and the weights were updated for 24 iterations. Fig. 3d repeated the same experiment as in Fig. 3a but with the learning rate searched from $(0.005, 0.01, 0.05, 0.1)$, which is wide enough to cover essentially all learning rates used to train deep neural networks in practice.

In Fig. 3e, there were 64 neurons in each layer (including input and output layers) for each network; weights were initialized via standard Xavier uniform initialization[68]. No activation function was used, that is, linear networks were investigated. Depths of networks (L) took values from $\{1, 2, \ldots, 24, 25\}$, as reported on the x axis. Input and target patterns were a pair of randomly generated patterns with a mean of 0 and standard deviation (s.d.) of 1. Learning rates of both learning rules were 0.001. Weights were updated for one iteration, and target alignment was measured. The whole experiment was repeated 27 times with each individual experiment reported as a point.

Simulations in Fig. 3f–h followed the experimental setup in Fig. 4a–h; these are described at the end of Biologically relevant tasks.

Biologically relevant tasks

In supervised learning simulations, fully connected networks in Fig. 4a–h were trained and tested on FashionMNIST[60], and convolutional neural networks[35] (Fig. 4i,j) were trained and tested on CIFAR-10 (ref. 36). With FashionMNIST, models were trained to perform classification of gray-scaled fashion item images into ten categories, such as trousers, pullovers and dresses. FashionMNIST was chosen because it is of moderate and appropriate difficulty for multilayer non-linear deep neural networks so that the comparisons with energy-based networks

are informative. Classification of the data in CIFAR-10 is more difficult, as it contains colored natural images belonging to categories such as cars, birds and cats and is thus only evaluated with convolutional neural networks. Both datasets consist of 60,000 training examples (that is, training set) and 10,000 test examples (that is, test set).

The experiments in Fig. 4a–h followed the configurations described below, except for the parameters investigated in specific panels (such as batch size, size of the dataset and size of the architecture), which were adjusted as stated in the descriptions of the specific experiments. The neural network was composed of four layers and 32 hidden neurons in each hidden layer. Note that the state-of-the-art MLP models of FashionMNIST are all quite large[69]. However, they are highly overparameterized and thus are not suitable to base our comparison on because the accuracy reaches more than 95% regardless of the learning rule due to the overparameterization. Thus, there was no space for demonstrating any meaningful comparison in these state-of-the-art overparameterized models. Overall, the size of the model on FashionMNIST demonstrated in this paper was a reasonable choice, with baseline models reaching reasonable performance (~0.12 test error for the standard machine learning setup) while maintaining enough room for demonstrating performance differences for different learning rules. The size of the input layer was 28 × 28 for FashionMNIST[60] gray scaled, and the size of the output layer was ten as the number of classes for both datasets. The weights were initialized from a normal distribution with a mean of 0 and s.d. of $\sqrt{\frac{2}{n^l+n^{l+1}}}$, where n^l and n^{l+1} are the numbers of neurons in the layer before and after the weight, respectively. This initialization is known as Xavier normal initialization[68]. The activation function $f()$ is sigmoid. We defined one iteration as updating the weights for one step based on a minibatch. Each iteration contained (1) a numerical integration procedure of relaxation of energy-based networks, which captures its continuous process; and (2) one update of weights at the end of the above procedure. The number of examples in a minibatch, called the batch size, was by default 32. One epoch comprised presenting the entire training set split over multiple minibatches. At the end of each epoch, the model was tested on the test set, and the classification error was recorded as the 'test error' of the epoch. The neural network was trained for 64 epochs, thus yielding 64 test errors. The mean of the test error over epochs, that is, during training progress, is an indicator of how fast the model learns, and the minimum of the test errors over epochs is an indicator of how well the model can learn, ignoring the possibility of overfitting due to training for too long. Learning rates were optimized independently for each configuration and each model. Each experiment was repeated ten times (unless stated otherwise), and the error bars represent the 68% confidence interval computed using bootstrap.

We now describe settings specific to individual experiments. In Fig. 4b, different batch sizes were tested (as shown on the x axis). In Fig. 4c, the batch size was set to 1. In continual learning of Fig. 4d, training alternated between two tasks. Task 1 involved classifying five randomly selected classes in a dataset, and task 2 involved classifying the remaining five classes. The whole network was shared by the two tasks; thus, different from the network used in other panels, the network only had five output neurons. This better corresponds to continual learning with multiple tasks in nature, because, for example, if humans learn to perform two different tasks, they typically use one brain and one pair of hands (that is, the whole network is shared), as they do not have two different pairs of hands (that is, humans share the output layers across tasks). Task 1 was trained for four iterations, task 2 was trained for four iterations, and the training continued until a total of 84 iterations was reached. After each iteration, error on the test set of each task was measured as 'test error'. In Fig. 4e, the mean of test error of both tasks during training of Fig. 4d at different learning rates is reported. In Fig. 4d–g investigating concept drifting[31,70,71], changes to class labels were made every 64 epochs, and the models were trained for 3,000 epochs in total. Thus, every 64 epochs, five of ten output neurons were selected, and the mapping from these five output neurons to the semantic meaning was pseudorandomly shuffled. In Fig. 4h, different numbers of data points per class (shown on the x axis) were included in the training set (subsets were randomly selected according to different seeds).

In Fig. 4i, we trained a convolutional network with prospective configuration and backpropagation, with the structure detailed in Fig. 4j. For each learning rule, we independently searched seven learning rates ranging from $\{0.0005, 0.00025, 0.0001, 0.000075, 0.00005, 0.000025, 0.00001\}$. Both learning rules were trained for 80 epochs, with a batch size of 200. Because training deep convolutional networks is more difficult and slower than training shallow fully connected networks, a few improvements were applied to both learning rules. Specifically, a weight decay of 0.01 and an Adam optimizer[72] were applied for both learning rules. To reduce running time, the weights were updated more frequently in predictive coding networks; that is, the weights were updated at all steps of inference instead of at the last step of inference. Inference was run for a fixed number of 16 iterations; thus, weights were updated 16 times for each batch of data. Thus, for fair comparison, backpropagation also updated weights 16 times on each batch of data. Training in each configuration (each learning rule and each learning rate) was repeated three times with different seeds.

To extend a predictive coding network to a convolutional neural network (or to any network with a layered structure[58,73]), we can define the forward function of a layer (that is, how the input of layer $l+1$ is computed from the neural activity of layer l) with weights $\boldsymbol{w}^l$ to be $\mathcal{F}_{\boldsymbol{w}^l}(\boldsymbol{x}^l)$. For example, for the MLPs described above, $\mathcal{F}_{\boldsymbol{w}^l}(\boldsymbol{x}^l) = \boldsymbol{w}^l f(\boldsymbol{x}^l)$. For a convolutional network, $\mathcal{F}_{\boldsymbol{w}^l}(\boldsymbol{x}^l)$ is a more complex function of $\boldsymbol{w}^l$ and $\boldsymbol{x}^l$, and also $\boldsymbol{w}^l$ and $\boldsymbol{x}^l$ are not simple matrix and vector anymore (to be defined later). Defining an ANN with $\mathcal{F}()$ would be (that is, Eq. (5) becomes) $\boldsymbol{x}^l = \mathcal{F}_{\boldsymbol{w}^{l-1}}(\boldsymbol{x}^{l-1})$. Defining an energy function of a predictive coding network with $\mathcal{F}()$ would be (that is, Eq. (6) becomes) $E^l = \frac{1}{2}\left[\boldsymbol{x}^l - \mathcal{F}_{\boldsymbol{w}^{l-1}}(\boldsymbol{x}^{l-1})\right]^2$. Thus, neural and weight dynamics would be (that is, Eqs. (12) and (13) become) $\Delta\boldsymbol{x}^l = -\gamma\boldsymbol{\varepsilon}^l + \frac{\partial\mathcal{F}_{\boldsymbol{w}^l}(\boldsymbol{x}^l)}{\partial\boldsymbol{x}^l}\boldsymbol{\varepsilon}^{l+1}$ and $\Delta\boldsymbol{w}^l = \alpha\boldsymbol{\varepsilon}^{l+1}\frac{\partial\mathcal{F}_{\boldsymbol{w}^l}(\boldsymbol{x}^l)}{\partial\boldsymbol{w}^l}$, respectively. As $\mathcal{F}_{\boldsymbol{w}^l}(\boldsymbol{x}^l)$ is defined, $\frac{\partial\mathcal{F}_{\boldsymbol{w}^l}(\boldsymbol{x}^l)}{\partial\boldsymbol{x}^l}$ and $\frac{\partial\mathcal{F}_{\boldsymbol{w}^l}(\boldsymbol{x}^l)}{\partial\boldsymbol{w}^l}$ are obtained via auto differentiation in PyTorch (https://pytorch.org/tutorials/beginner/basics/autogradqs_tutorial.html). Thus, training a convolutional predictive coding network is as simple as replacing lines 11 and 16 in Algorithm 1 with the above corresponding equations.

In the following, we define $\mathcal{F}_{\boldsymbol{w}^l}(\boldsymbol{x}^l)$ for convolutional networks. First, $\boldsymbol{x}^l \in \mathbb{R}^{c_l\times h_l\times w_l}$, where c_l, h_l and w_l are the number of features, height and width of the feature map, respectively. The numbers for each layer are presented in Fig. 4j in the format $c_l@h_l \times w_l$. For example, for the first layer (input layer), the shape was 3@32 × 32 as it is 32 × 32 colored images, that is, with three feature maps representing red, green and blue. We denote kernel size, stride and padding of this layer as k_l, s_l and p_l, respectively. The numbers for each layer are presented in Fig. 4j. Thus, $\boldsymbol{w}^l \in \mathbb{R}^{c_{l+1}\times c_l\times k_l\times k_l}$. Finally, $\boldsymbol{x}^{l+1}$ is obtained via

$$\boldsymbol{x}^{l+1}[c,x,y] = f\left(\boldsymbol{x}^l[:, xs_l - p_l : xs_l - p_l + k_l, ys_l - p_l : ys_l - p_l + k_l]\right) \cdot \boldsymbol{w}^l[c,:,:,:], \tag{14}$$

where $[a,b,\ldots]$ means indexing the tensor along each dimension, : means all indexes at that dimension, $a:b$ means slice of that dimension from index a to $b-1$, and $\cdot$ is dot product. In the above equation, if the slicing of $\boldsymbol{x}^l$ on the second and third dimensions, that is, $\boldsymbol{x}^l[:, xs_l - p_l : xs_l - p_l + k_l, ys_l - p_l : ys_l - p_l + k_l]$, is outside its defined range $\mathbb{R}^{c_l\times h_l\times w_l}$, the entries outside range are considered to be 0, known as padding mode of zeros.

In Fig. 3f, networks of 15 layers were trained and tested on the FashionMNIST[60] dataset. Learning rates in Fig. 3f were optimized

independently by a grid search over (5.0, 1.0, 0.5, 0.1, 0.05, 0.01, 0.005, 0.001, 0.0005, 0.0001, 0.00005, 0.00001, 0.000005) for each learning rule, as shown Fig. 3g; that is, each learning rule in Fig. 3f used the learning rate that gave a minimal point in the corresponding curve in Fig. 3g. The experiment in Fig. 3h investigated other network depths ($\{1, 2, 4, 6, 8, 10, 12, 14, 15\}$) in the same setup. Similar to Fig. 3f, the learning rate for each learning rule and each 'number of layers' was the optimal value (in terms of mean of test error as the y axis of the figure) independently searched from (5.0, 1.0, 0.5, 0.1, 0.05, 0.01, 0.005, 0.001, 0.0005, 0.0001, 0.00005, 0.00001, 0.000005). Hidden layers were always of size 64 in the above experiments. In the above experiment, only a part of the training set was used (60 data points per class) so that the test error was evaluated more frequently to reflect the difference on efficiency of the investigated learning rules. The activation function $f()$ used is LeakyReLU instead of the standard sigmoid because sigmoid results in difficulty in training deep neural networks. Other unmentioned details followed the defaults, as described above.

In the reinforcement learning experiments (Fig. 4k), we evaluated performance on three classic reinforcement learning problems: Acrobot[74,75], MountainCar[76] and CartPole[77]. We interacted with these environments via a unified interface by OpenAI Gym[78]. The observations s_t of these environments are vectors describing the status of the system, such as velocities and positions of different moving parts (for details, refer to the original articles or documentation from OpenAI Gym). Each entry of the observation s_t is normalized to mean 0 and s.d. 1 via Welford's online algorithm[79,80]. The action space of these environments is discrete. Thus, we can have a network taking in observation s_t and predicting the value (Q) of each action a_t with different output neurons. Such a network is known as an action-value network, in short, a Q network. In our experiment, the Q network contained two hidden layers, each of which contained 64 neurons, initialized the same way as the network used for supervised learning, described before. One can acquire the value of an action a_t at a given observation s_t by feeding s_t into the Q network and reading out the prediction on the output neuron corresponding to the action a_t; such a value is denoted $Q(s_t, a_t)$. The training of Q is a simple regression problem to target $\hat{R}_t$, obtained via Q learning with experience replay (summarized in Algorithm 2). Considering s_t to be $\boldsymbol{s}^{\text{in}}$ and $\hat{R}_t$ to be $\boldsymbol{s}^{\text{target}}$, the Q network can be trained with prospective configuration or backpropagation. Note that $\hat{R}_t$ is the target of the selected action a_t (that is, the target of one of the output neurons corresponds to the selected action a_t); thus, $\hat{R}_t$ is, in practice, considered to be $\boldsymbol{s}^{\text{target}}[a_t]$. For prospective configuration, it means that the rest of the output neurons except the one corresponding to a_t are freed; for backpropagation, it means that the error on these neurons is masked out.

A predictive coding network with slightly different settings from the defaults was used for prospective configuration. The integration step was fixed to be half of the default ($\gamma = 0.05$), and relaxation was performed for a fixed and smaller number of steps ($\mathcal{T} = 32$). This change was introduced because Q learning is more unstable (smaller integration step) and more expensive (smaller number of relaxation steps) than supervised learning tasks. To produce a smoother curve of 'sum of rewards per episode' in Fig. 4k from *SumRewardPerEpisode* in Algorithm 2, the *SumRewardPerEpisode* curve was averaged along *TrainingEpisode* with a sliding window with a length of 200. Each experiment was repeated with three random seeds, and the shadows represent 68% confidence interval across them. Learning rates were searched independently for each environment and each model from the range $\{0.05, 0.01, 0.005, 0.001, 0.0005, 0.0001\}$. The results reported in Fig. 4k are for the learning rates yielding the highest mean of 'sum of rewards per episode' over training episodes.

Algorithm 2. Q learning with experience replay

Input: Action-value network Q.
Result: Trained action-value network Q.
Initialize experience replay $\mathcal{R}$ of capacity 50000;
for $TrainingEpisode = 0$; $TrainingEpisode < 10000$; $TrainingEpisode = TrainingEpisode + 1$ **do**
  $\rho = \max(0.01, 0.08 - 0.01 * (TrainingEpisode/200))$; // Anneal probability of exploring
  Get initial observation s_t and set episode termination signal $d_t = False$;
  Initialize $SumRewardPerEpisode = 0$;
  while ! d_t **do** // Collect experience
    With probability ρ sample a random action a_t, otherwise select $a_t = \arg\max_a Q(s_t, a)$;
    Execute a_t, observe reward r_t, new observation r_{t+1} and d_t;
    Accumulate $SumRewardPerEpisode += r_t$;
    Store transition $(s_t, a_t, r_t, s_{t+1}, d_t)$ in $\mathcal{R}$;
    Set $s_t = s_{t+1}$;
  end
  if $length(\mathcal{R}) > 2000$ **then** // Replay and train
    for $epoch = 0$; $epoch < 10$; $epoch = epoch + 1$ **do**
      Sample random minibatch (size=60) of $(s_t, a_t, r_t, s_{t+1}, d_t)$ from $\mathcal{R}$;
      $\hat{R}_t = \begin{cases} r_t, & \text{if } d_t == True \\ r_t + 0.98 \max_a Q(s_{t+1}, a), & \text{otherwise} \end{cases}$;
      Set $\boldsymbol{s}^{\text{in}} = s_t$;
      Set $\boldsymbol{s}^{\text{target}}[a_t] = \hat{R}_t$;
      Train Q with $\boldsymbol{s}^{\text{in}}$ and $\boldsymbol{s}^{\text{target}}[a_t]$ with prospective configuration or backpropagation;
    end
  end
  Report $SumRewardPerEpisode$;
end

Simulation of motor learning

As shown in Fig. 5, we trained a network that included two input neurons, two hidden neurons and two output neurons. The two input neurons were one-to-one connected to the two hidden neurons, and the two hidden neurons were fully connected to the two output neurons. The two input neurons were considered to encode presenting the blue and red background, respectively. The two output neurons were considered to encode the prediction of the perturbations toward positive and negative directions, respectively. Presenting and not presenting a background color were encoded 1 and 0, respectively; presenting and not presenting perturbations of a particular direction were encoded 1 and 0, respectively. The weights were initialized from a normal distribution with mean 0 and an s.d. fitted to the behavioral data (see below), simulating that the participants had not built any associations before the experiments. Learning rates were independent for the two layers, as we expected the connections from perception to belief and from belief to predictions to have different degrees of plasticity. The two learning rates were also fitted to the data (see below).

The number of participants and training and testing trials follow exactly as described for the human experiment[38]. In particular, for each of the 24 simulated participants, the weights were initialized with a different seed of the random number generator. They each experienced two stages: training and testing. Note that the pretraining stage performed in the human experiment was not simulated here as its goal was to make human participants familiar with the setup and devices.

In the training stage, the model experienced 24 blocks of trials. In each block, the model was presented with the following sequence of trials, matching the original experiment[38]:

- The model was trained with two trials without perturbation, B_0 and R_0, with the order counterbalanced across consecutive blocks. Note that, in the human experiment, there were two trial types without perturbations (channel and washout trials), but they were simulated in the same way here as B_0 or R_0 trials because they both did not include any perturbations.
- The model was trained with 32 trials with perturbations, where there were equal numbers of B+ and R− within each of the 8 trials in a pseudorandom order.
- The model experienced two trials, B_0 and R_0, with the order counterbalanced across consecutive blocks.
- The model experienced $n \leftarrow \{14, 16, 18\}$ washout trials (equal numbers of B_0 and R_0 trials in a pseudorandom order), where $n \leftarrow \{a, b, c\}$ denotes sampling without replacement from a set of values a, b and c and replenishing the set whenever it becomes empty.
- The model experienced one triplet, where the exposure trial was either B+ or R−, counterbalanced across consecutive blocks. Here, a triplet consisted of three sequential trials: B_0, the specified exposure trial and B_0 again.
- The model experienced additional $n \leftarrow \{6, 8, 10\}$ washout trials (equal numbers of B_0 and R_0 trials in a pseudorandom order).
- The model experienced one triplet again, where the exposure trial was either B+ or R−, whichever was not used on the previous triplet.

In the testing stage, the model then experienced eight repetitions of four blocks of trials. In each block, one of the combinations of B+, R+, B− and R− was tested. The order of the four blocks was shuffled in each of the eight repetitions. In each block, the model first experienced $n \leftarrow \{2, 4, 6\}$ washout trials (equal numbers of B_0 and R_0 trials in a pseudorandom order). The model then experienced a triplet of trials, where the exposure trial was the combination (B+, R+, B− or R−) tested in a given block to assess single-trial learning of this combination. The change in adaption in the model was computed as the absolute value of the difference in the predictions of perturbations on the two B_0 trials in the above triplet, where the prediction of perturbation was computed as the difference between the activities of the two output neurons. The predictions were averaged over participants and the above repetitions.

The parameters of each learning rule were chosen such that the model best reproduced the change in adaptation shown in Fig 5f. In particular, we minimized the sum over set C of the four exposure trial types of the squared difference between average change in adaptation in experiment (d_c) and model (x_c):

$$\sum_{c \in C} (a x_c - d_c)^2. \tag{15}$$

The model predictions were additionally scaled by a coefficient a fitted to the data because the behavioral data and model outputs had different scales. An exhaustive search was performed over model parameters. The s.d. of initial weights could take values from $\{0.01, 0.05, 0.1\}$, and two learning rates for two layers could take values from $\{0.00005, 0.0001, 0.0005, 0.01, 0.05\}$. For each learning rule and each combination of the above model parameters, the coefficient a was then resolved analytically (restricted to be positive) to minimize the sum of the squared errors of Eq. (15).

Simulation of human reinforcement learning

As shown in Fig. 6b, we trained a network that included one input neuron, one hidden neuron and two output neurons. The input neuron was considered to encode being in the task, so it was set to 1 throughout the simulation. The two output neurons encoded the prediction of the value of the two choices. Reward and punishment were encoded as 1 and −1, respectively, because the participants were either winning or losing money. The model selected actions stochastically based on the predicted value of the two choices (encoded in the activity of two output neurons) according to the softmax rule (with a temperature of 1). The weights were initialized from a normal distribution of mean 0 and an s.d. fitted to experimental data (see below), simulating that the human participants had not built any associations before the experiments. The number of simulated participants (number of repetitions with different seeds) was set to 16, as in the human experiment[38]. The number of trials was not mentioned in the original paper, so we simulated for 128 trials for both learning rules.

To compare the ability of the two learning rules to account for the pattern of signal from the mPFC, for each of the rules, we optimized the parameters describing how the model is set up and learns (the s.d. of initial weights and the learning rate). Namely, we searched for the values of these parameters for which the model produces the most similar pattern of its output activity to that in the experiment. In particular, we minimized the sum over set C of four trial types in Fig. 6c of the squared difference between model predictions x_c and data d_c on mean mPFC signal:

$$\sum_{c \in C} (a x_c + b - d_c)^2. \tag{16}$$

The model predictions were additionally scaled by a coefficient a and offset by a bias b because the fMRI signal had different units and baseline than the model. To compute the model prediction for a given trial type, the activity of the output neuron corresponding to the chosen option was averaged across all trials of this type in the entire simulation. The scaled average activity from the model is plotted in Fig. 6c, where the error bars show the 68% confidence interval of the scaled activity. To fit the model to experimental data, the values of model parameters and the coefficient were found as described in the previous section. In particular, we used exhaustive grid search on the parameters. The models were simulated for all possible combinations of s.d. of initial weights and the learning rate from the following set: $\{0.01, 0.05, 0.1\}$. For each learning rule and each combination of the above model parameters, the coefficient a (restricted to be positive) and the bias b were then resolved analytically to minimize the sum of the squared error of Eq. (16).

Statistics and reproducibility

The work in this paper involved computer simulations, but due to random initialization of weight parameters, the simulations were repeated multiple times. No statistical method was used to predetermine the number of repetitions, but for simulations corresponding to behavioral or neurophysiological experiments, the number of repetitions was matched to the number of participants in the given experiment. No data were excluded from the analyses. Because the order of execution has no effect on the results of the numeric experiments, they were not randomized. The investigators were not blinded to outcome assessment.

To visualize the variability of simulation results, we either presented individual data points or error bars showing confidence intervals or box plots. Confidence intervals were computed using bootstrap throughout the paper, and detailed descriptions of the implementation can be found at https://seaborn.pydata.org/tutorial/error_bars.html#confidence-interval-error-bars. The details of the methods used to produce the box plots are available at https://seaborn.pydata.org/generated/seaborn.boxplot.html.

Reporting summary

Further information on research design is available in the Nature Portfolio Reporting Summary linked to this article.

Data availability

Learning tasks analyzed in Fig. 4a–j were built using the publicly available FashionMNIST[60] and CIFAR-10 (ref. 36) datasets. These datasets are incorporated in most machine learning libraries, and their original releases are available at https://github.com/zalandoresearch/fashion-mnist and https://www.cs.toronto.edu/~kriz/cifar.html, respectively. Reinforcement learning tasks analyzed in Fig. 4i were built using the publicly available simulators by OpenAI Gym[78]. Source data are provided with this paper.

Code availability

Complete code and full documentation reproducing all simulation results written in Python are publicly available at https://github.com/Yuhang-Song/Prospective-Configuration released under GNU General Public License v3.0 without any additional restrictions (for license details, see https://opensource.org/licenses/GPL-3.0 by the open source initiative).

References

61. Goodfellow, I., Bengio, Y. & Courville, A. *Deep Learning* (MIT Press Cambridge, 2016).
62. O'Reilly, R. C. Biologically plausible error-driven learning using local activation differences: the generalized recirculation algorithm. *Neural Comput.* **8**, 895–938 (1996).
63. Almeida, L. B. A learning rule for asynchronous perceptrons with feedback in a combinatorial environment. In *Artificial Neural Networks: Concept Learning* (ed. Diederich, J.) 102–111 (IEEE Computer Society Press, 1990).
64. Pineda, F. Generalization of back propagation to recurrent and higher order neural networks. In *Advances in Neural Information Processing Systems (NeurIPS)* (ed. Anderson, D.) 602–611 (Curran Associates, 1987).
65. Pineda, F. J. Dynamics and architecture for neural computation. *J. Complex.* **4**, 216–245 (1988).
66. Hebb, D. O. *The Organisation of Behaviour: A Neuropsychological Theory* (Science Editions New York, 1949).
67. Senn, W. et al. A neuronal least-action principle for real-time learning in cortical circuits. Preprint at *bioRxiv* https://doi.org/10.1101/2023.03.25.534198 (2023).
68. Glorot, X. & Bengio, Y. Understanding the difficulty of training deep feedforward neural networks. In *Proc. 13th International Conference on Artificial Intelligence and Statistics* (eds Teh, Y. W. & Titterington, M.) 249–256 (PMLR, 2010).
69. Tolstikhin, I. O. et al. Mlp-mixer: an all-mlp architecture for vision. In *Advances in Neural Information Processing Systems (NeurIPS)* (eds Ranzato, M. et al.) 24261–24272 (Curran Associates, 2021).
70. Žliobaitė, I. Learning under concept drift: an overview. Preprint at https://doi.org/10.48550/arXiv.1010.4784 (2010).
71. Tsymbal, A. *The Problem of Concept Drift: Definitions and Related Work*. Technical report, Computer Science Department, Trinity College Dublin (2004).
72. Kingma, D. P. & Ba, J. Adam: a method for stochastic optimization. https://doi.org/10.48550/arXiv.1412.6980 (2014).
73. Salvatori, T., Song, Y., Lukasiewicz, T., Bogacz, R. & Xu, Z. Reverse differentiation via predictive coding. In *Proc. 36th AAAI Conference on Artificial Intelligence* (Salvatori, T., Song, Y., Xu, Z., Lukasiewicz, T. & Bogacz, R.) 8150–8158 (Curran Associates, 2022).
74. Sutton, R. S. Generalization in reinforcement learning: successful examples using sparse coarse coding. In *Advances in Neural Information Processing Systems (NeurIPS)* (eds Touretzky, D. et al.) 1038–1044 (NIPS, 1995).
75. Geramifard, A., Dann, C., Klein, R. H., Dabney, W. & How, J. P. RLPy: a value-function-based reinforcement learning framework for education and research. *J. Mach. Learn. Res.* **16**, 1573–1578 (2015).
76. Moore, A. Efficient memory-based learning for robot control. Technical report, Carnegie Mellon Univ. (1990).
77. Barto, A. G., Sutton, R. S. & Anderson, C. W. Neuronlike adaptive elements that can solve difficult learning control problems. In *IEEE Transactions on Systems, Man, and Cybernetics*, 834–846 (1983).
78. Brockman, G. et al. OpenAI Gym. Preprint at https://doi.org/10.48550/arXiv.1606.01540 (2016).
79. Welford, B. P. Note on a method for calculating corrected sums of squares and products. *Technometrics* **4**, 419–420 (1962).
80. Knuth, D. E. *Art of Computer Programming*, Vol. 2 (Addison-Wesley Professional, 2014).

Acknowledgements

We thank T. Behrens for comments on the manuscript and A. Saxe and M. Witbrock for discussions. The presented research was supported by the following grants: China Scholarship Council under the State Scholarship Fund (Y.S.), JPMorgan AI Research Awards (Y.S.), Biotechnology and Biological Sciences Research Council grant BB/S006338/1 (R.B.), Medical Research Council grant MC_UU_00003/1 (R.B.), the Alan Turing Institute under the EPSRC grant EP/N510129/1 (T.L.), the AXA Research Fund (T.L.), National Natural Science Foundation of China grants 61906063 and 62276089 (Z.X.), Natural Science Foundation of Hebei Province, China, grant F2021202064 (Z.X.), Natural Science Foundation of Tianjin City, China, grant 19JCQNJC00400 (Z.X.), the '100 Talents Plan' of Hebei Province, China, grant E2019050017 (Z.X.) and the Yuanguang Scholar Fund of Hebei University of Technology, China (Z.X.). The funders had no role in study design, data collection and analysis, decision to publish or preparation of the manuscript. This research was also funded, in part, by JPMorgan Chase & Co. Any views or opinions expressed herein are solely those of the authors listed and may differ from the views and opinions expressed by JPMorgan Chase & Co. or its affiliates. This material is not a product of the Research Department of J.P. Morgan Securities, LLC. This material should not be construed as an individual recommendation for any particular client and is not intended as a recommendation of particular securities, financial instruments or strategies for a particular client. This material does not constitute a solicitation or offer in any jurisdiction.

Author contributions

Y.S. and R.B. conceived the project. Y.S., R.B., B.M. and T.S. contributed ideas for experiments and analysis. Y.S. and B.M. performed simulations. Y.S., B.M. and R.B. performed mathematical analyses. Y.S., T.L. and R.B. managed the project. T.L and Z.X. advised on the project. Y.S., R.B. and B.M. wrote the paper. T.S., T.L. and Z.X. provided revisions to the paper.

Competing interests

Y.S., B.M. and R.B. are shareholders in Fractile, Ltd., which designs artificial intelligence accelerator hardware. The remaining authors declare no competing interests.

Additional information

Supplementary information The online version contains supplementary material available at https://doi.org/10.1038/s41593-023-01514-1.

Correspondence and requests for materials should be addressed to Yuhang Song, Thomas Lukasiewicz, Zhenghua Xu or Rafal Bogacz.

Peer review information *Nature Neuroscience* thanks Karl Friston, Walter Senn, Friedemann Zenke and Joel Zylberberg for their contribution to the peer review of this work.

nature portfolio

Corresponding author(s): Rafal Bogacz, Yuhang Song, Thomas Lukasiewicz, Zhenghua Xu

Last updated by author(s): 26/09/23

Reporting Summary

Nature Portfolio wishes to improve the reproducibility of the work that we publish. This form provides structure for consistency and transparency in reporting. For further information on Nature Portfolio policies, see our Editorial Policies and the Editorial Policy Checklist.

Statistics

For all statistical analyses, confirm that the following items are present in the figure legend, table legend, main text, or Methods section.

n/a	Confirmed	
☐	☒	The exact sample size (*n*) for each experimental group/condition, given as a discrete number and unit of measurement
☐	☒	A statement on whether measurements were taken from distinct samples or whether the same sample was measured repeatedly
☒	☐	The statistical test(s) used AND whether they are one- or two-sided *Only common tests should be described solely by name; describe more complex techniques in the Methods section.*
☒	☐	A description of all covariates tested
☒	☐	A description of any assumptions or corrections, such as tests of normality and adjustment for multiple comparisons
☐	☒	A full description of the statistical parameters including central tendency (e.g. means) or other basic estimates (e.g. regression coefficient) AND variation (e.g. standard deviation) or associated estimates of uncertainty (e.g. confidence intervals)
☒	☐	For null hypothesis testing, the test statistic (e.g. *F*, *t*, *r*) with confidence intervals, effect sizes, degrees of freedom and *P* value noted *Give P values as exact values whenever suitable.*
☒	☐	For Bayesian analysis, information on the choice of priors and Markov chain Monte Carlo settings
☒	☐	For hierarchical and complex designs, identification of the appropriate level for tests and full reporting of outcomes
☒	☐	Estimates of effect sizes (e.g. Cohen's *d*, Pearson's *r*), indicating how they were calculated

Our web collection on statistics for biologists contains articles on many of the points above.

Software and code

Policy information about availability of computer code

Data collection	no new data were collected for this manuscript.
Data analysis	Complete code and full documentation reproducing all simulation results written in Python is publicly available at https://github.com/YuhangSong/Prospective-Configuration. It is released under GNU General Public License v3.0 without any additional restrictions (for license's details see https://opensource.org/licenses/GPL-3.0 by the open source initiative).

For manuscripts utilizing custom algorithms or software that are central to the research but not yet described in published literature, software must be made available to editors and reviewers. We strongly encourage code deposition in a community repository (e.g. GitHub). See the Nature Portfolio guidelines for submitting code & software for further information.

Data

Policy information about availability of data

All manuscripts must include a data availability statement. This statement should provide the following information, where applicable:

- Accession codes, unique identifiers, or web links for publicly available datasets
- A description of any restrictions on data availability
- For clinical datasets or third party data, please ensure that the statement adheres to our policy

Learning tasks analysed in Fig. 4a-j were built using the publicly available FashionMNIST and CIFAR-10 datasets. They are incorporated in most machine learning

libraries, and their original releases are available at https://github.com/zalandoresearch/fashion-mnist and https://www.cs.toronto.edu/~kriz/cifar.html, respectively. Reinforcement learning tasks analysed in Fig.4k were built using the publicly available simulators by OpenAI Gym https://www.gymlibrary.ml.

Human research participants

Policy information about studies involving human research participants and Sex and Gender in Research.

Reporting on sex and gender	*Use the terms sex (biological attribute) and gender (shaped by social and cultural circumstances) carefully in order to avoid confusing both terms. Indicate if findings apply to only one sex or gender; describe whether sex and gender were considered in study design whether sex and/or gender was determined based on self-reporting or assigned and methods used. Provide in the source data disaggregated sex and gender data where this information has been collected, and consent has been obtained for sharing of individual-level data; provide overall numbers in this Reporting Summary. Please state if this information has not been collected. Report sex- and gender-based analyses where performed, justify reasons for lack of sex- and gender-based analysis.*
Population characteristics	*Describe the covariate-relevant population characteristics of the human research participants (e.g. age, genotypic information, past and current diagnosis and treatment categories). If you filled out the behavioural & social sciences study design questions and have nothing to add here, write "See above."*
Recruitment	*Describe how participants were recruited. Outline any potential self-selection bias or other biases that may be present and how these are likely to impact results.*
Ethics oversight	*Identify the organization(s) that approved the study protocol.*

Note that full information on the approval of the study protocol must also be provided in the manuscript.

Field-specific reporting

Please select the one below that is the best fit for your research. If you are not sure, read the appropriate sections before making your selection.

☒ Life sciences ☐ Behavioural & social sciences ☐ Ecological, evolutionary & environmental sciences

For a reference copy of the document with all sections, see nature.com/documents/nr-reporting-summary-flat.pdf

Life sciences study design

All studies must disclose on these points even when the disclosure is negative.

Sample size	This study did not involve any data collections, but only computer simulations. Since the computer simulations involved random initialization of the models, they were repeated multiple times, and the exact number of repetition for each simulation is given in the manuscript. No statistical method was used to predetermine the number of repetitions, but for simulations corresponding to behavioural or neurophysiological experiments, the number of repetitions was matched to the number of subjects in the given experiment.
Data exclusions	No data were excluded.
Replication	All results of simulations can be replicated by running the code we made available.
Randomization	Since the order of execution has no effect on result of numeric experiments, they were not randomised.
Blinding	No blinding was performed, because the analysis and visualization of experimental data were performed automatically by computer code.

Reporting for specific materials, systems and methods

We require information from authors about some types of materials, experimental systems and methods used in many studies. Here, indicate whether each material, system or method listed is relevant to your study. If you are not sure if a list item applies to your research, read the appropriate section before selecting a response.

Materials & experimental systems

n/a	Involved in the study
☒	☐ Antibodies
☒	☐ Eukaryotic cell lines
☒	☐ Palaeontology and archaeology
☒	☐ Animals and other organisms
☒	☐ Clinical data
☒	☐ Dual use research of concern

Methods

n/a	Involved in the study
☒	☐ ChIP-seq
☒	☐ Flow cytometry
☒	☐ MRI-based neuroimaging

nature neuroscience

Article

https://doi.org/10.1038/s41593-023-01514-1

Inferring neural activity before plasticity as a foundation for learning beyond backpropagation

In the format provided by the authors and unedited

Inferring neural activity before plasticity as a foundation for learning beyond backpropagation

1 Supplementary Information

This document contains Supplementary Figures referred in the paper, followed by Supplementary Notes with additional description and analysis of the simulated models.

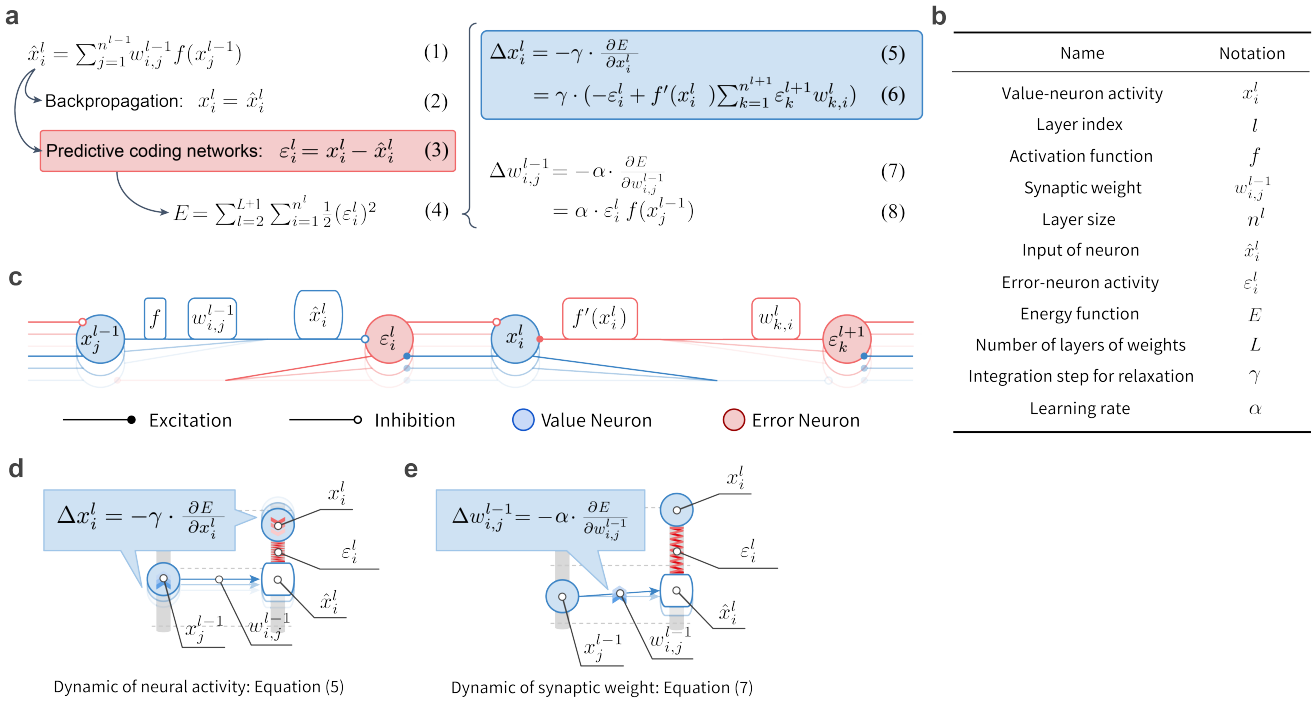

Name	Notation
Value-neuron activity	x_i^l
Layer index	l
Activation function	f
Synaptic weight	$w_{i,j}^{l-1}$
Layer size	n^l
Input of neuron	$\hat{x}_i^l$
Error-neuron activity	ε_i^l
Energy function	E
Number of layers of weights	L
Integration step for relaxation	γ
Learning rate	α

Supplementary Fig. 1

Predictive coding networks, neural implementation and corresponding energy machine. The figure shows a list of the equations describing the equilibrium-seeking dynamics and plasticity of predictive coding networks (panels a-b), how these equations map to a neural implementation, and how they map to the machine analog introduced in Fig. 2.

► **a** | List of equations describing predictive coding networks. Eq. (1) in this figure describes the input to a given layer $\hat{x}_i^l$ from the neurons in the previous layer x_j^{l-1}. In artificial neural networks trained with backpropagation, neural activities of a given layer x_i^l are set as the input to this layer $\hat{x}_i^l$ (Eq. (2)). In contrast, in predictive coding networks, neural activities of this layer x_i^l are **not** set as the input to this layer $\hat{x}_i^l$, instead an error ε_i^l is defined between them (Eq. (3)). Additionally, predictive coding networks define the energy E of the network to be the sum of all the squared errors $\frac{1}{2}\left(\varepsilon_i^l\right)^2$ (Eq. (4)). The dynamic of neural activity Δx_i^l in predictive coding networks is set to change the neural activity in proportion to the negative gradient of the energy with respect to the neural activity, so as to reduce the energy (Eq. (5)), which can be further derived as Eq. (6). The dynamic of synaptic weights $\Delta w_{i,j}^{l-1}$ of predictive coding networks is set to be in proportion to the negative gradient of the energy with respect to the weight, so as to reduce the energy (Eq. (7)), which can be further derived as Eq. (8).

► **b** | A list of symbols shared by all panels in the figure for easy reference.

► **c** | Mapping of equations describing predictive coding networks in panel a to a neural implementation. The neural implementation includes value neurons (blue) performing computations in Eq. (6), and separate error neurons encoding prediction errors (red) performing computations in Eq. (3), where positive sign is encoded by excitatory connections while negative sign is encoded by the inhibitory connections. It should be noticed that the weight dynamics $\Delta w_{i,j}^{l-1}$ is also realized locally: weight change described by Eq. (8). corresponds to simple Hebbian plasticity[1] in the architecture shown in panel a, i.e., the change in a weight is proportional to the product of activity of pre-synaptic and post-synaptic neurons. Different suggestions have been made on how this architecture could be realized in cortical circuits. An influential study[2] has suggested that error and value neurons correspond to separate neurons, so in such architecture the plasticity rule is precisely Hebbian, as explained above. Some other models[3] implementing predictive coding networks[4] include an error compartment (in apical dendrite) and a value compartment (in soma) within a single neuron. In such architecture the plasticity is still local as it depends on the product of activity in one neurons and potential of the apical dendrite in the other neuron.

► **d-e** | Mapping of equations describing predictive coding networks in panel a to the machine analog introduced in Fig. 2. The exact same set of equations describing predictive coding networks also describe a physical machine connected with rods, nodes and springs. ► **d** | The dynamic of neural activity Δx_i^l of predictive coding networks (Eq. (5)) describes relaxing the physical machine by moving the nodes. ► **e** | The dynamic of synaptic weight $\Delta w_{i,j}^{l-1}$ of predictive coding networks (Eq. (7)) describes relaxing the physical machine by tuning the rods.

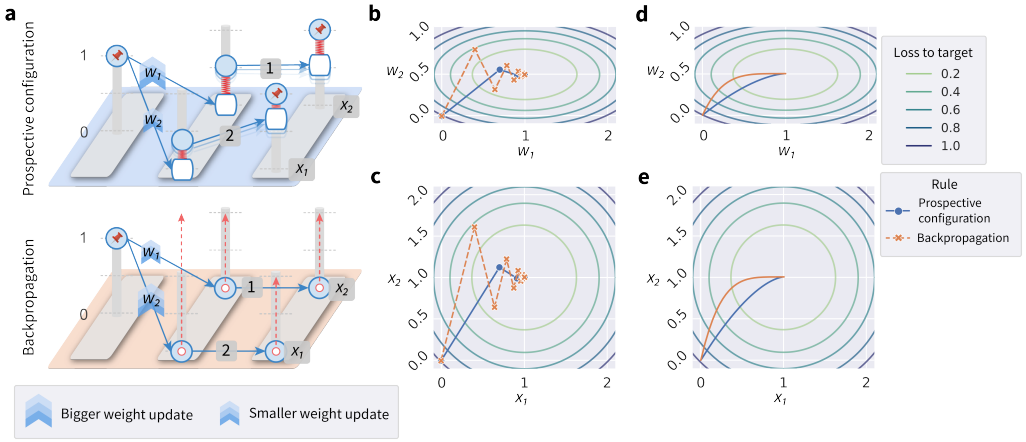

Supplementary Fig. 2

Differences in learning between prospective configuration and backpropagation. This figure shows an example of a simple network revealing striking differences in how errors are propagated and weights modified by the two algorithms. For this network it is possible to explicitly visualize how learning changes weights and outputs, and explicitly show that although backpropagation follows the gradient of loss in the space of weights, it does not in the space of outputs.

► **a** | Setup of the example. In this example, we consider a network consisting of 1 input neuron, 2 hidden neurons and 2 output neurons, with the structure shown with the energy machine. The input is always 1 and the target of both output neurons are both 1. The weights in the first layer are initialized to 0, while in the second layer to 1 (top) and 2 (bottom). We visualize with the energy machine how prospective configuration and backpropagation learn differently in this example. Prospective configuration assigns larger error to the top hidden neurons than the bottom, and hence would increase w_1 more than w_2. By contrast, backpropagation does the opposite: since the backpropagated errors are scaled by the weights to output layer, the error for the bottom hidden neuron is higher than for the top. Importantly, in this learning problem, weight w_2 does not need to be modified as much as w_1, because any changes in w_2 will be amplified by the high weight to the output neuron. Prospective configuration indeed modifies w_2 less than w_1, while backpropagation does the opposite. This suggests that backpropagation does not modify the weights optimally to move output toward the target, and we will illustrate it in the following panels.

► **b** | Landscape of the weights (w_1 and w_2). We consider a setup in which the network only learns the two weights in the first layer: w_1 and w_2, while the weights in the second layer are fixed all the time during the training. This is so that the weight space is small (only two dimensional, so that we can visualize the landscape of weights); and we choose to learn the two weights in the first layer instead the second (last) layer so that the problem is not trivial. All the combinations of weights on the same contour line gives the same loss to the target (in short, loss), where we can see the combination of $w_1 = 1$ and $w_2 = 0.5$ gives loss of 0. Assuming the weights (w_1, w_2) start from $(0, 0)$, backpropagation (orange) takes steps following the direction orthogonal to the contour lines, i.e. the direction of local gradient descent. It is well-known that backpropagation cannot have more global vision of the minimal point of the landscape: thus, often forms the trajectory of learning as the orange curve, "bouncing" towards the global minimum point. Prospective configuration (blue), on the contrary, although does not follow gradient in the weight space (blue line is not orthogonal to the contour lines), it moves more directly to the global minimum of the landscape. This is exactly due to the mechanism of prospective configuration giving the learning rule a more global view of the system: as mentioned above, prospective configuration infers that since

the bottom weight of second layer is larger (= 2) than the top one (= 1), it only needs small error being assigned to the bottom neuron of the hidden layer so as to correct the error on the bottom output.

▶ **c** | Landscape of the outputs (x_1 and x_2). The panel shows changes in output neurons' activity, x_1 and x_2, resulting from the weight updates in panel b. As in panel b, the contour lines indicate the loss. Comparing panels b and c reveals that changes of backpropagation (orange) are orthogonal to the loss contour lines in weight space, but not in output neuron space; while changes of prospective configuration (blue) are not orthogonal to loss contour lines in weight space, but are closer to being orthogonal in output neuron space. Overall, the comparison reveals fundamental difference between backpropagation and prospective configuration: backpropagation does local gradient decent in weight space (local means it only sees the infinitely small area around it current state); while prospective configuration infers the configuration of neuron activities that reduces the loss in the output space, thus, the trajectory in the weight space is fundamentally different from that for backpropagation. This fundamental difference leads to advantage of prospective configuration over backpropagation: it moves more directly towards the global minimum in the weight space and output space. Learning rate in this panel is the same as the learning rate used in the corresponding learning rule in panel b.

▶ **d-e** | The same experiments as b and c but with a small learning rate $\alpha = 0.05$ for both learning rules. As can be seen in the two panels, the notable difference between the two learning rules persists despite the learning rate being sufficiently small (the trajectory being sufficiently smooth).

Implementation details. In panels b and c, learning rate for backpropagation in this figure is set to $\alpha = 0.4$, while that for prospective configuration is solved so that it produces the same magnitude of weight change ($\sqrt{\Delta w_1^2 + \Delta w_2^2}$) during the first iteration as backpropagation. Weights are updated for 15 iterations in panels b and c, and for 150 iterations in panels d and e. Details of the learning rules are described in the Methods section and also in Supplementary Notes, Section 2.1.

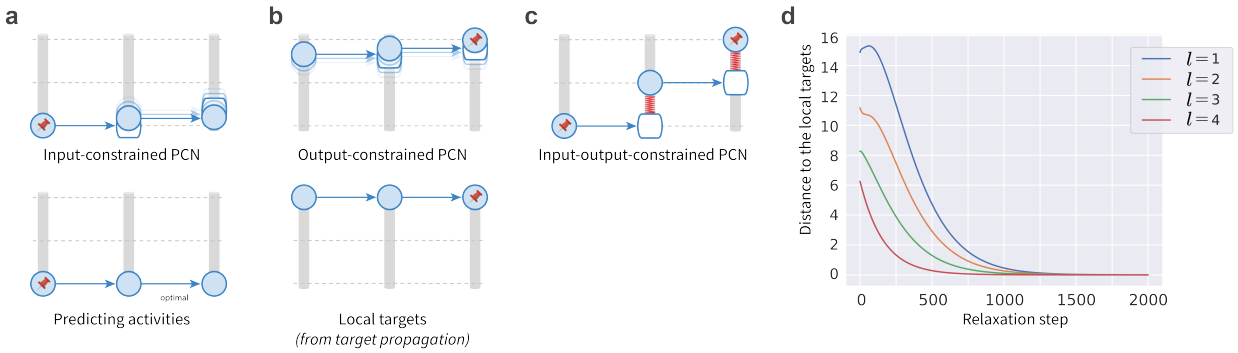

Supplementary Fig. 3

Relationship of prospective configuration to target propagation. Prospective configuration is related to another influential algorithm of credit assignment — target propagation[5]. Since target propagation has target alignment equal to 1[6], this relationship provides an explanation for the high target alignment of prospective configuration. Target propagation is an algorithm, which explicitly computes the neural activity in hidden layers required to produce the desired target pattern. We call these values local targets. We demonstrate that one of energy-based networks, predictive coding networks[7,8] (PCNs) tends to move the activity during relaxation towards these local targets. The relationship of PCNs to target propagation can be visualized with the proposed energy machine in Fig. 2, hence panels a–c illustrate how the neural activity in a PCN depends on whether inputs and outputs are constrained, and these properties are formally proved in Supplementary Notes, Section 2.2.

▶ **a** | With only input neurons constrained (and outputs unconstrained) PCNs can generate prediction about the output, and hence we refer to this pattern of neural activity as the predicting activity.

▶ **b** | With only output neurons constrained (and inputs unconstrained), the neural activity of PCNs relaxes to the local target from target propagation. This happens because with only outputs constrained, other nodes have a freedom to move to values that generate the outputs, and when the energy reduces to 0 (as shown in the bottom display) all neurons must have the activity generating the target output.

▶ **c** | With both input and output neurons constrained, the neural activity of PCNs relaxes to the weighted sum of the local target from target propagation and the predicting activity. Note that the position of the hidden node is in between the positions from panels a and b.

▶ **d** | The distance between the neural activity to the local target at different layers along the relaxation progress in output-constrained PCNs. Here, the neural activity of the output-constrained PCNs converges to the local target, and the layers closer to the output layer (larger l) converge to the local target earlier than the others, which is as expected from the physical intuition of the energy machine.

Implementation details. We train the models to predict a target pattern from an input pattern (both randomly generated from $\mathcal{N}(0,1)$, and the input and target patterns are of 5 and 1 entries, respectively). The structure of the networks is $5 \to 5 \to 5 \to 5 \to 1$. There is no activation function, i.e., it is a linear network. For the computation of the local target in target propagation, refer to the original paper[5]. The mean square difference is used to measure the distance to the local target.

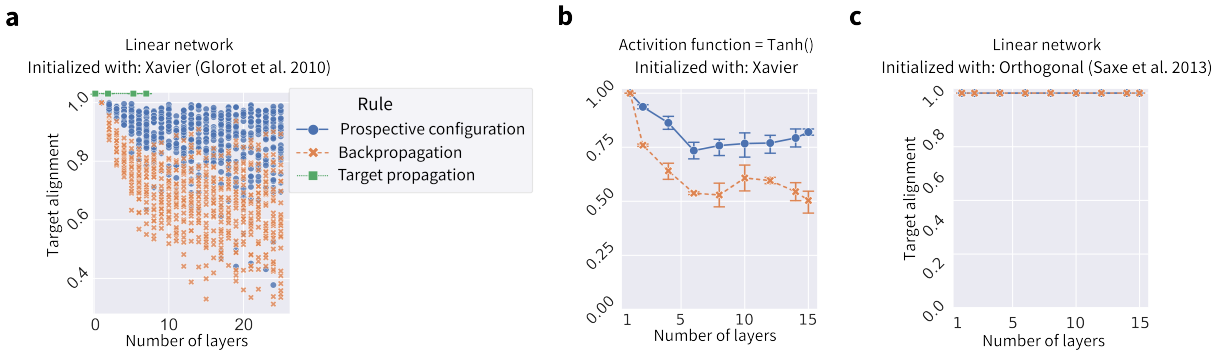

Supplementary Fig. 4

Target alignment in deep neural networks with different learning algorithms, non-linearities and initializations. This figure extends the analyses from Fig. 3e in the main paper of target alignment in randomly generated networks with different depth.

► **a** | Target alignment for target propagation in deep linear network initialized with standard Xavier normal initialization[9]. For comparison, the results presented in Fig. 3e of the main paper for predictive coding networks and backpropagation are also shown. The results for target propagation are only shown for networks with up to 5 layers, because the algorithm became numerically unstable for deeper networks. The target alignment of target propagation is equal to 1 as implied by previous analytic work[6] (for details see Supplementary Notes, Section 2.4.2).

► **b** | Target alignment for networks with a non-linear (*Tanh*) activation function, initialized with standard Xavier normal initialization[9]. The higher value of target alignment for predictive coding networks than backpropagation shown in panel a generalizes to networks with non-linearity.

► **c** | Target alignment of linear networks with orthogonal initialization (where weight in each layer satisfy $\left(\boldsymbol{w}^l\right)^T \boldsymbol{w}^l = \boldsymbol{I}$)[10]. Saxe et al.[10] discovered that with such initialization weights evolve independently of each other during learning, thus, learning times can be independent of depth, even for arbitrarily deep linear networks. As shown in the figure, interestingly, orthogonal initialization gives target alignment of 1 for both learning rules. We also demonstrated this analytically in Supplementary Notes, Section 2.4.3. This perfect target alignment can be intuitively expected, because the independence of weights mentioned above is related to a lack of interference, and it further illustrates that reduction in target alignment is caused by interference between weights.

Each experiment in panels b-c is repeated with $n = 3$ random seeds. Error bars and bands represent the 68% confidence interval.

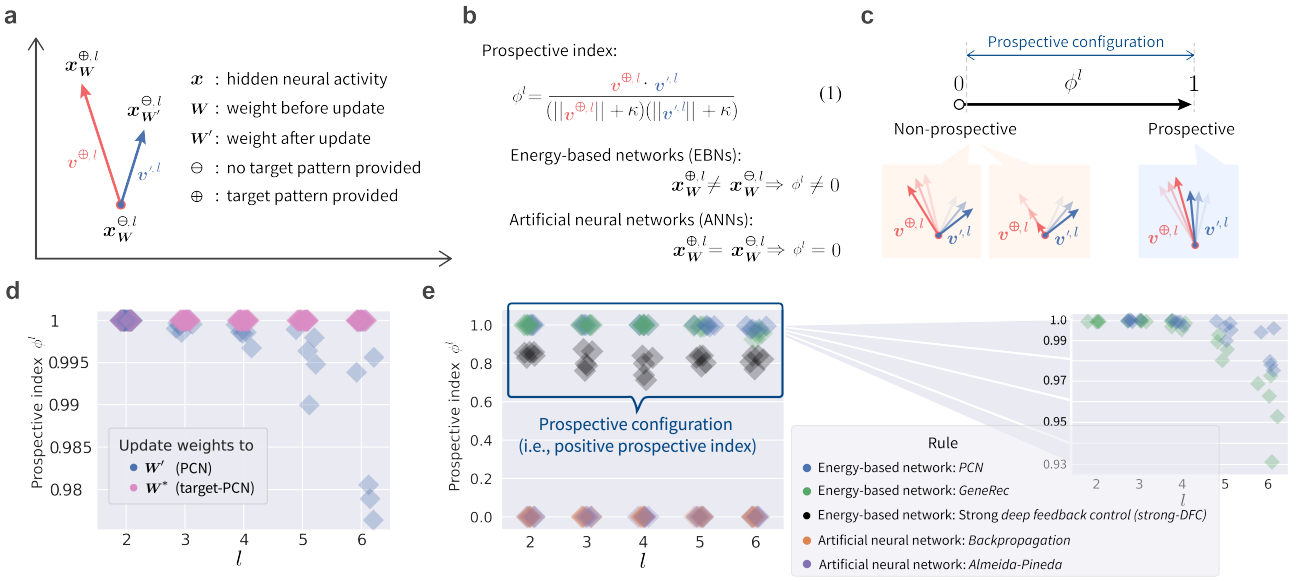

Supplementary Fig. 5

Formal definition of prospective configuration. Formal definition of prospective configuration with prospective index (panels a–c), a metric that one can measure for any learning model. With this metric, we show that prospective configuration is present in different *energy-based networks* (EBNs), but not in *artificial neural networks* (ANNs) (panels d–e).

▶ a | To introduce the prospective index, we consider the hidden neural activity $\boldsymbol{x}^l$ in layer l, at three moments of time. First, a learning iteration starts from $\boldsymbol{x}^l$ under the current weights $\boldsymbol{W}$ without target pattern provided $\ominus$: $\boldsymbol{x}_{\boldsymbol{W}}^{\ominus,l}$. Second, a target pattern is provided $\oplus$, and neural activity settles to $\boldsymbol{x}_{\boldsymbol{W}}^{\oplus,l}$. Third, $\boldsymbol{W}$ is updated to $\boldsymbol{W}'$, the target pattern is removed $\ominus$, and the neural activity settles to $\boldsymbol{x}_{\boldsymbol{W}'}^{\ominus,l}$. We define two vectors $\boldsymbol{v}^{\oplus,l}$ and $\boldsymbol{v}'^{,l}$, representing the direction of the neural activity changes as a result of the target pattern being given $\ominus \to \oplus$ and the weights being updated $\boldsymbol{W} \to \boldsymbol{W}'$, respectively.

▶ b | The prospective index ϕ^l is the cosine similarity of $\boldsymbol{v}^{\oplus,l}$ and $\boldsymbol{v}'^{,l}$. A small constant $\kappa = 0.00001$ is added in the denominator to ensure that the prospective index is still defined if the length of one of the vectors is 0 (in which case the prospective index in equal to 0). For EBNs, the neural activity settles to a new configuration when the target pattern is provided, i.e., $\boldsymbol{x}_{\boldsymbol{W}}^{\oplus,l} \neq \boldsymbol{x}_{\boldsymbol{W}}^{\ominus,l}$, so ϕ^l is non-zero; for ANNs, the neural activity stays unchanged when the target pattern is provided, i.e., $\boldsymbol{x}_{\boldsymbol{W}}^{\oplus,l} = \boldsymbol{x}_{\boldsymbol{W}}^{\ominus,l}$, so ϕ^l is zero.

▶ c | A positive ϕ^l implies that $\boldsymbol{v}^{\oplus,l}$ and $\boldsymbol{v}'^{,l}$ are pointing in the same direction, i.e., the neural activity after the target pattern provided $\boldsymbol{x}_{\boldsymbol{W}}^{\oplus,l}$ is similar to the neural activity after the weight update $\boldsymbol{x}_{\boldsymbol{W}'}^{\ominus,l}$, i.e., is prospective. We define the models following the principle of prospective configuration as those with positive ϕ^l (averaged over all layers). Additionally, prospective index close to 1 implies that a weight update rule in a model is able to consolidate the pattern of activity following relaxation, so a similar pattern is reinstated during prediction on the next trial.

▶ d | The prospective index ϕ^l of different layers l in PCNs and a variant of PCNs called target-PCNs. Several observations can be made, and they are explained and proved in Supplementary Notes, Section 2.3.

▶ e | The prospective index ϕ^l of different EBNs and ANNs. Here, we can see that all EBNs produce positive ϕ^l, i.e., the prospective configuration is commonly observed in EBNs, but not in ANNs. Among the EBNs, *Deep Feedback Control*[11] (DFC) was proposed to work with "infinitely weak nudging", as in equilibrium propagation[12]. More recent work demonstrates that it also works with "strong control"[13,14]

(thus, called strong-DFC), i.e., with the natural form of EBNs. The prospective index was measured for this strong-DFC model and shows it belongs to one of EBNs that process prospective configuration. Details of the simulated strong-DFC model can be found in Supplementary Notes, Section 2.1.

Implementation details. We train various models to predict a target pattern from an input pattern (both randomly generated from $\mathcal{N}(0,1)$). The structure of the networks is $64 \to 64 \to 64 \to 64 \to 64 \to 64 \to 64$. The weights are initialized using Xavier normal initialization[9] (described in the Methods). No activation function was used. Batch size is set to 1. The models were trained for one iteration (i.e., one update of the weights), the prospective index was then measured for this update. Prospective indices of input and output layers are not reported. This is because the input and output layers are held fixed during learning; thus, the prospective index is not defined for them. Experiments were repeated 5 times. The EBNs investigated include PCNs[7,8], target-PCNs, and *GeneRec*[15], while the ANNs investigated include backpropagation and *Almeida-Pineda*[16–18]. Details of all simulated models are given in Supplementary Notes, Section 2.1.

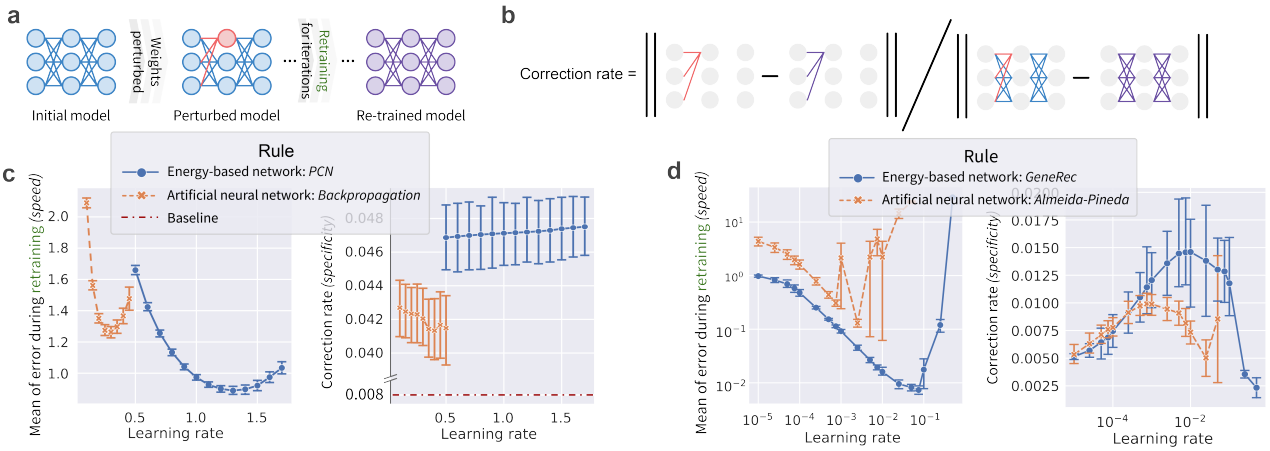

Supplementary Fig. 6

Prospective configuration yields a more accurate weight modification. A numerical experiment (panels a–b) verifies that *energy-based networks* (EBNs) yield a more accurate weight modification than *artificial neural networks* (ANNs) (panels c–d). The following intuition can be provided for why the prospective configuration enables an accurate weight modification. In EBNs, if more error is assigned to a neuron, this neuron will settle to a prospective activity that reduces the error. The prospective activity of this neuron is then propagated through the network, resulting in less error being assigned to other neurons, thus the error being assigned more accurately.

▶ **a** | Experimental procedure: we take a pre-trained model (illustration here does not reflect the real size of the model), randomly select a hidden neuron and perturb the synaptic weights connecting to this neuron (red), then retrain this model on the same pattern for a fixed number of iterations. During retraining, an optimal learning agent is expected to identify that the error in the output neurons is due to the perturbed weights, thus, (1) correct the error faster, and (2) correct the perturbed weights more. We refer to the above two properties as *speed* and *specificity*. Speed can be measured with the mean of error over retraining iterations (the lower, the better).

▶ **b** | Specificity can be measured by correction rate (the higher, the better): the ratio of how much the perturbed weights are corrected compared to how much all the weights (in all layers) are corrected after all retraining iterations.

▶ **c** | A comparison between an EBN, predictive coding network[7,8] (PCN), and an ANN, trained with backpropagation. In the right plot, there is an additional baseline, which is the number of perturbed weights divided by the number of all the weights, indicating the expected correction rate if a learning rule randomly assigns errors.

▶ **d** | The same comparison as in panel c, but for another EBN, namely, *GeneRec*[15]. GeneRec describes learning in recurrent networks, and ANN with this architecture is not trained by standard backpropagation, but by a variant of backpropagation, called *Almeida-Pineda*[16–18].

Implementation details. We first pre-train the models to predict a target pattern from an input pattern (both randomly generated from $\mathcal{N}(0,1)$ and of 32 entries). The structure of the networks is $32 \to 32 \to 32 \to 32$. The pre-training session is sufficiently long (1000 iterations) to reach convergence. Then, one neuron is randomly selected from the $(32+32)$ hidden neurons, and all weights connecting to this neuron are "flipped" (i.e., multiplied by -1). Current weights of the network are recorded as $\boldsymbol{W}_b$. The part of current weights that were just flipped are recorded as $\boldsymbol{W}_b^f$. The network is then re-trained on the same pattern for 64 iterations. After each re-training iteration, the model makes a prediction. The square difference

between the prediction and the target pattern is recorded as the "error during re-training" of this iteration. After the entire re-training session, the "errors during re-training" are averaged over the 64 re-training iterations, producing the left plots of panels c–d. Current weights of the network are recorded as $\boldsymbol{W}_a$. The part of current weights that were flipped before the re-training session are recorded as $\boldsymbol{W}_a^f$. The *correction rate* is computed as $\| \boldsymbol{W}_a^f - \boldsymbol{W}_b^f \| \ / \ \| \boldsymbol{W}_a - \boldsymbol{W}_b \|$, which produces the right plots of panels c–d. Each configuration was repeated $n = 20$ times, and the error bars represent 68% confidence intervals.

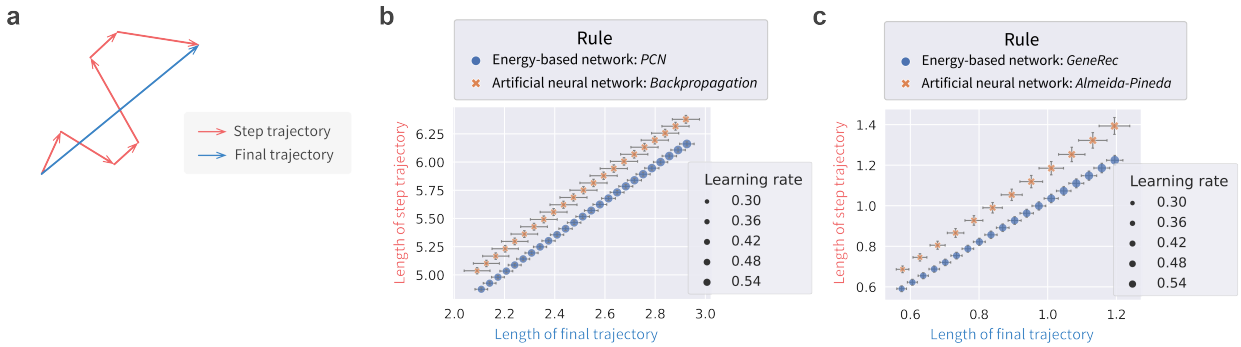

Supplementary Fig. 7

Prospective configuration produces less erratic weight modification. An experiment verifies that *energy-based networks* (EBNs) (i.e., prospective configuration), produce a less erratic weight modification than *artificial neural networks* (ANNs) (i.e., backpropagation).

▶ **a** | Experimental procedure. The weights are updated for a fixed number of steps on a fixed number of data points, which produces the step trajectory in the weight space (each red arrow corresponds to one weights update). Connecting the start and end points of the step trajectory (i.e., the initial and final weights of the model) produces the final trajectory (blue). A learning rule with less erratic weight modification would produce a shorter step trajectory relative to the final trajectory. This property of less erratic weight modification is also desirable for biological systems, because each weight modification costs metabolic energy.

▶ **b** | Comparison of the length of step and final trajectories between EBN, predictive coding network (PCN), and an ANN, trained with backpropagation. Note that the length of both trajectories depends on the learning rate. Thus, in panels b–c, we present the length of the step and final trajectory on y and x axis, respectively; each point is from a specific learning rate (represented by the size of the marker; the legend does not enumerate all sizes). In such plots, when the two learning rules produce roughly the same length of final trajectory (which could be from different learning rates), one can compare the length of their step trajectory.

▶ **c** | The same comparison as in panel c, but for another EBN, namely, *GeneRec*[15]. GeneRec describes learning in recurrent networks, and ANN with this architecture is not trained by standard backpropagation, but by a variant of backpropagation, called *Almeida-Pineda*[16–18].

Implementation details. We train the models to predict a target pattern from an input pattern (both randomly generated from $\mathcal{N}(0,1)$ and of 32 entries), and there are 32 pairs of them (32 data points). The structure of the networks is $32 \to 32 \to 32 \to 32$. The batch size is one, as biological systems update the weights after each experience. The training is conducted for 64 epochs (one epoch iterates over all 32 data points). At the end of each epoch, current weights of the network are recorded as one set. Thus, it results in a sequence of 64 sets of weights. Each set of weights is used as one point to construct the step trajectory. The first and last sets of weights are used to construct the final trajectory. The length of the step and final trajectories can then be computed and reported in Supplementary Figs. 7b–c. For each combination of learning rule and learning rate, simulation is repeated $n = 20$ times with different seeds, and the error bars represent 68% confidence intervals.

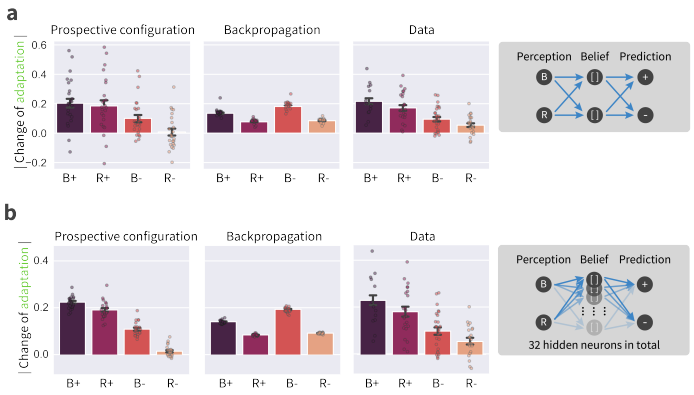

Supplementary Fig. 8

Motor learning experiment with fully-connected structure and more hidden neurons. In the experiments explaining biological observations, for simplicity, we simulated minimal networks necessary to perform these tasks, but it is important to establish if task structure can be discovered and learned by the networks without specifying network structure. Thus, here we repeat the motor learning experiment in Fig. 5 with general fully-connected structure (panel a) and 32 hidden neurons (panel b). Insets illustrate the structure of the networks. In both cases, prospective configuration is able to discover the task structure itself and reproduce the experimental observations; while backpropagation cannot. One should also notice that the variance of the simulation results (spread of changes in adaptation) decreases with increase of the network size.

Each experiment is repeated with $n = 24$ random seeds. Error bars and bands represent the 68% confidence interval.

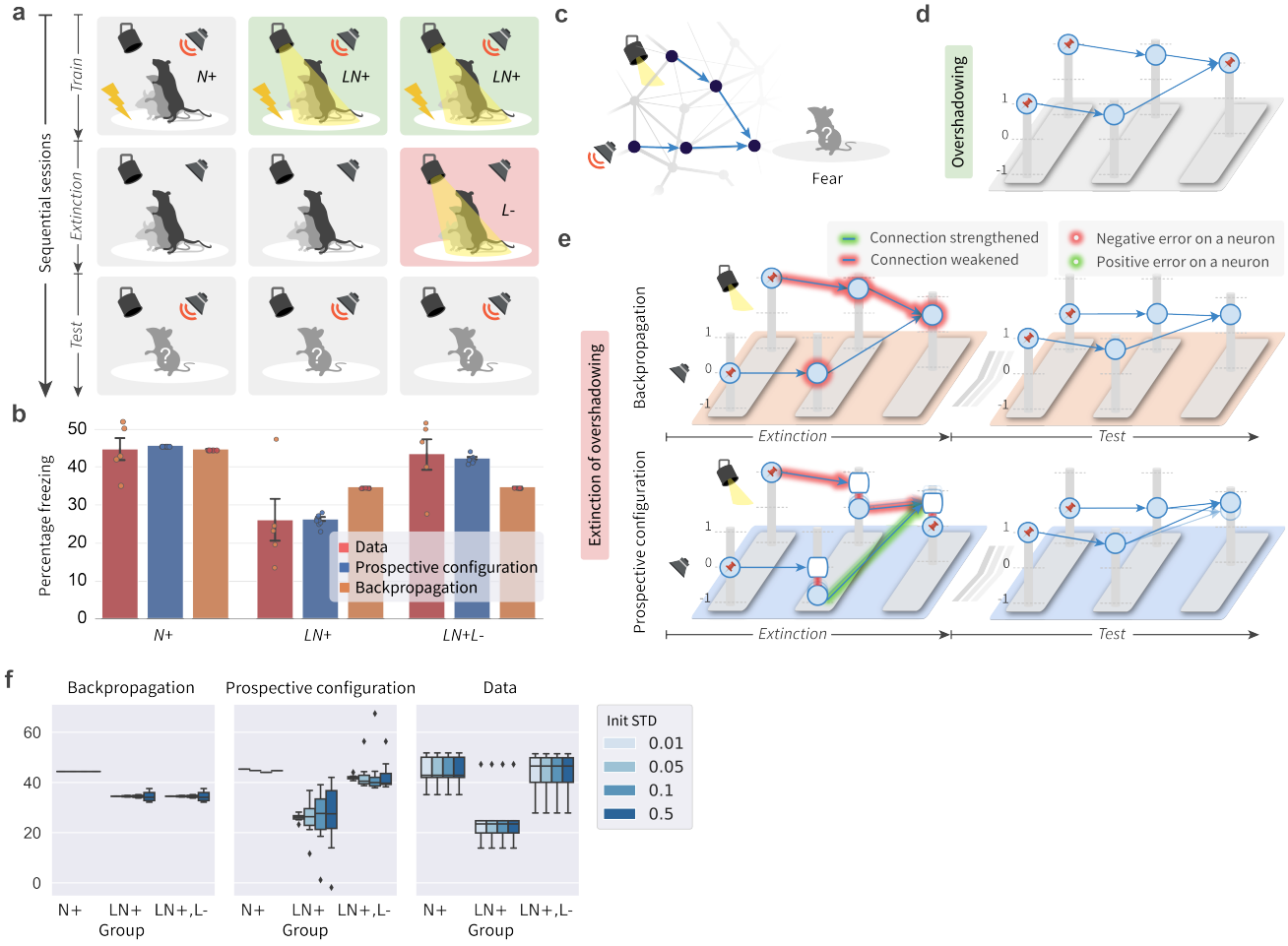

Supplementary Fig. 9

Prospective configuration explains extinction of overshadowing in fear conditioning. The extinction of overshadowing effect[19] can be accurately reproduced and explained by prospective configuration, but not backpropagation (comparing "Data" against "Prospective configuration" and "Backpropagation" in panel b).

► **a** | Experimental procedure. Rats were divided into three groups, corresponding to three columns. Each group underwent three sessions sequentially, corresponding to the top three rows, namely, train, extinction, and test. The goal of the training session was to associate fear (+) with different presented stimuli *N* or *LN* depending on the group: rats experienced an electric shock paired with different stimuli, where *N* and *L* stands for noise and light, respectively. Next, during the extinction session no shock was given, and for the third group the light was presented but without the shock, aiming to eliminate the fear (-) of light (*L*). Finally, all groups underwent a test session measuring how much fear was associated with the noise: the noise was presented and the percentage of freezing of rats was measured.

► **b** | Experimental and simulation results. The bar chart plots the percentage of freezing during test for each group, both measured in the animal experiments[19] (i.e., Data) and simulated by the two learning rules. Two effects are present in experimental data. First, comparing the groups *N*+ and *LN*+ demonstrates the overshadowing effect: there is less fear of noise if the noise had been compounded with light when paired with shock *LN*+ than if the noise alone had been paired with shock *N*+ (that is, light overshadows noise in a conditioned fear experiment). This effect can be accounted for by the canonical

model of error-driven learning — the Rescorla-Wagner model[20], and consequently it can be also produced by both error-driven models we consider — backpropagation and prospective configuration (explained in panel d). Second, comparing the groups *LN+* and *LN+L-* shows the striking effect of extinction of overshadowing: presenting the light without the shock increases the fear response to the non-presented stimulus — noise. This effect is not produced by backpropagation, but can be reproduced by prospective configuration (explained in panel e).

▶ c | The neural architecture considered: both stimuli are processed by hidden neurons (i.e., intermediate neurons corresponding to visual and auditory cortices) and are then combined to produce the prediction of electric shock (i.e., fear).

▶ d | Explanation of overshadowing effect, i.e., the reduced percentage freezing comparing group *LN+* against *N+*. With the energy machine introduced in Fig. 2, the diagram illustrates the state of the network after the *Train* sessions in groups *LN+* and *LN+L-*. The network learns to predict a shock (i.e. produces output of 1), on the basis of two stimuli, hence each of the inputs to the output neuron must be 0.5. Therefore, if only one stimulus is presented, the output of the network is reduced to 0.5. The network shown in this panel is acting as the starting point of learning in panel e.

▶ e | Explanation of extinction of overshadowing effect, i.e., the increased percentage freezing after noise in group *LN+L-* in comparison to *LN+*. This effect suggests that during extinction trials, where light is presented without a shock, the animals increased fear prediction to noise. As shown in this panel, backpropagation (top) cannot explain this, since the error cannot be backpropagated to and drive a weight modification on a non-activated branch where no stimuli are presented; prospective configuration (bottom), however, can account for this. Specifically, on the non-activated branch, the hidden neural activity decreases from zero to a small negative value (it may correspond to a neural activity decreasing below the baseline[21]). Since a weight modification depends on the product of the presynaptic activity and the postsynaptic activity representing the error, which are both negative here, the weight on the non-activated branch is strengthened.

▶ f | Robustness to different standard deviations of initial weights. We also simulated networks with different standard deviations of initial weights (ranging from 0.01 to 0.5, represented by the depth of the colour). It is shown that prospective configuration fits better to the data measured in the animal experiments than backpropagation, regardless of the standard deviation of initial weights. The box plots show the quartiles of the percentage of freezing, the line in the middle indicates the median, while the whiskers extend to show the rest of the distribution, except for the points that are determined to be outliers, which are shown separately.

Each experiment in panels b and f is repeated with $n = 8$ random seeds. Error bars and bands represent the 68% confidence interval.

Implementation details. As shown in panel c, the simulated network includes 2 input, 2 hidden, and 1 output neurons. The weights are initialized from a normal distribution of mean 0 and standard deviation 0.01, reflecting that the animals have not built an association between stimulus and electric shock before the experiments. Presenting or not presenting the stimulus (noise, light, or shock) is encoded as 1 and 0, respectively. The two input neurons are considered to be the visual and auditory neurons; thus, their activity corresponds to perceiving light and noise, respectively. The output neuron is considered to encode the prediction of the electric shock. The training and extinction sessions are both simulated for 32 iterations with the learning rate of 0.01. In the test session, the model makes a prediction with the presented stimulus (noise only). As in the Methods section, we denote by x_c the prediction for each group c from a set $C = \{N+, LN+, LN+L-\}$. To map the prediction to the percentage of freezing, it is scaled by a coefficient a (as the neural activity and the measure of freezing have different units) and shifted by

a bias b (as the rats may have some tendency to freeze after salient stimuli even if they had not been associated with a shock). The numbers reported in panel b are these scaled predictions. The coefficient a (constrained to be positive) and bias b are optimized for prospective configuration and backpropagation independently, analogously as described in the Methods section, i.e. their values that minimize summed squared error given below are found analytically.

$$\sum_{c \in C} (a x_c + b - d_c)^2 \tag{1}$$

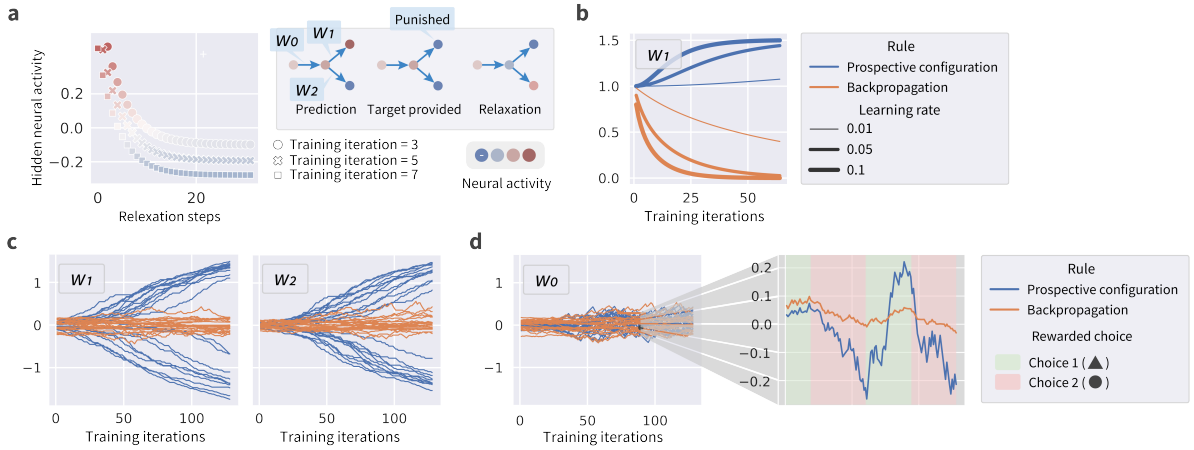

Supplementary Fig. 10

Inference of rewarded choice in the models of human reinforcement learning in Fig. 6. To shed light on the difference between prospective configuration and backpropagation in this task we first simulate an "idealized" version of the task, where the rewards and punishments are delivered deterministically, and the reversal only occurs once at the beginning of training (panels a and b), and then we show that insights from this idealized version translate to the full task from the human experiment (panels c and d).

▶ **a** | Here, we inspect prospective configuration at the first few training iterations: during relaxation, the hidden neuron is able to infer its prospective configuration, i.e., negative hidden activity encoding that the rewarded choice has reversed. The structure of the network is shown in the inset, it starts from ($\{W_0 = 1, W_1 = 1, W_2 = -1\}$) and is trained for 64 trials in total.

▶ **b** | Here, we show that such inference by prospective configuration results in an increase of W_1: since it has inferred from the punishment that the rewarded choice has reversed to a non-rewarded one, such punishment strengthens the connection from the latent state representing non-rewarded choice to a punishment. By contrast, in backpropagation W_1 is decreased: since it receives a punishment without updating the latent state (still encoding that the rewarded choice has not changed), it weakens the connection from the latent state to a reward.

▶ **c** | Here, we show that the W_1 and W_2 in the simulation of the full task with stochastic rewards. The weights follow a similar pattern as in the simplified task, i.e., their magnitude increases in prospective configuration. This signifies that the network learns that the rewards from the two options are jointly determined by a hidden state. This increase of the magnitude of W_1 and W_2 enables the network to infer the hidden state from the feedback, and learn the task structure (as described for panel b).

▶ **d** | Here, we show the evolution of W_0 in the full task. In prospective configuration, this weight remains closer to 0 than W_1 and W_2. Inset shows W_0 on one of the simulation in the main plot, where it is demonstrated that prospective configuration easily flips W_0 as the rewarded choice changes, while backpropagation has difficulty in accomplishing this. The reason of such behavior is as follows: thanks to large magnitude of W_1 and W_2 in prospective configuration, an error on the output unit results in a large error on the hidden unit, so the network is able to quickly flip the sign of W_0 whenever the observation mismatches the expectation. This results in an increased expectation on the Switch trials (Fig. 6c).

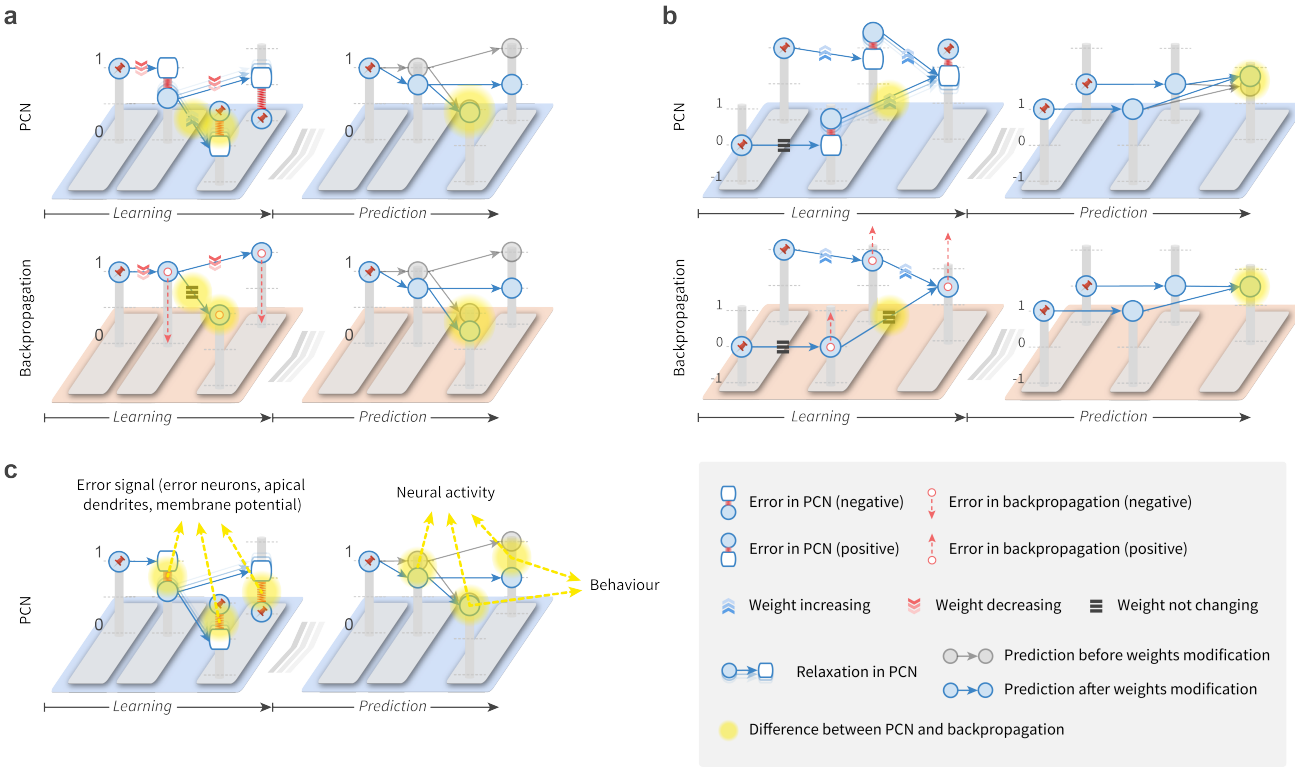

Supplementary Fig. 11

Experimental predictions of prospective configuration and backpropagation. To provide examples of experimental predictions of prospective configuration, panels a-b (and Supplementary Fig. 12) illustrate different behaviour of the learning rules in simple network motifs, which are minimal networks displaying given behaviour. Two motifs in this figure have been already analysed earlier in the paper, but there we focused on differences corresponding to experimentally observed effects, while in this figure we also add other qualitative differences that reveal a range of untested predictions of prospective configuration. Here, we consider a *predictive coding network*[7,8] (PCN) with the energy machine in Fig. 2, however, a similar analysis can be applied to other energy-based networks, which also follow the principle of prospective configuration. In each panel, the top and bottom rows demonstrate the prediction of PCNs and backpropagation, respectively. The left column adds the differences in the prediction errors during learning and the resulting weight update. The right column demonstrates the neuron activity before (transparent) and after (opaque) weight update. The differences between the rules are highlighted in yellow. Experimental predictions following from them can be derived as summarized in panel c.

► **a** | The error may spread to the branch where the prediction is correctly made. This motif has been compared with experimental data in Fig. 6, but here we focus on the effect illustrated in Fig. 1 and Fig. 2d, which despite being intuitive, has not been tested experimentally to our knowledge. The panel adds that an error on one output in PCN results in prediction error on the other, correctly predicted output. This produces an increase of the weight of the correct output neuron, which compensates for the decrease of the weight from the input, and enables the network to make correct prediction on the next trial.

► **b** | The error may cause a weight change in the sensory regions associated with absent stimuli. The panel shows a similar motif as the one investigated in Supplementary Fig. 9. The difference is that Supplementary Fig. 9 introduces negative error while this panel introduces positive error on the same architecture. Interestingly, introducing negative (Supplementary Fig. 9) or positive (this panel) error to the

same architecture produce a similar effect in the PCN, i.e. an increased predicted output for the stimulus not presented during learning.

► c | Observing model behaviour in experiments. The diagram summarizes how the differences illustrated in previous panels could be measured in experiments. The key difference in models' behaviour during learning is the difference in error signals. However, currently it is not clear how the prediction errors are represented in the cortical circuits. Three hypotheses have been proposed in the literature that errors are encoded in: activity of separate error neurons[2,7,22], membrane potential of value neurons[23,24], membrane potential in apical dendrites of value neurons[3,4]. Nevertheless, if the future research establishes how errors are encoded, it will be possible to test the predictions related to errors during learning. For example, one can design a task corresponding to panel a, where predictions in two modalities have to be made on the basis of a stimulus. One can then test if omission in one modality results in error signals in the brain region corresponding to the correctly predicted modality. The models also differ in the neural activity of the value nodes during the next trial following the learning. Such predictions are easier to test, because if the model makes a prediction without observing any supervised signal, then all errors are equal to 0 in PCNs, so the neural activity should reflect just the activity of value nodes. Additionally, the differences in the activity of the output value neurons should be testable in behavioural experiments. For example, panel b makes a behavioural prediction (presenting light with stronger shock should also increase freezing for tone) that can be tested in a similar way as described in Supplementary Fig. 9. Testing this prediction would also validate our explanation of the experimental result in Supplementary Fig. 9.

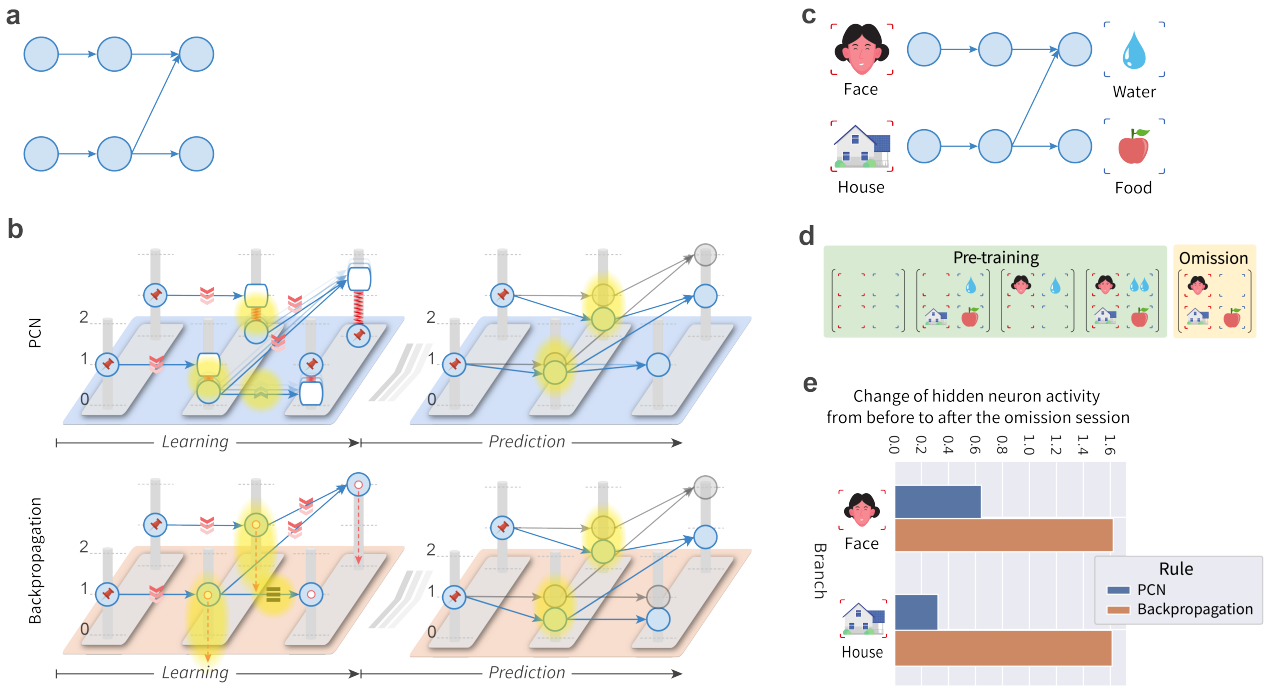

Supplementary Fig. 12

Experimental predictions concerning errors assigned to hidden nodes. The figure demonstrates a striking difference in how prospective configuration and backpropagation assign error to hidden nodes. Namely, in prospective configuration, the error assigned to a hidden node is reduced if the node is also connected to correctly predicted outputs. This difference is illustrated in a motif (panel a), for which we illustrate behaviour of learning rules with the energy machine (panel b), and describe a sample experiment testing model predictions (panels c–d) . Finally, we report the simulation results of the two learning rules (panel e), confirming that they indeed make distinct predictions for this motif.

► **a** | In this motif, two stimuli are presented and two predictions are made. One stimulus contributes to only one prediction, while the other stimulus contributes to both predictions.

► **b** | Comparison of learning rules' behaviour with the energy machine (notation as in Supplementary Fig. 11). The diagrams illustrate a network containing the motif (panel a), in a situations where one of the predicted outputs (top output) is omitted. A negative error is introduced to the prediction determined by both stimuli. Thus, we would expect the error to be assigned to hidden neurons on both branches. Both learning rules do so, however, they assign errors differently. PCNs allocate less error on the bottom hidden neuron than the top hidden neuron, because the bottom hidden neuron also contributes to another output that was correctly predicted, while backpropagation assigns the same error to both hidden neurons. This is also a nice example where prospective configuration (PCNs) demonstrates more intelligent behavior.

► **c** | Experimental stimuli. To test this motif, it is important to choose stimuli for which neural activity of "hidden" neurons can be easily measured. In case of a human experiment, inputs could contain faces and houses, because the hidden neurons would correspond to the brain regions known to be specifically excited by these particular types of stimuli, and the activity of these regions could be easily distinguished in an experiment[25]. The outputs could correspond to reward modalities (e.g. water and food). In case of a human experiment, these could be "virtual rewards" the participants are instructed to gather, while for animals, these could be the actual rewards.

► **d** | Experimental procedure. The motif shown in panel c could arise in brain networks from training

with examples shown in the green box. To test differences in behaviour of learning rules, partial omission trials could be presented, in which one of the expected outputs is omitted, as shown in the orange box.

► **e** | Results of simulations. We pre-train the models with the examples in the green box in panel d for a sufficient number of iterations until convergence, and then we train the model with the omission using the example in the orange box in panel d for one trial. We measure the change of hidden neural activity on both branches from before to after the above omission session. The graph shows simulation results of such change in hidden activity: PCNs predict different changes on different branches, while backpropagation predicts the same change on different branches (consistent with illustration in panel b, right).

Implementation details. Presenting and not presenting a stimulus (face, house, water, or food) are encoded as 1 and 0, respectively. Presenting two drops of water is encoded as 2. The network is initialized to the pre-trained connection pattern demonstrated in Supplementary Figs. 12c, i.e., the weights visible on the panel are set to one and other weights are set to zero. Such pattern of weights would arise from pre-training with the four examples in Supplementary Figs. 12d (in the green "Pre-training" box), but for simplicity, we do not simulate such pre-training but just set the weights as explained before. Next, to measure the activity of hidden units of such network during prediction, we set both inputs to 1 and record the hidden neural activity of the two branches. Subsequently, the model is presented with the omission trial shown in the orange box and the weights are updated once. Finally, to measure weight changes resulting from training on the subsequent prediction trial, we set both inputs to 1 and record the hidden neural activity of the two branches for the second time. The change of the hidden neuron activity from before to after the omission session can thus be computed for both branches.

2 Supplementary Notes

In this supplement, we present additional description and analysis of the simulated models. In Section 2.1, we provide details of all models simulated in the paper. In Section 2.2, we discuss relationship between prospective configuration and target propagation. In Section 2.3, we analyse prospective index of PCNs. In Section 2.4, we analyse target alignment of various learning models.

2.1 Details of simulated models

This section gives more details of all simulated models. The general idea of *energy-based networks* (EBNs) and *artificial neural networks* (ANNs), and one of EBNs, *predictive coding network*[7,8] (PCN), have been described in the Main article and Methods. PCN is again included here along with other simulated models to provide descriptions in a unified form, facilitating the reproduction of our reported results. Complete code and full documentation reproducing all simulation results written in Python is made publicly available at https://github.com/YuhangSong/Prospective-Configuration.

Algorithms 1 to 5 describe how the four models simulated in this paper predict and learn. These four models are: PCN, backpropagation, *GeneRec*[15], and *Almeida-Pineda*[16–18]. Among the four models, PCN and GeneRec are the two EBNs we investigate; backpropagation and Almeida-Pineda are the two ANNs we investigate. Specifically, PCN is compared against backpropagation, because it has been established that PCN are closely related to backpropagation[8,26] and they make the same prediction with the same weights and input pattern[8]. Therefore we simulated prediction in these two algorithms in the same way (Algorithm 1). However, they learn differently (c.f. Algorithm 2 and Algorithm 1 in the Methods of the main article). The other EBN, GeneRec, describes learning in recurrent networks, and ANN in this architecture is not trained by standard backpropagation, but a modified version proposed by Almeida and Pineda[16–18] (thus called the *Almeida-Pineda* algorithm). Thus, GeneRec should be compared against Almeida-Pineda because they make same prediction with the same weights and input pattern[15]. Therefore we simulated prediction in these two algorithms in the same way (Algorithm 3). But they learn differently (c.f. Algorithms 4 and 5). In a word, PCN and backpropagation are EBN and ANN working in feed-forward architecture, respectively; GeneRec and Almeida-Pineda are EBN and ANN working in recurrent architecture, respectively.

Algorithm 1: Predict with backpropagation or *predictive coding network*[7,8] (PCN)

Input: input pattern $\boldsymbol{s}^{\text{in}}$; synaptic weights $\{\boldsymbol{w}^1, \boldsymbol{w}^2, \cdots, \boldsymbol{w}^L\}$
Result: activity of output neurons $\boldsymbol{x}^{L+1}$

$\boldsymbol{x}^1 = \boldsymbol{s}^{\text{in}}$; // Clamp input neurons to input pattern
for $l = 1;\ l < L+1;\ l = l+1$ **do** // Forward pass of the network
  $\boldsymbol{x}^{l+1} = \boldsymbol{w}^l f\left(\boldsymbol{x}^l\right)$;
end

Particularly, PCN & Backpropagation work in a network where prediction is made from the input through a series of forward weights $\{\boldsymbol{w}^1, \boldsymbol{w}^2, \cdots, \boldsymbol{w}^L\}$; GeneRec & Almeida-Pineda works in a network where prediction is made from input through a mixture of forward weights $\{\boldsymbol{w}^1, \boldsymbol{w}^2, \cdots, \boldsymbol{w}^L\}$ and backward weights $\{\boldsymbol{m}^1, \boldsymbol{m}^2, \cdots, \boldsymbol{m}^L\}$. The forward weights $\{\boldsymbol{w}^1, \boldsymbol{w}^2, \cdots, \boldsymbol{w}^L\}$ and backward weights $\{\boldsymbol{m}^1, \boldsymbol{m}^2, \cdots, \boldsymbol{m}^L\}$ are not necessarily related. This architecture is also similar to the continuous Hopfield model[27,28]. Unlike in some previous studies[12], here, we focus on layered networks, where the sets of neurons at adjacent layers $\boldsymbol{x}^l$ and $\boldsymbol{x}^{l+1}$ are connected by synaptic weights. Thus, we define two sets of

weights for GeneRec & Almeida-Pineda that works in the recurrent network: $\boldsymbol{w}^l$ is the forward weights connecting from $\boldsymbol{x}^l$ to $\boldsymbol{x}^{l+1}$; $\boldsymbol{m}^l$ is the backward weights connecting from $\boldsymbol{x}^{l+1}$ to $\boldsymbol{x}^l$.

Algorithm 2: Learn with backpropagation

Input: input pattern $\boldsymbol{s}^{\text{in}}$; target pattern $\boldsymbol{s}^{\text{target}}$; synaptic weights $\left\{\boldsymbol{w}^1, \boldsymbol{w}^2, \cdots, \boldsymbol{w}^L\right\}$
Output: updated synaptic weights $\left\{\boldsymbol{w}^1, \boldsymbol{w}^2, \cdots, \boldsymbol{w}^L\right\}$

$\boldsymbol{x}^1 = \boldsymbol{s}^{\text{in}}$; // Clamp input neurons to input pattern
for $l = 1;\ l < L+1;\ l = l+1$ **do** // Forward pass of the network
  $\boldsymbol{x}^{l+1} = \boldsymbol{w}^l f\left(\boldsymbol{x}^l\right)$;
end
$\boldsymbol{\varepsilon}^{L+1} = \boldsymbol{s}^{\text{target}} - \boldsymbol{x}^{L+1}$; // Compute error of the output neurons
for $l = L+1;\ l > 2;\ l = l-1$ **do** // Backpropagation of error
  $\boldsymbol{\varepsilon}^{l-1} = f'\left(\boldsymbol{x}^{l-1}\right) \circ \left(\left(\boldsymbol{w}^{l-1}\right)^T \boldsymbol{\varepsilon}^l\right)$;
end
for $l = 1;\ l < L+1;\ l = l+1$ **do** // Update weights
  $\Delta \boldsymbol{w}^l = \alpha \boldsymbol{\varepsilon}^{l+1} \left(f\left(\boldsymbol{x}^l\right)\right)^T$;
  $\boldsymbol{w}^l = \boldsymbol{w}^l + \Delta \boldsymbol{w}^l$;
end

Also note that GeneRec has been explored and re-discovered in recent works[29,30] showing how a closely related algorithm resembles backpropagation when the backward weights are the transposes of the forward weights $\boldsymbol{m}^l = \left(\boldsymbol{w}^l\right)^T$ (or for a fully-connected network in their context $w_{i,j} = w_{j,i}$), and how the extreme version of the algorithm approximate backpropagation[12].

Supplementary Fig. 5 additionally investigates *Strong Deep Feedback Control*[13,14] (strong-DFC). *Deep Feedback Control*[11] (DFC) was proposed to work with "infinitely weak nudging", as in equilibrium propagation[12]. More recent work demonstrates that it also works with "strong control"[13,14] (thus, called strong-DFC), i.e., with the natural form of EBNs. Thus, in this paper we investigate strong-DFC. In strong-DFC (or DFC in general), backward weights $\boldsymbol{m}^l$ do not connect from layer $l+1$ to layer l as in other models investigated in the paper. Instead, $\boldsymbol{m}^l$ connects from the output layer $L+1$ to layer l. We use the provided code in `https://github.com/mariacer/strong_dfc` to simulate strong-DFC. All hyper parameters are kept as is in the provided code. We remove the activation function of the last layer in the original implementation[11], to keep consistent with the rest of the models investigated in this paper, thus, providing a fair comparison. Derivation and motivation of the model can be found in the original paper[13,14].

Some common notations in the algorithms are: α is the learning rate for weights update; γ and $\mathscr{T}$ are the integration step and length of relaxation, respectively (specific to the two EBNs, PCN and GeneRec); $\boldsymbol{s}^{\text{in}}$ and $\boldsymbol{s}^{\text{target}}$ are the input and target patterns, respectively. For Almeida-Pineda, which requires additional iterative process to propagate error, β and $\mathscr{K}$ are the integration step and length of this iterative process, respectively. In our simulation, we use $\beta = 0.01$ and $\mathscr{K} = 1600$.

All simulated models work in mini-batch mode, that is to say, one iteration is to update the weights for one step on a mini-batch of data randomly sampled from the training set for classification tasks. The above sampling is without replacement, i.e., the same examples will not be sampled again before the completion of a epoch, which is when the entire training set has been sampled once. For example, considering a dataset of 1000 examples with a batch-size (number of examples in a mini-batch) of 10, then each iteration

would update weights for one step on 10 examples, and it will take 100 such iterations to complete one epoch. To implement the Algorithms 1 to 5 described below in mini-batch mode, one can simply add an extra-dimension, the size of which is batch-size, to all the neuron-specific vectors in the algorithms such as $\boldsymbol{x}^l$, $\boldsymbol{\epsilon}^l$ and etc., and then reduce this dimension by summing over it when computing weight update $\Delta \boldsymbol{w}^l$ (and $\Delta \boldsymbol{m}^l$ if the model is GeneRec or Almeida-Pineda).

Note that learning with Almeida-Pineda involves relaxation of the model, i.e., updating neural activity, in lines 5-12 of Algorithm 4. However, its function is to make a prediction with current weights and input pattern so that the error on the output neurons can be computed (in the following line 13), similar as the function of "forward pass" in backpropagation in lines 2-4 of Algorithm 2. The neural activity in the Almeida-Pineda model is fixed during spreading of error, like in backpropagation. Thus, Almeida-Pineda is classified as an ANN rather than an EBN (which updates neural activity during spreading of error).

Algorithm 3: Predict with *Almeida-Pineda*[16–18] or *GeneRec*[15]

Input: input pattern $\boldsymbol{s}^{\text{in}}$; forward and backward synaptic weights $\left\{\boldsymbol{w}^1, \boldsymbol{w}^2, \cdots, \boldsymbol{w}^L\right\}$ and $\left\{\boldsymbol{m}^1, \boldsymbol{m}^2, \cdots, \boldsymbol{m}^L\right\}$

Result: activity of output neurons $\boldsymbol{x}^{L+1}$

1 $\boldsymbol{x}^1 = \boldsymbol{s}^{\text{in}}$; // Clamp input neurons to input pattern
2 **for** $l = 2;\ l < L+2;\ l = l+1$ **do** // Initialize $\boldsymbol{x}$
3 $\quad \boldsymbol{x}^l = \boldsymbol{0}$;
4 **end**
5 **for** $t = 0;\ t < \mathscr{T};\ t = t+1$ **do** // Relaxation
6 $\quad$ **for** $l = 2;\ l < L+1;\ l = l+1$ **do**
7 $\quad\quad \Delta \boldsymbol{x}^l = \gamma\left(-\boldsymbol{x}^l + \boldsymbol{m}^l f\left(\boldsymbol{x}^{l+1}\right) + \boldsymbol{w}^{l-1} f\left(\boldsymbol{x}^{l-1}\right)\right)$;
8 $\quad\quad \boldsymbol{x}^l = \boldsymbol{x}^l + \Delta \boldsymbol{x}^l$;
9 $\quad$ **end**
10 $\quad \Delta \boldsymbol{x}^{L+1} = \gamma\left(-\boldsymbol{x}^{L+1} + \boldsymbol{w}^L f\left(\boldsymbol{x}^L\right)\right)$;
11 $\quad \boldsymbol{x}^{L+1} = \boldsymbol{x}^{L+1} + \Delta \boldsymbol{x}^{L+1}$;
12 **end**

Algorithm 4: Learn with *Almeida-Pineda*[16–18]

Input: input pattern $\boldsymbol{s}^{\text{in}}$; target pattern $\boldsymbol{s}^{\text{target}}$; forward and backward synaptic weights $\{\boldsymbol{w}^1, \boldsymbol{w}^2, \cdots, \boldsymbol{w}^L\}$ and $\{\boldsymbol{m}^1, \boldsymbol{m}^2, \cdots, \boldsymbol{m}^L\}$

Output: updated forward and backward synaptic weights $\{\boldsymbol{w}^1, \boldsymbol{w}^2, \cdots, \boldsymbol{w}^L\}$ and $\{\boldsymbol{m}^1, \boldsymbol{m}^2, \cdots, \boldsymbol{m}^L\}$

$\boldsymbol{x}^1 = \boldsymbol{s}^{\text{in}}$; // Clamp input neurons to input pattern

for $l = 2;\ l < L+2;\ l = l+1$ **do** // Initialize $\boldsymbol{x}$

  $\boldsymbol{x}^l = \boldsymbol{0}$;

end

for $t = 0;\ t < \mathscr{T};\ t = t+1$ **do** // Relaxation

  for $l = 2;\ l < L+1;\ l = l+1$ **do**

    $\Delta \boldsymbol{x}^l = \gamma\left(-\boldsymbol{x}^l + \boldsymbol{m}^l f\left(\boldsymbol{x}^{l+1}\right) + \boldsymbol{w}^{l-1} f\left(\boldsymbol{x}^{l-1}\right)\right)$;

    $\boldsymbol{x}^l = \boldsymbol{x}^l + \Delta \boldsymbol{x}^l$;

  end

  $\Delta \boldsymbol{x}^{L+1} = \gamma\left(-\boldsymbol{x}^{L+1} + \boldsymbol{w}^L f\left(\boldsymbol{x}^L\right)\right)$;

  $\boldsymbol{x}^{L+1} = \boldsymbol{x}^{L+1} + \Delta \boldsymbol{x}^{L+1}$;

end

$\boldsymbol{\varepsilon}^{L+1} = \boldsymbol{s}^{\text{target}} - \boldsymbol{x}^{L+1}$; // Compute error of the output neurons

for $l = 1;\ l < L+1;\ l = l+1$ **do** // Initialize $\boldsymbol{\varepsilon}$

  $\boldsymbol{\varepsilon}^l = \boldsymbol{0}$;

end

for $t = 1;\ t < \mathscr{K}+1;\ t = t+1$ **do** // Backpropagation of error

  for $l = 2;\ l < L+1;\ l = l+1$ **do**

    $\Delta \boldsymbol{\varepsilon}^l = \beta\left(-\boldsymbol{\varepsilon}^l + f'\left(\boldsymbol{x}^l\right) \circ \left(\boldsymbol{m}^l \boldsymbol{\varepsilon}^{l+1}\right) + f'\left(\boldsymbol{x}^l\right) \circ \left(\boldsymbol{w}^{l-1} \boldsymbol{\varepsilon}^{l-1}\right)\right)$;

    $\boldsymbol{\varepsilon}^l = \boldsymbol{\varepsilon}^l + \Delta \boldsymbol{\varepsilon}^l$;

  end

  $\Delta \boldsymbol{\varepsilon}^1 = \beta\left(-\boldsymbol{\varepsilon}^1 + f'\left(\boldsymbol{x}^1\right) \circ \left(\boldsymbol{m}^1 \boldsymbol{\varepsilon}^2\right)\right)$;

  $\boldsymbol{\varepsilon}^1 = \boldsymbol{\varepsilon}^1 + \Delta \boldsymbol{\varepsilon}^1$;

end

for $l = 1;\ l < L+1;\ l = l+1$ **do** // Update weights

  $\Delta \boldsymbol{w}^l = \alpha \boldsymbol{\varepsilon}^{l+1} \left(f\left(\boldsymbol{x}^l\right)\right)^T$;

  $\boldsymbol{w}^l = \boldsymbol{w}^l + \Delta \boldsymbol{w}^l$;

  $\Delta \boldsymbol{m}^l = \alpha \boldsymbol{\varepsilon}^l \left(f\left(\boldsymbol{x}^{l+1}\right)\right)^T$;

  $\boldsymbol{m}^l = \boldsymbol{m}^l + \Delta \boldsymbol{m}^l$;

end

Algorithm 5: Learn with *GeneRec*[15]

Input: input pattern $\boldsymbol{s}^{\text{in}}$; target pattern $\boldsymbol{s}^{\text{target}}$; forward and backward synaptic weights $\{\boldsymbol{w}^1, \boldsymbol{w}^2, \cdots, \boldsymbol{w}^L\}$ and $\{\boldsymbol{m}^1, \boldsymbol{m}^2, \cdots, \boldsymbol{m}^L\}$

Output: updated forward and backward synaptic weights $\{\boldsymbol{w}^1, \boldsymbol{w}^2, \cdots, \boldsymbol{w}^L\}$ and $\{\boldsymbol{m}^1, \boldsymbol{m}^2, \cdots, \boldsymbol{m}^L\}$

$\boldsymbol{x}^1 = \boldsymbol{s}^{\text{in}}$; // Clamp input neurons to input pattern

for $l = 2;\ l < L+2;\ l = l+1$ **do** // Initialize $\boldsymbol{x}$

  $\boldsymbol{x}^l = \boldsymbol{0}$;

end

for $t = 0;\ t < \mathscr{T};\ t = t+1$ **do** // Relaxation

  for $l = 2;\ l < L+1;\ l = l+1$ **do**

    $\Delta \boldsymbol{x}^l = \gamma\left(-\boldsymbol{x}^l + \boldsymbol{m}^l f\left(\boldsymbol{x}^{l+1}\right) + \boldsymbol{w}^{l-1} f\left(\boldsymbol{x}^{l-1}\right)\right)$;

    $\boldsymbol{x}^l = \boldsymbol{x}^l + \Delta \boldsymbol{x}^l$;

  end

  $\Delta \boldsymbol{x}^{L+1} = \gamma\left(-\boldsymbol{x}^{L+1} + \boldsymbol{w}^L f\left(\boldsymbol{x}^L\right)\right)$;

  $\boldsymbol{x}^{L+1} = \boldsymbol{x}^{L+1} + \Delta \boldsymbol{x}^{L+1}$;

end

for $l = 1;\ l < L+1;\ l = l+1$ **do** // Update weights (negative phase)

  $\Delta \boldsymbol{w}^l = -\alpha f\left(\boldsymbol{x}^{l+1}\right)\left(f\left(\boldsymbol{x}^l\right)\right)^T$;

  $\boldsymbol{w}^l = \boldsymbol{w}^l + \Delta \boldsymbol{w}^l$;

  $\Delta \boldsymbol{m}^l = -\alpha f\left(\boldsymbol{x}^l\right)\left(f\left(\boldsymbol{x}^{l+1}\right)\right)^T$;

  $\boldsymbol{m}^l = \boldsymbol{m}^l + \Delta \boldsymbol{m}^l$;

end

$\boldsymbol{x}^{L+1} = \boldsymbol{s}^{\text{target}}$; // Clamp output neurons to target pattern

for $t = 0;\ t < \mathscr{T};\ t = t+1$ **do** // Relaxation

  for $l = 2;\ l < L+1;\ l = l+1$ **do**

    $\Delta \boldsymbol{x}^l = \gamma\left(-\boldsymbol{x}^l + \boldsymbol{m}^l f\left(\boldsymbol{x}^{l+1}\right) + \boldsymbol{w}^{l-1} f\left(\boldsymbol{x}^{l-1}\right)\right)$;

    $\boldsymbol{x}^l = \boldsymbol{x}^l + \Delta \boldsymbol{x}^l$;

  end

end

for $l = 1;\ l < L+1;\ l = l+1$ **do** // Update weights (positive phase)

  $\Delta \boldsymbol{w}^l = \alpha f\left(\boldsymbol{x}^{l+1}\right)\left(f\left(\boldsymbol{x}^l\right)\right)^T$;

  $\boldsymbol{w}^l = \boldsymbol{w}^l + \Delta \boldsymbol{w}^l$;

  $\Delta \boldsymbol{m}^l = \alpha f\left(\boldsymbol{x}^l\right)\left(f\left(\boldsymbol{x}^{l+1}\right)\right)^T$;

  $\boldsymbol{m}^l = \boldsymbol{m}^l + \Delta \boldsymbol{m}^l$;

end

2.2 Relationships of predictive coding networks to target propagation (Supplementary Fig. 3)

In Supplementary Fig. 3, we illustrate that prospective configuration, particularly, *predictive coding network*[7,8] (PCN), has close a relationship to target propagation[31]. In this section, we formally prove these observations.

Note that these relationships of PCNs to target propagation on one hand build interesting connections to existing work, on the other hand serve as a step in providing a mathematical explanation of the target alignment of PCNs, as discussed in the later Section 2.4.4.

2.2.1 Target propagation

Algorithm 6: Learn with target-propagation

Input: input pattern $\boldsymbol{s}^{\text{in}}$; target pattern $\boldsymbol{s}^{\text{target}}$; synaptic weights $\left\{\boldsymbol{w}^1, \boldsymbol{w}^2, \cdots, \boldsymbol{w}^L\right\}$

Output: updated synaptic weights $\left\{\boldsymbol{w}^1, \boldsymbol{w}^2, \cdots, \boldsymbol{w}^L\right\}$

$\boldsymbol{x}^1 = \boldsymbol{s}^{\text{in}}$; // Clamp input neurons to input pattern

for $l = 1;\ l < L+1;\ l = l+1$ **do** // Forward pass of the network

  $\boldsymbol{x}^{l+1} = \boldsymbol{w}^l f\left(\boldsymbol{x}^l\right)$;

end

$\tilde{\boldsymbol{x}}^{L+1} = \boldsymbol{s}^{\text{target}}$;

$\boldsymbol{\varepsilon}^{L+1} = \tilde{\boldsymbol{x}}^{L+1} - \boldsymbol{x}^{L+1}$;

for $l = L+1;\ l > 2;\ l = l-1$ **do** // Target-propagation

  $\tilde{\boldsymbol{x}}^{l-1} = f^{-1}\left(\left(\boldsymbol{w}^{l-1}\right)^{-1}\tilde{\boldsymbol{x}}^l\right)$;

  $\boldsymbol{\varepsilon}^{l-1} = \tilde{\boldsymbol{x}}^{l-1} - \boldsymbol{x}^{l-1}$;

end

for $l = 1;\ l < L+1;\ l = l+1$ **do** // Update weights

  $\Delta\boldsymbol{w}^l = \alpha\boldsymbol{\varepsilon}^{l+1}\left(f\left(\boldsymbol{x}^l\right)\right)^T$;

  $\boldsymbol{w}^l = \boldsymbol{w}^l + \Delta\boldsymbol{w}^l$;

end

We first briefly review target propagation. The key insight behind target propagation is that rather than updating weights based on a gradient of a loss function, one can instead attempt to explicitly compute what are the optimal activity for the neurons so that they can produce the desired target pattern, and then update the weights so as to nudge the current neural activity towards the optimal activity directly. We call these optimal activity *local target* since if the neurons take this activity, the network would produce the desired target pattern. Importantly, we can directly compute the local target in terms of the *inverses* of the weights and activation functions. Namely, suppose that we have a three-layer network with activation functions $f()$, weight matrices $\boldsymbol{w}^1, \boldsymbol{w}^2, \boldsymbol{w}^3$ and an input pattern $\boldsymbol{s}^{\text{in}}$. The output of this network is $\boldsymbol{x}^4 = \boldsymbol{w}^3 f\left(\boldsymbol{w}^2 f\left(\boldsymbol{w}^1 f\left(\boldsymbol{s}^{\text{in}}\right)\right)\right)$. Suppose instead that we do not want the network to output $\boldsymbol{x}^4$ for a given $\boldsymbol{s}^{\text{in}}$ but rather a given target pattern $\boldsymbol{s}^{\text{target}}$. Then, the activity at the first layer $\tilde{\boldsymbol{x}}^1$ that would produce this desired activity can be exactly computed by inverting[1] the network $\tilde{\boldsymbol{x}}^1 = f^{-1}\left(\left(\boldsymbol{w}^1\right)^{-1} f^{-1}\left(\left(\boldsymbol{w}^2\right)^{-1} f^{-1}\left(\left(\boldsymbol{w}^3\right)^{-1}\boldsymbol{s}^{\text{target}}\right)\right)\right)$. From this, we can define a recursion of one local target in terms of another at the layer above,

$$\begin{aligned} \tilde{\boldsymbol{x}}^l &= f^{-1}\left(\left(\boldsymbol{w}^l\right)^{-1}\tilde{\boldsymbol{x}}^{l+1}\right) \\ \tilde{\boldsymbol{x}}^{L+1} &= \boldsymbol{s}^{\text{target}} \end{aligned} \tag{2}$$

Based on these targets we can define the errors in target propagation as $\boldsymbol{\varepsilon}^l = \tilde{\boldsymbol{x}}^l - \boldsymbol{x}^l$. These errors drive the update of weights according to:

$$\Delta\boldsymbol{w}^l = \alpha\boldsymbol{\varepsilon}^{l+1}\left(f\left(\boldsymbol{x}^l\right)\right)^T \tag{3}$$

[1] Note that in realistic networks the weight matrices are not all square so an exact inverse $\left(\boldsymbol{w}^l\right)^{-1}$ does not exist. Instead, we can compute approximations of the inverse using the Moore-Penrose pseudoinverse[32] $\left(\boldsymbol{w}^l\right)^{\dagger}$, which is the least squares solution to the optimization problem $\arg\min_{\boldsymbol{w}} \left\|\boldsymbol{I} - \boldsymbol{w}^l\boldsymbol{w}\right\|$.

This algorithm is summarized in Algorithm 6.

2.2.2 *Analyses of the relationships*

Now we formally prove the below observations in Supplementary Fig. 3 about how prospective configuration, particularly PCN, has close a relationship to target propagation[5]. In other words, we formally prove that

- In an output-constrained PCN, neural activity after relaxation converges to the local target;
- In an input-output-constrained PCN, neural activity after relaxation approaches to the weighted sum of the predicting activity and the local target.

In the above, predicting activity refer to the neural activity when the model is making prediction, and they are the same for both backpropagation and PCN as they compute the same neural activity when making a prediction.

Output-constrained PCN As mentioned, we first investigate the "output-constrained PCN": in this PCN input neurons are not clamped to the input pattern but output neurons are clamped to the target pattern. We show that in this PCN, the activity after relaxation is precisely equal to the local target. Since $\boldsymbol{x}^1$ is not constrained to the input pattern, we can look at its dynamic by setting $l = 1$ in Eq. 12 in the Methods of the main article. Since there is no error term or error nodes at the input layer, there is only the later term left when setting $l = 1$ in Eq. 12 in the Methods of the main article (note that here we write in matrix & vector form):

$$\Delta \boldsymbol{x}^1 = \gamma f'\left(\boldsymbol{x}^1\right) \circ \left(\left(\boldsymbol{w}^1\right)^T \boldsymbol{\varepsilon}^2\right) \tag{4}$$

$$= \gamma f'\left(\boldsymbol{x}^1\right) \circ \left(\left(\boldsymbol{w}^1\right)^T \left(\boldsymbol{x}^2 - \boldsymbol{w}^1 f\left(\boldsymbol{x}^1\right)\right)\right) \tag{5}$$

Considering the above dynamic has converged, we can set $\Delta \boldsymbol{x}^1 = \boldsymbol{0}$ in the above equation and solving for $\boldsymbol{x}^1$, then we can obtain the converged value of $\boldsymbol{x}^1$:

$$\boldsymbol{x}^1 = f^{-1}\left(\left(\boldsymbol{w}^1\right)^{-1} \boldsymbol{x}^2\right) \tag{6}$$

Now we look at the dynamic of $\boldsymbol{x}^2$ by setting $l = 2$ in Eq. 12 in the Methods of the main article:

$$\Delta \boldsymbol{x}^2 = \gamma\left(-\boldsymbol{\varepsilon}^2 + f'\left(\boldsymbol{x}^2\right) \circ \left(\left(\boldsymbol{w}^2\right)^T \boldsymbol{\varepsilon}^3\right)\right) \tag{7}$$

$$= \gamma\left(-\left(\boldsymbol{x}^2 - \boldsymbol{w}^1 f\left(\boldsymbol{x}^1\right)\right) + f'\left(\boldsymbol{x}^2\right) \circ \left(\left(\boldsymbol{w}^2\right)^T \left(\boldsymbol{x}^3 - \boldsymbol{w}^2 f\left(\boldsymbol{x}^2\right)\right)\right)\right) \tag{8}$$

Putting the solved $\boldsymbol{x}^1$, i.e., Eq. (6), into the above Eq., we have:

$$\Delta \boldsymbol{x}^2 = \gamma f'\left(\boldsymbol{x}^2\right) \circ \left(\left(\boldsymbol{w}^2\right)^T \left(\boldsymbol{x}^3 - \boldsymbol{w}^2 f\left(\boldsymbol{x}^2\right)\right)\right) \tag{9}$$

Considering the above dynamic has converged, we can set $\Delta \boldsymbol{x}^2 = \boldsymbol{0}$ in the above equation and solving for $\boldsymbol{x}^2$, then we can obtain the converged value of $\boldsymbol{x}^2$:

$$\boldsymbol{x}^2 = f^{-1}\left(\left(\boldsymbol{w}^2\right)^{-1} \boldsymbol{x}^3\right) \tag{10}$$

One can now see the proof goes recursively until $l = L$ and $\boldsymbol{x}^{L+1}$ is fixed to the target pattern $\boldsymbol{s}^{\text{target}}$:

$$\begin{aligned} \boldsymbol{x}^l &= f^{-1}\left(\left(\boldsymbol{w}^l\right)^{-1}\boldsymbol{x}^{l+1}\right) \\ \boldsymbol{x}^{L+1} &= \boldsymbol{s}^{\text{target}} \end{aligned} \tag{11}$$

which is exactly the recursive formula of the local target in target propagation, i.e., Eq. (2). Thus, neural activity of output-constrained PCN after relaxation equals to the local target.

Input-output-constrained PCN Secondly, we investigate the "input-output-constrained PCN": in this PCN both input and output neurons are clamped to the input and target patterns, respectively. We show that in this PCN, the activity after relaxation are the weighted sum of the predicting activity and the local target. Particularly, since in an input-output-constrained PCN we can only solve for the equilibrium after relaxation analytically in the linear case, we prove this for a linear PCN. Nevertheless, the analysis still provides useful insights. Looking at the network dynamics at a given layer l, i.e., Eq. 12 in the Methods of the main article, we can write the dynamics in the linear case as,

$$\Delta\boldsymbol{x}^l = \gamma\left(-\left(\boldsymbol{x}^l - \boldsymbol{w}^{l-1}\boldsymbol{x}^{l-1}\right) + \left(\boldsymbol{w}^l\right)^T\left(\boldsymbol{x}^{l+1} - \boldsymbol{w}^l\boldsymbol{x}^l\right)\right) \tag{12}$$

If we then set $\Delta\boldsymbol{x}^l = \boldsymbol{0}$ and solve for $\boldsymbol{x}^l$, we obtain,

$$\Delta\boldsymbol{x}^l = \boldsymbol{0} \implies -\left(\boldsymbol{x}^l - \boldsymbol{w}^{l-1}\boldsymbol{x}^{l-1}\right) + \left(\boldsymbol{w}^l\right)^T\left(\boldsymbol{x}^{l+1} - \boldsymbol{w}^l\boldsymbol{x}^l\right) = \boldsymbol{0} \tag{13}$$

$$\implies -\boldsymbol{x}^l + \boldsymbol{w}^{l-1}\boldsymbol{x}^{l-1} + \left(\boldsymbol{w}^l\right)^T\boldsymbol{x}^{l+1} - \left(\boldsymbol{w}^l\right)^T\boldsymbol{w}^l\boldsymbol{x}^l = \boldsymbol{0} \tag{14}$$

$$\implies \boldsymbol{x}^l + \left(\boldsymbol{w}^l\right)^T\boldsymbol{w}^l\boldsymbol{x}^l = \boldsymbol{w}^{l-1}\boldsymbol{x}^{l-1} + \left(\boldsymbol{w}^l\right)^T\boldsymbol{x}^{l+1} \tag{15}$$

$$\implies \left(\boldsymbol{I} + \left(\boldsymbol{w}^l\right)^T\boldsymbol{w}^l\right)\boldsymbol{x}^l = \boldsymbol{w}^{l-1}\boldsymbol{x}^{l-1} + \left(\boldsymbol{w}^l\right)^T\boldsymbol{x}^{l+1} \tag{16}$$

$$\implies \boldsymbol{x}^l = \left(\boldsymbol{I} + \left(\boldsymbol{w}^l\right)^T\boldsymbol{w}^l\right)^{-1}\left(\boldsymbol{w}^{l-1}\boldsymbol{x}^{l-1} + \left(\boldsymbol{w}^l\right)^T\boldsymbol{x}^{l+1}\right) \tag{17}$$

If we assume that the norm of the weights is large compared to the identity matrix $\boldsymbol{I}$, i.e., we consider $\left(\boldsymbol{I} + \left(\boldsymbol{w}^l\right)^T\boldsymbol{w}^l\right)^{-1} \approx \left(\left(\boldsymbol{w}^l\right)^T\boldsymbol{w}^l\right)^{-1}$, the above equilibrium solution can further be approximated by:

$$\implies \boldsymbol{x}^l \approx \left(\left(\boldsymbol{w}^l\right)^T\boldsymbol{w}^l\right)^{-1}\left(\boldsymbol{w}^{l-1}\boldsymbol{x}^{l-1} + \left(\boldsymbol{w}^l\right)^T\boldsymbol{x}^{l+1}\right) \tag{18}$$

$$\implies \boldsymbol{x}^l \approx \underbrace{\left(\left(\boldsymbol{w}^l\right)^T\boldsymbol{w}^l\right)^{-1}}_{\text{constant}}\ \underbrace{\boldsymbol{w}^{l-1}\boldsymbol{x}^{l-1}}_{\substack{\text{predicting activity} \\ \text{for backpropagation and PCN}}} + \underbrace{\left(\boldsymbol{w}^l\right)^{-1}\boldsymbol{x}^{l+1}}_{\substack{\text{local target} \\ \text{from target propagation}}} \tag{19}$$

where the equilibrium solution is simply the weighted sum of the predicting activity and the local target.

In summary, during relaxation the activity in PCNs tends to move from the predicting activity towards the local target that would be computed by target propagation. These relationships on one hand build interesting connections to existing work, on the other hand serve as a step in providing a mathematical explanation of the target alignment of PCNs, as discussed in the later Section 2.4.4.

2.3 Prospective index of predictive coding networks (Supplementary Fig. 5)

This section formally proves two properties of the prospective index ϕ^l of a *predictive coding network*[7,8] (PCN), that can be observed in Supplementary Fig. 5d. To briefly recap, prospective index ϕ^l quantifies to what extent the hidden neural activity of the network following clamping output neurons to a target pattern is shifting toward the hidden neural activity following subsequent weight modification. Below we show two properties visible in Supplementary Fig. 5d:

- Firstly, prospective index of the first hidden layer (ϕ^2) in a PCN is always one.
- Secondly, the prospective index in other layer is close to one because, the weights $\boldsymbol{W}$ in PCN are updated towards a configuration $\boldsymbol{W}^*$ whose prospective index is one.

Note that these observations of high prospective index of PCNs on one hand formally define what we proposed as "prospective configuration" and distinguishes itself from backpropagation, on the other hand serve as a step in providing a mathematical explanation of the target alignment of PCNs, as discussed in the later Section 2.4.4.

2.3.1 Prospective index of the first hidden layer of PCN is always one

We assume that the model does not make a perfect prediction with the current weights, so that the error in the prediction drives the learning. As defined in Supplementary Fig. 5a, vectors $\boldsymbol{v}^{\oplus,l}$ and $\boldsymbol{v}'^{,l}$ describe the changes in hidden neuron activity, due to target pattern being provided and learning respectively. Specifically for layer $l = 2$, these vectors are:

$$\boldsymbol{v}^{\oplus,2} = \boldsymbol{x}_{\boldsymbol{W}}^{\oplus,2} - \boldsymbol{x}_{\boldsymbol{W}}^{\ominus,2} \tag{20}$$

$$\boldsymbol{v}'^{,2} = \boldsymbol{x}_{\boldsymbol{W}'}^{\ominus,2} - \boldsymbol{x}_{\boldsymbol{W}}^{\ominus,2} \tag{21}$$

We will now show that for PCN the above vectors $\boldsymbol{v}^{\oplus,2}$ and $\boldsymbol{v}'^{,2}$ point in the same direction. The change in activity due to learning $\boldsymbol{v}'^{,2}$ is equal to

$$\boldsymbol{v}'^{,2} = \boldsymbol{w}'^{,1} f\left(\boldsymbol{x}_{\boldsymbol{W}'}^{\ominus,1}\right) - \boldsymbol{w}^1 f\left(\boldsymbol{x}_{\boldsymbol{W}}^{\ominus,1}\right) \tag{22}$$

Since the value nodes of the first (input) layer $\boldsymbol{x}^1$ are always fixed to the input signal $\boldsymbol{s}^{\text{in}}$, the above Eq. (22) can further be written as,

$$\begin{aligned}\boldsymbol{v}'^{,2} &= \boldsymbol{w}'^{,1} f\left(\boldsymbol{s}^{\text{in}}\right) - \boldsymbol{w}^1 f\left(\boldsymbol{s}^{\text{in}}\right) \\ &= \left(\boldsymbol{w}'^{,1} - \boldsymbol{w}^1\right) f\left(\boldsymbol{s}^{\text{in}}\right) \\ &= \Delta\boldsymbol{w}^1 f\left(\boldsymbol{s}^{\text{in}}\right)\end{aligned} \tag{23}$$

Using Eqs. 13 and 11 in the Methods of the main article, we write

$$\boldsymbol{v}'^{,2} = \alpha\left(\boldsymbol{x}_{\boldsymbol{W}}^{\oplus,2} - \hat{\boldsymbol{x}}_{\boldsymbol{W}}^{\oplus,2}\right)\left(f\left(\boldsymbol{s}^{\text{in}}\right)\right)^T f\left(\boldsymbol{s}^{\text{in}}\right) \tag{24}$$

In Eq. (24), $\hat{\boldsymbol{x}}^l$ denotes inputs to neurons in layer l, i.e., $\hat{\boldsymbol{x}}^l = \boldsymbol{w}^{l-1} f\left(\boldsymbol{x}^{l-1}\right)$. Note that $\hat{\boldsymbol{x}}_{\boldsymbol{W}}^{\oplus,2} = \boldsymbol{x}_{\boldsymbol{W}}^{\ominus,2}$, because both of these quantities are equal to $\boldsymbol{w}^1 f\left(\boldsymbol{s}^{\text{in}}\right)$ (the input of the first hidden layer ($l = 2$) does not change

in response to output neuron being clamped). Using $\hat{\boldsymbol{x}}_{\boldsymbol{W}}^{\oplus,2} = \boldsymbol{x}_{\boldsymbol{W}}^{\ominus,2}$, the above Eq. (24) can further be written as,

$$\boldsymbol{v}'^{,2} = \left(\boldsymbol{x}_{\boldsymbol{W}}^{\oplus,2} - \boldsymbol{x}_{\boldsymbol{W}}^{\ominus,2}\right) \alpha \left(f\left(\boldsymbol{s}^{\text{in}}\right)\right)^T f\left(\boldsymbol{s}^{\text{in}}\right) \tag{25}$$

Note that $\alpha \left(f\left(\boldsymbol{s}^{\text{in}}\right)\right)^T f\left(\boldsymbol{s}^{\text{in}}\right)$ is a positive scalar (if at least one entry in the input pattern is non-zero). Comparing Eqs. (20) and (25), we can see that vectors $\boldsymbol{v}'^{,2}$ and $\boldsymbol{v}^{\oplus,2}$ are just scaled versions of each other, hence the cos of the angle between them is equal to 1, and thus prospective index is also equal to 1 (in the limit of $\kappa \to 0$).

2.3.2 Weights in PCN are updated towards a configuration with prospective index of one

As seen in Supplementary Fig. 5d, the prospective index for layers $l > 2$ is very close to one. To provide an intuition for why this is the case, in this section we demonstrate how PCNs would need to be modified to have prospective index equal to 1. We will refer to such modified model as target-PCN, and calculate its prospective index.

As in the previous section, we assume that the model does not make a perfect prediction with the current weights, so that the error in the prediction drives the learning. We start with recapping what happens in sequence in one iteration of the standard PCN.

1. Start from relaxation with only input neurons clamped to input pattern ($\ominus$) and with current weight $\boldsymbol{W}$, the hidden neuron activity settles to: $\boldsymbol{x}_{\boldsymbol{W}}^{\ominus,l}$

2. Both input and output neurons are clamped to the input and target pattern respectively ($\oplus$) and then the hidden neuron activity is relaxed to: $\boldsymbol{x}_{\boldsymbol{W}}^{\oplus,l}$

3. Weights $\boldsymbol{W}$ are updated for one step to $\boldsymbol{W}'$ to decrease the energy, while hidden neuron activity stays still from the last step: $\boldsymbol{x}_{\boldsymbol{W}}^{\oplus,l}$

4. Output neurons are freed but the input neuron is still clamped to the input pattern and then the hidden neuron activity is relaxed to: $\boldsymbol{x}_{\boldsymbol{W}'}^{\ominus,l}$

In the above step 3, weights are updated for one step from $\boldsymbol{W}$ to $\boldsymbol{W}'$. However, one can investigate the case of updating weights $\boldsymbol{W}$ for many steps until convergence $\boldsymbol{W}^*$ in the above step 3. This will result in weights $\boldsymbol{W}^*$ that represents: "the target towards which the weights $\boldsymbol{W}$ are updated". Thus, we call this variant "target-PCN" and it is summarized in Algorithm 7. Specifically, the procedure of target-PCN is to replace the above steps 3 and 4 of standard PCN with:

3. Weights are updated for many steps from $\boldsymbol{W}$ to $\boldsymbol{W}^*$ to decrease the energy till convergence, while hidden neuron activity stays still from the last step: $\boldsymbol{x}_{\boldsymbol{W}}^{\oplus,l}$;

4. Output neurons are freed but the input neuron is still clamped to the input pattern and then the hidden neuron activity is relaxed to: $\boldsymbol{x}_{\boldsymbol{W}^*}^{\ominus,l}$;

Algorithm 7: Learn with target-PCN

Input: input pattern $\boldsymbol{s}^{\text{in}}$; target pattern $\boldsymbol{s}^{\text{target}}$; synaptic weights $\left\{\boldsymbol{w}^1, \boldsymbol{w}^2, \cdots, \boldsymbol{w}^L\right\}$
Output: updated synaptic weights $\left\{\boldsymbol{w}^1, \boldsymbol{w}^2, \cdots, \boldsymbol{w}^L\right\}$

$\boldsymbol{x}^1 = \boldsymbol{s}^{\text{in}}$; // Clamp input neurons to input pattern
$\boldsymbol{x}^{L+1} = \boldsymbol{s}^{\text{target}}$; // Clamp output neurons to target pattern
for $t = 0;\ t < \mathscr{T};\ t = t+1$ **do** // Relaxation
  for $l = 1;\ l < L+1;\ l = l+1$ **do**
    $\hat{\boldsymbol{x}}^{l+1} = \boldsymbol{w}^l f\left(\boldsymbol{x}^l\right)$;
    $\boldsymbol{\varepsilon}^{l+1} = \boldsymbol{x}^{l+1} - \hat{\boldsymbol{x}}^{l+1}$;
  end
  for $l = 2;\ l < L+1;\ l = l+1$ **do**
    $\Delta \boldsymbol{x}^l = \gamma\left(-\boldsymbol{\varepsilon}^l + f'\left(\boldsymbol{x}^l\right) \circ \left(\left(\boldsymbol{w}^l\right)^T \boldsymbol{\varepsilon}^{l+1}\right)\right)$;
    $\boldsymbol{x}^l = \boldsymbol{x}^l + \Delta \boldsymbol{x}^l$;
  end
end
while $\left\{\boldsymbol{w}^1, \boldsymbol{w}^2, \cdots, \boldsymbol{w}^L\right\}$ *not converged* **do** // Update weights till convergence
  for $l = 1;\ l < L+1;\ l = l+1$ **do**
    $\hat{\boldsymbol{x}}^{l+1} = \boldsymbol{w}^l f\left(\boldsymbol{x}^l\right)$;
    $\boldsymbol{\varepsilon}^{l+1} = \boldsymbol{x}^{l+1} - \hat{\boldsymbol{x}}^{l+1}$;
  end
  for $l = 1;\ l < L+1;\ l = l+1$ **do** // Update weights
    $\Delta \boldsymbol{w}^l = \alpha \boldsymbol{\varepsilon}^{l+1}\left(f\left(\boldsymbol{x}^l\right)\right)^T$;
    $\boldsymbol{w}^l = \boldsymbol{w}^l + \Delta \boldsymbol{w}^l$;
  end
end

In the following, we demonstrate prospective index of target-PCN is one for all layers. First, we should notice that the minimum of energy E of PCN is zero, since the energy function is a sum of quadratic terms, i.e., Eq. 6 in the Methods of the main article. Then, we should notice that such energy E of PCN can be optimized to its minimum of zero by optimizing only $\boldsymbol{W}$. Particularly, the local energy term of layer l is:

$$\begin{aligned}\frac{1}{2}\left(\boldsymbol{\varepsilon}^l\right)^T \boldsymbol{\varepsilon}^l &= \frac{1}{2}\left(\boldsymbol{x}^l - \hat{\boldsymbol{x}}^l\right)^T \left(\boldsymbol{x}^l - \hat{\boldsymbol{x}}^l\right) \\ &= \frac{1}{2}\left(\boldsymbol{x}^l - \boldsymbol{w}^{l-1} f\left(\boldsymbol{x}^{l-1}\right)\right)^T \left(\boldsymbol{x}^l - \boldsymbol{w}^{l-1} f\left(\boldsymbol{x}^{l-1}\right)\right)\end{aligned} \tag{26}$$

In the above Eq., $\boldsymbol{x}^l - \boldsymbol{w}^{l-1} f\left(\boldsymbol{x}^{l-1}\right)$ can be optimized to produce a zero vector by optimizing only $\boldsymbol{w}^{l-1}$, as long as $f\left(\boldsymbol{x}^{l-1}\right)$ is not a zero vector. Specifically, let us denote all the non-zero entries in $f\left(\boldsymbol{x}^{l-1}\right)$ by $\left\{f\left(x_i^{l-1}\right)\right\}_{i \in I}$, where I is the set of indices i so that $f\left(x_i^{l-1}\right)$ is non-zero. Since $f\left(\boldsymbol{x}^{l-1}\right)$ is not a zero vector, $I \neq \emptyset$. To demonstrate that there exists a solution for $\left\{w_{j,i}^{l-1}\right\}_{i \in I}$ so that $x_j^l = \sum_{i \in I} w_{j,i}^{l-1} f\left(x_i^{l-1}\right)$, we construct an example of such solution. Such sample solution is to pick one index g from I, then have $w_{j,g}^{l-1} = \frac{x_j^l}{f\left(x_i^{l-1}\right)}$ and $\left\{w_{j,i}^{l-1} = 0 : i \in I, i \notin \{g\}\right\}$. Thus, as long as $f\left(\boldsymbol{x}^{l-1}\right)$ is not a zero vector ($I \neq \emptyset$), there exists a solution of $\boldsymbol{w}^{l-1}$ that makes $\boldsymbol{x}^l - \boldsymbol{w}^{l-1} f\left(\boldsymbol{x}^{l-1}\right)$ a zero vector.

Thus, in step 3 of the target-PCN, the energy of the network is at its minimum of zero. This further implies that in the step 4 of the target-PCN, the neural activity does not move, i.e.,

$$\boldsymbol{x}_{\boldsymbol{W}^*}^{\ominus,l} = \boldsymbol{x}_{\boldsymbol{W}}^{\oplus,l} \tag{27}$$

According to the definition of prospective index in Supplementary Figs. 5a-b, the prospective index of this target-PCN ($\phi^{*,l}$) is:

$$\begin{aligned}
\phi^{*,l} &= \frac{\boldsymbol{v}^{\oplus,l} \cdot \boldsymbol{v}^{*,l}}{\left(||\boldsymbol{v}^{\oplus,l}|| + \kappa\right)\left(||\boldsymbol{v}^{*,l}|| + \kappa\right)} \\
&\approx cos\left(\boldsymbol{v}^{\oplus,l}, \boldsymbol{v}^{*,l}\right) \\
&= cos\left(\overrightarrow{\boldsymbol{x}_{\boldsymbol{W}}^{\ominus,l}\boldsymbol{x}_{\boldsymbol{W}}^{\oplus,l}}, \overrightarrow{\boldsymbol{x}_{\boldsymbol{W}}^{\ominus,l}\boldsymbol{x}_{\boldsymbol{W}^*}^{\ominus,l}}\right) \\
&= cos\left(\overrightarrow{\boldsymbol{x}_{\boldsymbol{W}}^{\ominus,l}\boldsymbol{x}_{\boldsymbol{W}}^{\oplus,l}}, \overrightarrow{\boldsymbol{x}_{\boldsymbol{W}}^{\ominus,l}\boldsymbol{x}_{\boldsymbol{W}}^{\oplus,l}}\right) \text{ according to Eq. (27)} \\
&= 1
\end{aligned} \tag{28}$$

This theoretical result is further confirmed by empirical observation in Supplementary Fig. 5d. Since the standard PCN modifies the weights in a similar direction as target-PCN, it is likely to have a similar prospective index.

In summary, PCN has a high prospective index. This on one hand formally defines what we proposed as "prospective configuration" and distinguishes itself from backpropagation, on the other hand serve as a step in providing a mathematical explanation of the target alignment of PCNs, as discussed in the later Section 2.4.4.

2.4 Target alignment

In this section we provide a mathematical analysis of target alignment. First, we show that the target alignment is equal to 1 for various networks that do not include hidden layers. Next we demonstrate that target propagation produces target alignment of 1. The third subsections identifies a special condition under which backpropagation produces target alignment of 1. The last subsection addresses the question of why predictive coding networks (PCNs) have higher target alignment than backpropagation, using several findings in earlier sections.

2.4.1 Target alignment for networks without hidden layers (Fig. 3e)

Fig. 3e shows that target alignment for models without hidden layers, trained either with prospective configuration or backpropagation, is exactly one, and here we prove this property analytically. Without hidden layers, prospective configuration and backpropagation are identical algorithms. In a linear network, the change of the weight $\boldsymbol{w}^1$ is:

$$\Delta \boldsymbol{w}^1 = \alpha \boldsymbol{\varepsilon}^2 \left(\boldsymbol{x}^1\right)^T \tag{29}$$

We denote output after learning by $\boldsymbol{x}'^2$. The change of the output $\boldsymbol{x}'^2 - \boldsymbol{x}^2$ is:

$$\boldsymbol{x}'^2 - \boldsymbol{x}^2 = \boldsymbol{w}'^{,2}\boldsymbol{x}^1 - \boldsymbol{w}^2\boldsymbol{x}^1 \tag{30}$$

$$= \Delta \boldsymbol{w}^1 \boldsymbol{x}^1 \tag{31}$$

$$= \alpha \boldsymbol{\varepsilon}^2 \left(\boldsymbol{x}^1\right)^T \boldsymbol{x}^1 \tag{32}$$

Here $\left(\boldsymbol{x}^1\right)^T \boldsymbol{x}^1$ is a positive scalar (if at least one entry in $\boldsymbol{x}^1$ is non-zero). Thus,

$$\boldsymbol{x}'^2 - \boldsymbol{x}^2 \sim \boldsymbol{\varepsilon}^2 \tag{33}$$

According to the definition of target alignment, which is the cosine similarity of the direction of the target (i.e., $\boldsymbol{\varepsilon}^2$) and the direction of learning (i.e., $\boldsymbol{x}'^2 - \boldsymbol{x}^2$), target alignment of this network is exactly one. This conclusion also applies to network with a nonlinear activation function.

2.4.2 Target alignment of target propagation (Supplementary Fig. 4a)

This subsection demonstrates that target alignment of target propagation is equal to 1. Such target alignment equal to 1 for target propagation is implied by Theorem 5 in the study of Meulemans et al.[6]. They show that if a network is linear and weights in each layer are invertible, then "parameter updates push the output activation along the negative gradient direction in the output space"[6]. Simulations in Supplementary Fig. 4a illustrate that the target alignment of target propagation is indeed equal to 1. For completeness we include in this paper a simple direct proof of this result (which we will also use in the next section).

For linear networks with invertible weights, the relationship between errors in adjacent layers in target propagation is:

$$\boldsymbol{\varepsilon}^l = \left(\boldsymbol{w}^l\right)^{-1} \boldsymbol{\varepsilon}^{l+1} \tag{34}$$

The activity of output neurons after the weight modification is:

$$\boldsymbol{x}'^{L+1} = \left(\boldsymbol{w}^L + \alpha \boldsymbol{\varepsilon}^{L+1} \left(\boldsymbol{x}^L\right)^T\right) \boldsymbol{w}'^{,L-1} \cdots \boldsymbol{w}'^{,1} \boldsymbol{x}^1 \tag{35}$$

$$= \boldsymbol{w}^L \boldsymbol{w}'^{,L-1} \cdots \boldsymbol{w}'^{,1} \boldsymbol{x}^1 + \boldsymbol{\varepsilon}^{L+1} \alpha \left(\boldsymbol{x}^L\right)^T \boldsymbol{w}'^{,L-1} \cdots \boldsymbol{w}'^{,1} \boldsymbol{x}^1 \tag{36}$$

Term $\alpha \left(\boldsymbol{x}^L\right)^T \boldsymbol{w}'^{,L-1} \cdots \boldsymbol{w}'^{,1} \boldsymbol{x}^1$ is a scalar, so let us denote it by c_L. Expanding $\boldsymbol{w}'^{,L-1}$ and using Eq. (34), we obtain:

$$\boldsymbol{x}'^{L+1} = \boldsymbol{w}^L \left(\boldsymbol{w}^{L_1} + \alpha \boldsymbol{\varepsilon}^L \left(\boldsymbol{x}^{L-1}\right)^T\right) \cdots \boldsymbol{w}'^{,1} \boldsymbol{x}^1 + c_L \boldsymbol{\varepsilon}^{L+1} \tag{37}$$

$$= \boldsymbol{w}^L \boldsymbol{w}^{L-1} \cdots \boldsymbol{w}'^{,1} \boldsymbol{x}^1 + \boldsymbol{w}^L \left(\boldsymbol{w}^L\right)^{-1} \boldsymbol{\varepsilon}^{L+1} \alpha \left(\boldsymbol{x}^{L-1}\right)^T \cdots \boldsymbol{w}'^{,1} \boldsymbol{x}^1 + c_L \boldsymbol{\varepsilon}^{L+1} \tag{38}$$

Note that $\boldsymbol{w}^L \left(\boldsymbol{w}^L\right)^{-1}$ is equal to the identity, so can be removed from the above equation, and $\alpha \left(\boldsymbol{x}^{L-1}\right)^T \cdots \boldsymbol{w}'^{,1} \boldsymbol{x}^1$ is a scalar, so denote it by c_{L-1}. Expanding all terms $\boldsymbol{w}'^{,l}$ analogously as above, we eventually obtain:

$$\boldsymbol{x}'^{L+1} = \boldsymbol{w}^L \cdots \boldsymbol{w}^1 \boldsymbol{x}^1 + \left(c_L + \cdots + c_1\right) \boldsymbol{\varepsilon}^{L+1} \tag{39}$$

Since the output before weight update was $\boldsymbol{w}^L \cdots \boldsymbol{w}^1 \boldsymbol{x}^1$, the change in the output is proportional to the direction towards target $\boldsymbol{\varepsilon}^{L+1}$, hence the target alignment is equal to 1. Given the similarity between target propagation and PCNs described in Section 2.2, the PCNs should also have target alignment relatively close to 1, as we will discuss further in Section 2.4.4.

It is also important to note that target propagation diverges from prospective configuration, when the feedback weights through which targets are propagated get small. This is implied by Eqs. (18) and (19) in Section 2.2, showing the relationship of predicting activity of backpropagation, local target of target propagation, and neural activities of PCN. Specifically, while deriving Eq. (19) (stating that neural activity in PCNs is a linear combination of predictive activity and local target from target propagation), an

assumption had to be made that the norm of the feedback weights $\boldsymbol{w}^l$ is large compared to the identity matrix $\boldsymbol{I}$. For example, if all feedback weights are equal to $\boldsymbol{w}^l_{i,j} = 0$, the neural activity $\boldsymbol{x}^l$ will be just equal to the predicting activity.

Since target propagation has a desirable property of perfect target alignment, one may ask if the brain can employ target propagation rather than prospective configuration as is main learning principle. However, energy-based networks have several advantages over target propagation both in terms of computational properties and relationship with experimental data. Since target propagation requires computation of multiple matrix inverses, it is numerically unstable, so for example in Supplementary Fig. 4a we only show the result for networks with up to 5 layers, because we were unable to perform target propagation in deeper networks due to numerical instabilities. PCNs offer a nice alternative which is related to target propagation, but is numerically stable (e.g., avoids propagating targets by infinitely large inverse matrices when a weight matrix is zero). Furthermore, target propagation does not modify the activity of the neurons during relaxation, so it does not follow prospective configuration. Consequently, in the case of the network in Fig. 1 target propagation would not compensate the weight to olfactory output, because such compensation relies on updating the activity of the hidden neuron. Theory reviewed in this section implies that target propagation only produces target alignment equal to 1 if the weights are invertable, but this is not the case in the network in Fig. 1, so target propagation would not produce unity target alignment for this problem. Moreover, target propagation would not be able to reproduce the patterns of behaviour and neural activity in Figs. 5, 6 and Supplementary Fig. 9, because reproducing these data relies on modifying activity of hidden neurons after feedback, and target propagation does not do it.

2.4.3 Target alignment for orthogonal initialization (Supplementary Fig. 4c)

This subsection identifies one special conditions under which backpropagation produces target alignment of 1. Specifically, simulations in Supplementary Fig. 4c show that target alignment is equal to 1 for backpropagation in linear networks, when the weights are initialized to orthogonal values $\left(\boldsymbol{w}^l\right)^T = \boldsymbol{w}^l$. This observation can be explained using results from the previous section: when weights are orthogonal, then $\left(\boldsymbol{w}^l\right)^T = \left(\boldsymbol{w}^l\right)^{-1}$, hence the relationship between errors in adjacent layers is the same as for target propagation (Eq. (34)). Consequently, the same argument can be applied to backpropagation on linear networks with orthogonal initialization to show that it has target alignment equal to 1.

2.4.4 Target alignment of predictive coding networks

The subsection addresses the question of why PCNs have higher target alignment than backpropagation, using several findings in earlier sections. Specifically, to justify why PCNs have high target alignment, we can combine 3 facts that we demonstrate in earlier sections, and summarize here:

1. Target alignment of target propagation is equal to 1. This is shown in Section 2.4.2.

2. When target pattern is provided to output neurons in PCNs, during relaxation the neural activity in hidden layers converges to values related to local targets in target propagation. This is shown in Section 2.2.

3. Weight modification in PCNs reinforces the pattern of activity to which it converged during relaxation. In other words, predicting activity changes as a result of weight modification in the direction of the equilibrium reached during relaxation. This is shown in Section 2.3.

According to fact 3, learning in PCNs reinforces the equilibrium activity, which, according to fact 2, is largely dependent on the local targets. Therefore, the changes in activity in hidden layers due to learning in

PCNs are similar to those in target propagation, and hence the changes in the output activity are also likely to be similar, and the two algorithms should also share a similarity in target alignment. According to fact 1, target propagation has target alignment of 1, so the PCNs should also share a similar target alignment.

References

[1] Donald Olding Hebb. *The organisation of behaviour: A neuropsychological theory*. Science Editions New York, 1949.

[2] Andre M Bastos et al. "Canonical microcircuits for predictive coding". In: *Neuron* 76.4 (2012), pp. 695–711.

[3] João Sacramento et al. "Dendritic cortical microcircuits approximate the backpropagation algorithm". In: *Advances in Neural Information Processing Systems (NeurIPS)*. 2018, pp. 8721–8732.

[4] James CR Whittington and Rafal Bogacz. "Theories of error back-propagation in the brain". In: *Trends in Cognitive Sciences* (2019).

[5] Dong-Hyun Lee et al. "Difference target propagation". In: *Joint European Conference on Machine Learning and Knowledge Discovery in Databases*. Springer. 2015, pp. 498–515.

[6] Alexander Meulemans et al. "A theoretical framework for target propagation". In: *Advances in Neural Information Processing Systems* 33 (2020), pp. 20024–20036.

[7] Rajesh PN Rao and Dana H Ballard. "Predictive coding in the visual cortex: A functional interpretation of some extra-classical receptive-field effects". In: *Nature Neuroscience* 2.1 (1999), pp. 79–87.

[8] James CR Whittington and Rafal Bogacz. "An approximation of the error backpropagation algorithm in a predictive coding network with local hebbian synaptic plasticity". In: *Neural Computation* 29.5 (2017), pp. 1229–1262.

[9] Xavier Glorot and Yoshua Bengio. "Understanding the difficulty of training deep feedforward neural networks". In: *Proceedings of the thirteenth international conference on artificial intelligence and statistics*. JMLR Workshop and Conference Proceedings. 2010, pp. 249–256.

[10] Andrew M Saxe, James L McClelland, and Surya Ganguli. "Exact solutions to the nonlinear dynamics of learning in deep linear neural networks". In: *arXiv preprint arXiv:1312.6120* (2013).

[11] Alexander Meulemans et al. "Credit assignment in neural networks through deep feedback control". In: *Advances in Neural Information Processing Systems* 34 (2021), pp. 4674–4687.

[12] Benjamin Scellier and Yoshua Bengio. "Equilibrium propagation: Bridging the gap between energy-based models and backpropagation". In: *Frontiers in Computational Neuroscience* 11 (2017), p. 24.

[13] Alexander Meulemans et al. "Minimizing control for credit assignment with strong feedback". In: *International Conference on Machine Learning*. PMLR. 2022, pp. 15458–15483.

[14] Alexander Meulemans et al. "The least-control principle for learning at equilibrium". In: *arXiv preprint arXiv:2207.01332* (2022).

[15] Randall C O'Reilly. "Biologically plausible error-driven learning using local activation differences: The generalized recirculation algorithm". In: *Neural Computation* 8.5 (1996), pp. 895–938.

[16] Luis B Almeida. "A learning rule for asynchronous perceptrons with feedback in a combinatorial environment". In: *Artificial Neural Networks: Concept Learning*. IEEE Computer Society Press, 1990, pp. 102–111.

[17] Fernando Pineda. “Generalization of back propagation to recurrent and higher order neural networks”. In: *Advances in Neural Information Processing Systems (NeurIPS)*. 1987, pp. 602–611.

[18] Fernando J Pineda. “Dynamics and architecture for Neural Computation”. In: *Journal of Complexity* 4.3 (1988), pp. 216–245.

[19] Mark A Kaufman and Robert C Bolles. “A nonassociative aspect of overshadowing”. In: *Bulletin of the Psychonomic Society* 18.6 (1981), pp. 318–320.

[20] Robert A Rescorla. “A theory of Pavlovian conditioning: Variations in the effectiveness of reinforcement and nonreinforcement”. In: *Current research and theory* (1972), pp. 64–99.

[21] Georg B Keller and Thomas D Mrsic-Flogel. “Predictive processing: A canonical cortical computation”. In: *Neuron* 100.2 (2018), pp. 424–435.

[22] Alexander Attinger, Bo Wang, and Georg B Keller. “Visuomotor coupling shapes the functional development of mouse visual cortex”. In: *Cell* 169.7 (2017), pp. 1291–1302.

[23] Martin Boerlin, Christian K Machens, and Sophie Denève. “Predictive coding of dynamical variables in balanced spiking networks”. In: *PLoS Computational Biology* 9.11 (2013), e1003258.

[24] Wieland Brendel et al. “Learning to represent signals spike by spike”. In: *PLoS Computational Biology* 16.3 (2020), e1007692.

[25] Hauke R Heekeren et al. “A general mechanism for perceptual decision-making in the human brain”. In: *Nature* 431.7010 (2004), pp. 859–862.

[26] Yuhang Song et al. “Can the brain do backpropagation?—Exact implementation of backpropagation in predictive coding networks”. In: *Advances in Neural Information Processing Systems (NeurIPS)*. Vol. 33. Europe PMC Funders, 2020, p. 22566.

[27] Dmitry Krotov and John J Hopfield. “Dense associative memory for pattern recognition”. In: *Advances in Neural Information Processing Systems (NeurIPS)*. Vol. 29. 2016, pp. 1172–1180.

[28] Victor Soto, Alberto Suárez, and Gonzalo Martínez-Muñoz. “An urn model for majority voting in classification ensembles”. In: *Advances in Neural Information Processing Systems (NeurIPS)*. Neural Information Processing Systems Foundation, 2016.

[29] Yoshua Bengio and Asja Fischer. “Early inference in energy-based models approximates back-propagation”. In: *arXiv preprint arXiv:1510.02777* (2015).

[30] Yoshua Bengio et al. “STDP as presynaptic activity times rate of change of postsynaptic activity”. In: *arXiv preprint arXiv:1509.05936* (2015).

[31] Yoshua Bengio. “How auto-encoders could provide credit assignment in deep networks via target propagation”. In: *arXiv preprint arXiv:1407.7906* (2014).

[32] Roger Penrose. “A generalized inverse for matrices”. In: *Mathematical proceedings of the Cambridge philosophical society*. Vol. 51. Cambridge University Press. 1955, pp. 406–413.